IN MEMORY OF WILHELM JORDAN

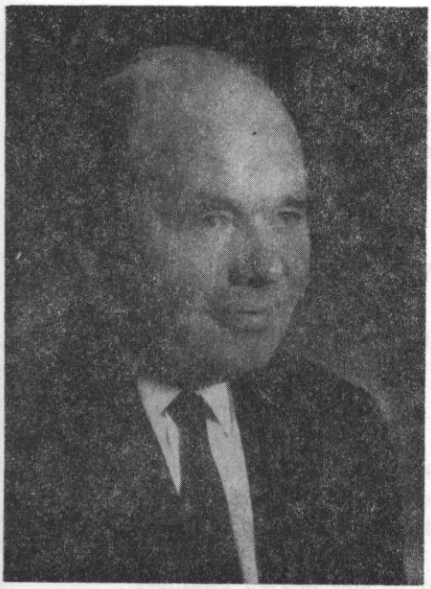

Dr. Wilhelm Lassen Jordan, an outstanding Danish acoustician, a worldrenowned expert in the field of interior acoustics, died, aged 72, on 3 February, 1982.

After graduation in 1933 from the Royal Technical Institute in Kopenhagen and obtaining the doctor's degree in 1941, over the nearly 40 successive years he has been outstandingly active as designer and consultant in interior acoustics, particularly in the domain of concert, theatre, and conference halls and studios of radio and television stations. Of the many of this designs in a large number of countries, most recognition was given to the buildings of the Danish radio in Kopenhagen (1940-1953), New York State Theater (1961-1965), Metropolitan Opera in New York (1962-1967), Sydney House (1957-1974), and many concert halls, including those in Oslo (1966-1977), Stockholm (1973-1979), Dublin (1976-1981), and Odense (1977-1981). He has been active until the final end. He died in Sydney while working on a new acoustical design of the opera hall in Sydney with 1550 seats in order that in addition to operas also theatrical plays could be staged there.

In his investigations he concentrated on the determination of simple, objective criteria of evaluation of the quality of concert and theatre halls. His experience of many years in acoustical designing of halls he contained in the recently published book *Acoustical Design of Concert Halls and Theatres* whose scientific and practical significance cannot be overestimated.

Wilhelm L. Jordan has been also hightly evaluated by Polish acousticians. They and he have always been in direct contact and he has often expressed his interest in our country.

ARCHIVES OF ACOUSTICS
7, 2, 83-106 (1982)

QUASI-NONLINEAR DISTORTION OF SIGNALS IN CLOSED SPACE FOR AN UNSTEADY STATE

STEFAN CZARNECKI

Department of Aeroacoustics, Institute of Fundamental Technological Research of Polish Academy of Sciences
(00-049 Warsaw, ul. Świętokrzyska 21)

WŁADYSŁAW WYGNAŃSKI

Chopin Academy of Music (00-368 Warsaw, ul. Okólnik 2)

This paper discusses the possibility of signal distortions occurring in closed space for the rise and decay of signals. A theoretical analysis is conducted for a simplified case in which the character of phenomena is analyzed in relation to the value of the ratio of the time delay between successive signals and their period.

The later part of this paper gives experimental results which confirm the possibility of distortions occurring in real conditions. It also discusses the possibility of the occurrence of phase, frequency and amplitude modulation and gives examples of signal shape distortion in its rising, obtained in two concert halls in the Academy of Music, Warsaw.

A subjective analysis was performed of the audibility of distortions in simulated signals which were programmed with a regular kind of distortion. The results of distortion audibility in % and the subjective analysis of the audibility of distortions in real conditions have shown that these distortions can be perceived with their short duration of the order of several or a dozen or so milliseconds.

1. Introduction

Among the variety of criteria for evaluating the acoustic quality of concert halls, theatres and auditoria, which will here be called auditoria, some refer to the initial time of sound rise and decay in enclosures.

Both in evaluating the masking effect of the first reflection with respect to the direct wave [6, 16] and in energy analysis of the first reflection with respect to all reflected waves [11, 13], these criteria involve a value of 50 ms calculated from the arrival or decay time of the direct wave as an essential value from the point of view of subjective analysis. The arbitrarily assumed notions of the rise time *TR* and the early decay time *EDT* of signals contain, according to JORDAN [7], essential data characterizing the properties of interiors.

These criteria can in general be called macroscopic, since they involve primarily energy relations without investigating the structure of signals [12].

It is well known that reflected waves affect the structure of a signal in an enclosure for an unsteady state. However, investigations in this field, which could be called microscopic approach investigations, have not been performed extensively so far. This approach was suggested in the 1950s and partly developed in the following years [2, 4, 14]; however, the lack of subjective evaluation methods for a „microscopic distinguishing" of the structure of the acoustic field failed to provide conditions to show the necessity for these investigations to be carried on.

The recently developed methods for subjective evaluation of acoustic signals and the use of FFT analysis of signals have encouraged the present authors to continue the microscopic approach investigations mentioned above.

The starting point in the present paper is the treatment of the delays with which particular reflected waves reach the observation point at the rise time of a signal as nonlinear, step-like time functions [2, 3]. For particular reflected waves these functions take a value of zero in the period in which the wave of a given reflection has not yet reached the observation point and a value of one when the wave of a given reflection has reached the observation point.

Assuming the linearity of phenomena in the amplitude domain, it is possible to superpose particular reflected waves, each of which contains a relevant step-like, i.e., nonlinear, time function resulting from the delay in its arrival at the observation point. As a result of the nonlinearity mentioned above, when the sound rises or decays at the observation point, the resultant signal shows the properties of a distorted signal.

Since the nonlinear properties of the resultant signal result from time characteristics and not from amplitude ones, the distortions thus caused will be called quasi-nonlinear distortions.

It is much more difficult to define nonlinear distortions resulting from nonlinear amplitude dependencies for unsteady-state than those for steady-state conditions. It is still more difficult to define quasi-nonlinear distortions.

In view of the above, the present paper does not attempt to define precisely the notion of transient signal distortions in an enclosure and their quantitative evaluation and is limited to a comparative analysis of the instantaneous spectrum of a distorted signal caused by the effect of the delays of particular re-

flected waves with respect to a reference signal in which the effect of reflected waves is absent.

reference is in this case a signal obtained in anechoic conditions, or (in practice) a signal in which the direct wave dominates. Thus, each signal for an unsteady state of sound in the enclosure in which reflected waves occur is a distorted signal. This paper attempts to grasp the character of these distortions and to evaluate their subjective audibility.

The aim of this paper is to analyze the effect of quasi-nonlinear distortions in the three aspects:

– theoretically, for a simplified case which can be described analytically;

– experimentally, in order to determine whether the phenomena described in the theoretical part occur in real conditions;

– subjectively, in order to define the audibility of differences between a distorted signal and an undistorted one for different durations of distortion.

The present investigations are preliminary and are limited to an examination of sinusoidal signals. In the future, these investigations will include real speech and music signals in a larger number of halls, and also other methods of psychoacoustic evaluation.

2. Theoretical analysis

It is known that Sabine's statistical theory is good for description of the acoustic field of enclosures in the case when the condition of a regular distribution of sound energy density in reflected waves, i.e. for a good diffusion of sound energy, is satisfied [1].

In unsteady-state of sound in an interior, i.e. when the sound rises or decays in an interior, this condition leads to an exponential increase or an exponential decrease in the SPL of waves reflected in an arbitrarily chosen observation point. In practice the curves of the rise or decay of sound in an interior deviate greatly from theoretical curves (most so for sinusoidal signals), in particular in the beginning of the rise or decay of sound. This is caused by an insufficient, from the point of view of the laws of statistics, number of the waves of the first reflections and by the effect of phase displacements between particular reflected waves whose sound pressure amplitudes are much higher than the amplitudes of the waves of the later reflections. This effect is one of the basic reasons why sinusoidal signals are not used in measurements of the reverberation time and why the first time section corresponding to a drop in SPL of 5 dB with respect to the steady-state level is eliminated from the decay curve.

This approach is fully justified in terms of measurement technique; it leads, however, to the loss of some data about the properties of a hall in the early rise or decay period. These data could be valuable in the future development of new criteria for evaluating halls.

In an unsteady state of sound in an enclosure the method of image sources [10,15] is useful in analysis of the acoustic field, particularly for the first reflections. This method consists in replacing the surfaces limiting the interior with an array of image sources with such properties and spatial arrangement that the sound distribution of the acoustic field in the interior represented by means of image sources corresponds to the sound distribution of this field in real conditions.

Of the major properties of the above representation used in the present paper, it is necessary to mention the following;

— the surfaces limiting the interior are planes;

— the sound power of the image source of the nth order is equal to the sound power of the real source multiplied by the factor β^n, where β is the coefficient of reflections from the planes limiting the interior;

— all image sources are started at the same time as the real source with the same phase;

— the distance of a given image source from the observation point is equal to the passage path of the wave emitted by the source Z and reaching the observation point X after a given number of reflections;

— in terms of amplitude acoustic signals fall within the limits of linear acoustics, which permits the use of a superposition of signals.

These assumptions make it possible to write the following formula for the instantaneous value of sound pressure in an unsteady state when the signal rises in the interior, from the time when the direct wave reaches the observation point till the time when the nth reflected wave does so,

$$p(t) = 1(t-\tau_0)p_0 \sin \omega_0(t-\tau_0) + \ldots + 1(t-\tau_n)\varrho_n \sin \omega_0(t-\tau_n), \tag{1}$$

where p_0 and p_n are the sound pressure amplitudes of the direct wave and of the nth wave reflected at the observation point X, respectively. The functions $1(t-\tau_0)$ and $1\ (t-\tau_n)$ are unit step-functions representing, respectively, the delays τ_0 and τ_n with which the direct and the nth reflected waves reach the observation point X with respect to the time $t = 0$ when the source is started:

$$\begin{aligned} &1(t-\tau_0) = 0 \quad \text{for } t < \tau_0, \\ &1(t-\tau_0) = 1 \quad \text{for } t \geqslant \tau_0, \\ &\ldots\ldots\ldots\ldots\ldots \\ &1(t-\tau_n) = 0 \quad \text{for } t < \tau_n, \\ &1(t-\tau_n) = 1 \quad \text{for } t \geqslant \tau_n. \end{aligned} \tag{2}$$

Considering relation (2), equation (1) can be represented in the form of the following sum

$$p(t) = \sum_{i=0}^{n} 1(t-\tau_i)p_i \sin \omega_0(t-\tau_i), \tag{3}$$

where n is the number of reflected waves under observation.

For successive values of the number n with known values of the sound pressure amplitudes p_i and the delays τ_i, it is possible to plot changes in the resultant signal as a function of time in the process of sound rise in the interior for some arbitrarily chosen observation point X. For arbitrary values of the amplitudes p_i and the delays τ_i it is, however, impossible to present the sum expressed in formula (3) in simple analytical form. This is possible only in a simplified case under the following assumptions:

– the sound level amplitudes of particular reflected waves are the same and equal to the amplitude p_0 of the direct wave,

$$p_i = p_0; \tag{4}$$

– successive reflected waves reach the observation point X at the same time intervals τ, which leads to the conditions

$$\tau_i = i\tau. \tag{5}$$

This case does not occur in real enclosures and can exist only in the conditions of the plane wave field limited by two parallel planes with the reflection coefficient $\beta = 1$, in the Kundt tube, for example. Consideration of the above simplified case aims, however, at investigating the character of sound pressure variations in an unsteady state, while experimental investigations in halls should verify whether the phenomena occurring in the simplified case occur in real conditions.

Assuming, for simplification, as the initial moment of the sound rise in the interior the moment when the direct wave reaches the observation point, i.e. $\tau = 0$, it is possible to write the expression of the instantaneous value of the sound pressure after n reflected waves have reached the observation point in the form

$$p(t) = \sum_{i=1}^{n} 1(t-i\tau)p_0 \sin \omega_0(t-i\tau). \tag{6}$$

The expression of the sum of sinusoidal signals with the same amplitude and argument which changes by a constant value as a step-function can be represented in analytical form, according to the general relation (5),

$$p_{n-1}(t) = \sum_{i=0}^{n-1} p_0 \sin(x+iy) = p_0 \sin\frac{ny}{2} \operatorname{cosec}\frac{y}{2} \sin\left[x+(n-1)\frac{y}{2}\right]. \tag{7}$$

Changing the number of the terms in the series in formula (7) to n and substituting

$$y = \omega_0\tau, \tag{8}$$

$$y = \omega_0\tau, \tag{9}$$

it is possible to write expression (6) of the sum of sinusoidal signals delayed in time and shifted in phase after n reflected waves have reached the observation point X in the form

$$p_n(t) = 1(t_n - n\tau)p_0 \frac{\sin\left[(n+1)\frac{\omega_0\tau}{2}\right]\sin\left(\omega_0 t - n\frac{\omega_0\tau}{2}\right)}{\sin\frac{\omega_0\tau}{2}}. \tag{10}$$

After the time t_n in which the nth reflected wave reaches the observation point, i.e. for $t_n \gg n\tau$, the function

$$1(t_n - n\tau) = 1, \tag{11}$$

while the step-like changes in a signal caused by the arrival of successive reflected waves at the observation point are expressed in expression (10) by varying the number n, which can be written in the form

$$n = \mathrm{ent}\left(\frac{t_n}{\tau}\right) = f(St). \tag{12}$$

This notation signifies that as successive reflected waves reach the observation point, the value of the number n is changed in a step-like manner, taking the least value of the integer in the quotient t_n/τ. The above step-like changes in the number n form a nonlinear time function which has been written in the general form as $f(St)$.

In further considerations it is convenient to use the ratio of the delay τ between successive reflections and the period T of the signal,

$$\gamma = \frac{\tau}{T} = \frac{\omega_0\tau}{2\pi}. \tag{13}$$

Substitution of relations (12) and (13) into expression (10) makes it possible to write

$$p_n(t) = p_0 \frac{\sin[f(St)+1]\pi\gamma}{\sin\pi\gamma}\sin[\omega_0 t - f(St)\pi\gamma]. \tag{14}$$

In the above expression the step time function $f(St)$ occurs twice: once as a change in amplitude and once as change in phase. It follows therefore that in an unsteady state of sound in an enclosure, i.e. in the time range $0 < t < \tau_n$, an effect corresponding to simultaneous amplitude and phase modulation of the signal occurs at the observation point X.

It is known that signal modulation can only occur under the conditions in which nonlinear effects occur. In the present case nonlinearity does not apply to the amplitude relations of the system but to the time relations resulting from delays introduced by the system. Therefore, in order to distinguish them from

the commonly used notion of nonlinearity, signal distortions considered here were called quasi-nonlinear distortions at the beginning of the paper. In considering the hall as a delaying system which is nonlinear as a function of time, it should be expected that the quasi-nonlinear distortions introduced should influence the character of the frequency spectrum in the unsteady-state of the signal.

The effect of amplitude and phase modulation resulting from formula (14) depends essentially on the coefficient γ expressed in relation (13), representing the ratio of the delay τ between two successive waves reaching the observation point X and the period T of the signal.

It is possible to distinguish here four characteristic ranges of the coefficient γ, leading to qualitatively different effects.

I. $\gamma \leqslant 0.5$, i.e. $\omega_0 \tau \leqslant \pi$.

In this case the delay τ between successive waves reaching the observation point X is lower than half the period T of the signal, causing distortions in the shape of the curve of the signal to occur in the first phase of the sound rise in an interior, analogous to nonlinear distortions. This shape can be determined easily from formula (14) by calculating successive values of $p_n(t)$ for successive numbers n. The shape of a distorted signal can repeat at regular time intervals, if the condition

$$\omega_0 \tau = \frac{2\pi}{k}, \tag{15}$$

where k is an arbitrary positive number, is satisfied.

For example, when $\gamma = 0.5$, i.e. $\omega_0 \tau = \pi$, from formula (12)

$$p_n(t) = p_0 \frac{\sin\left[(n+1)\frac{\pi}{2}\right]}{\sin\frac{\pi}{2}} \sin\left(\omega_0 t - 4\frac{\pi}{2}\right). \tag{16}$$

It can be easily seen that in the present case for odd values of n the instantaneous value of the signal amplitude is equal to 0, while for even values of n the instantaneous value of the signal amplitude takes the values of p_0 (Fig. 1a).

The instantaneous changes in the values of the amplitude within one period which occur in the present case cannot be called amplitude modulation. The distortions in the shape of the curve of the signal can be regarded as the effect of phase modulation.

II. $0.5 < \gamma < 1.5$, i.e. $\pi < \omega_0 \tau < 3\pi$.

In this case the phase shift occurring for each period T of the signal causes, in addition to change in the signal shape, an effect corresponding to frequency

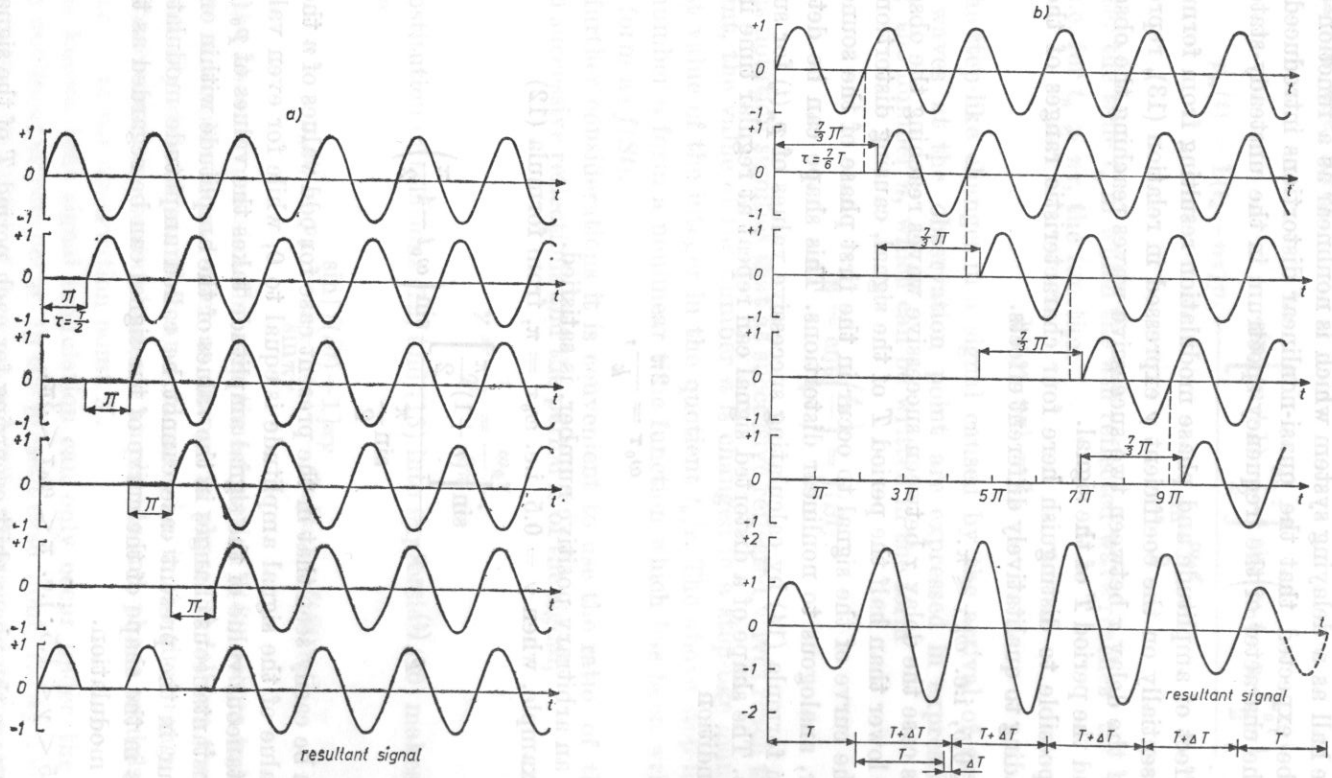

a) distortion in signal shape, $\tau = T/2$ $(\gamma = 1/2)$

b) frequency change $\tau = 7/6\ T$ $(\gamma = 7/6)$

Fig. 1. Characteristic cases of the rise of a sinusoidal signal in enclosure for constant values of the delays of successivesignals by the value τ

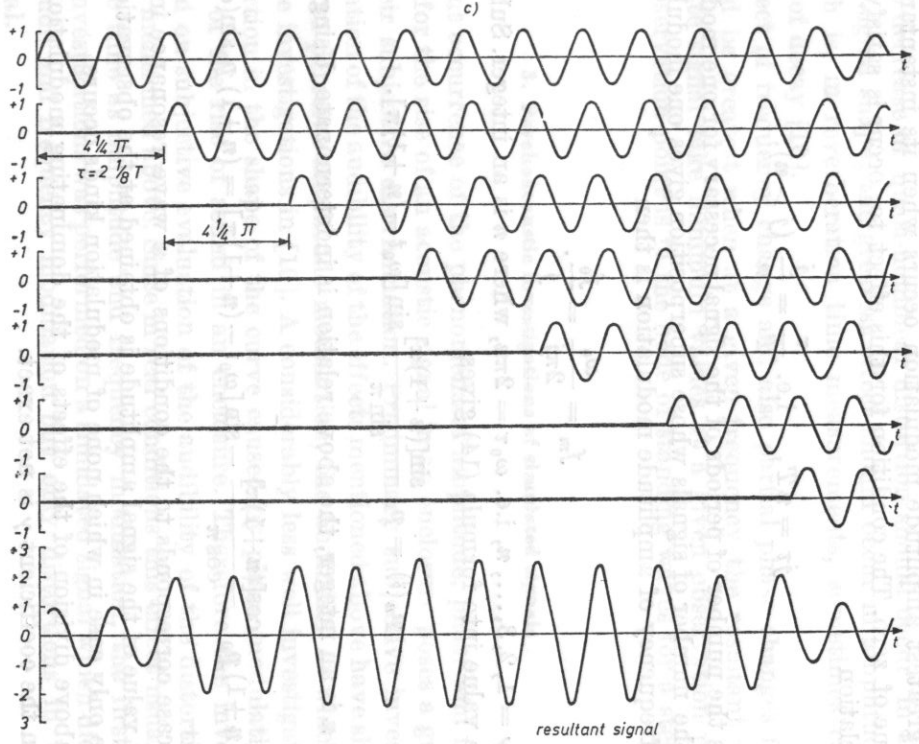

c) amplitude modulation $\tau = 2\,1/8\,T$ $(\gamma = 4\,1/4)$

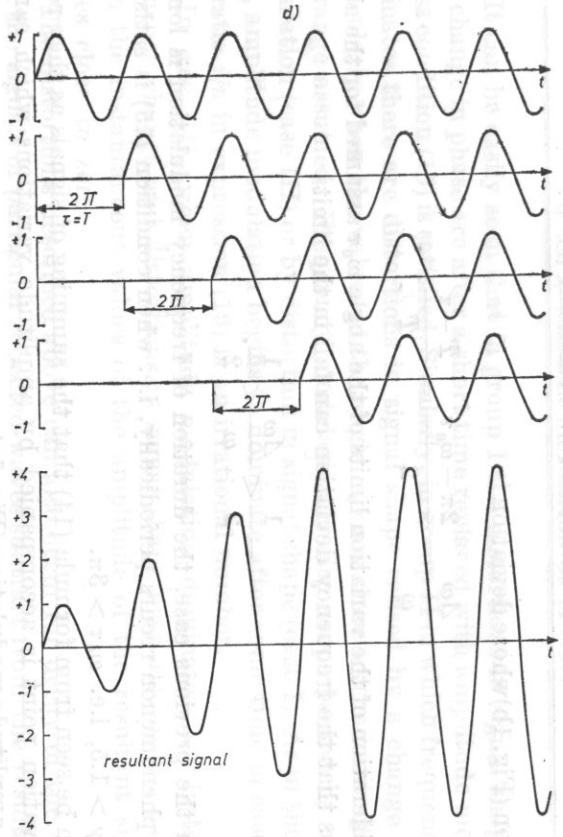

d) summing of signals in phase (wave resonance), $\tau = T$ $(\gamma = 1)$

modulation (Fig. 1b)whose deviation is

$$\frac{\Delta\omega}{\omega} = \frac{2\pi - \omega_0\tau}{2} = \frac{T-\tau}{T}. \tag{17}$$

Consideration of the variation limits of the angle $\omega_0\tau$ assumed for the above case shows that the frequency deviation can fall in the limits

$$-\frac{1}{2} < \frac{\Delta\omega}{\omega} < \frac{1}{2}. \tag{18}$$

As in the previous case, the duration of frequency modulation is longest when the phenomenon recurs periodically, i.e. when condition (15) is satisfied.

III. $\gamma > 1.5$, i.e. $\omega_0\tau > 3\pi$.

It can be seen from formula (14) that the summing of signals as they reach the observation point is accompanied by amplitude variations which can be treated as amplitude modulation (Fig. 1c).

The greatest amplitude modulation occurs when its instantaneous values ake a value of zero. The condition for this effect to occur is satisfying the following relation

$$j\tau = nT, \quad \text{i.e.} \quad \frac{\tau}{T} = \frac{j}{n} \quad (j > n), \tag{19}$$

where j is the number of periods of the signal necessary for one modulation period, n is the number of signals whose superposition gives one modulation cycle.

The frequency of amplitude modulation is then

$$f_m = \frac{\omega_0}{2\pi j} = \frac{f_0}{j}. \tag{20}$$

IV. $\gamma = 1, 2, 3, \ldots, n$, i.e. $\omega_0\tau = 2\pi n$, where n is an integer. Substitution of the above value into formula (14) gives

$$p_n(t) = p_0 \frac{\sin[(n+1)\pi]}{\sin\pi} \sin[\omega_0 t - (n+1)\pi]. \tag{21}$$

Since n is an integer, the above relation is indeterminate. Using de l'Hospital's rule

$$p_n(t) = (n+1)\, p_0 \frac{\cos[(n+1)\pi]}{\cos\pi} - \sin[\omega_0 t - (n+1)\pi] = (n+1)\, p_0 \sin(\omega_0 t). \tag{22}$$

This case corresponds to the conditions of a wave resonance in which the maximum value of the signal amplitude is obtained at the observation point X. This is the only case in which none of modulation kinds occurs.

The above division of the effects of the dominating modulation kinds depending on the coefficient γ is not exact.

It can be easily seen that in group I the distortions in signal shape caused by a change in phase are after a short time replaced with amplitude modulation, unless condition (15) is satisfied. Similarly, in group II in which frequency change dominates there are distortions in signal shape caused by a change in phase, particularly when the values of the angle $\omega_0\tau$ are close to the limiting values of the range assumed. Frequency modulation is also accompanied by amplitude modulation (case III) or by distortion in signal shape (case I). As in the previous case, amplitude modulation begins to dominate after some time in case II when the ratio j/n in expression (19) is an irrational number.

In case III, when amplitude modulation dominates, an instantaneous frequency change and distortions in signal shape may also occur, particularly when the instantaneous values of the amplitude of the resultant signal take values close to zero.

The distortions described above can also occur for decay of the signal but then the signals of particular reflected waves subtract from the resultant signal in a steady state, which decreases the influence of the effects mentioned above. The greatest decrease of quasi-nonlinear distortion should occur in the effect of distorted signal shape; the greatest effect should occur in amplitude modulation, which is, in reverberation time measurements, sometimes called the lrregularity of decay [10].

The effect of frequency change and also partial phase changes for sound decay should be greatest when at a given frequency the resultant values of a steady-state signal take minimum values at a given observation point, i.e. when the observation point is in the node of standing waves for a steady-state condition.

3. Psychoacoustic investigations of simulated signals

The joint occurrence of the phenomena of amplitude, phase and frequency modulation for the rise of an acoustic signal in an enclosure poses a great difficulty in their subjective discrimination. Preliminary subjective investigations of the evaluation of the audibility of the effects mentioned above have shown that it is easiest to perceive amplitude modulation, the audibility of which was the object of the investigations in [19]. A considerably less well investigated effect is the distortion in the shape of the curve caused by phase modulation in the first period of the rise of sound in an enclosure. Therefore the investigation concentrated on subjective evaluation of the audibility of the distortion in the curve shape mentioned above. Since in real conditions this effect usually occurs at the same time as amplitude and frequency modulation, the first stage of subjective investigations was performed on a simulated signal which did not contain amplitude and frequency modulation but only distortions in the shape of the signal.

The simulated signal was a sinusoid with a continuously controlled number of half-sinusoids cut-off by the digital system (Fig. 2) [17].

When n denotes the number of distorted periods, the signal under investigation is described by relation (16) for numbers less than n; or it is an undistorted sinusoidal signal for numbers greater than n. The investigations were performed on signals for the numbers n equal to 1, 2, 4, 8, 16, which when recorded on magnetic tape alternating with undistorted signals in a random order were reproduced through headphones. The investigations were performed for frequencies of 250 Hz, 800 Hz and 2.5 kHz. Several measurement series, 10 signals each, were performed for each of the above frequencies.

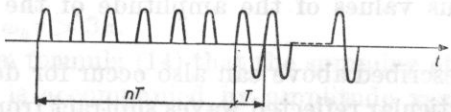

Fig. 2. An example of distorted simulated signal for subjective investigations of the evaluation of the audibility of changes in the signal shape (n is the number of periods of the distorted signal)

15 listeners participated in the investigations. Their task was to evaluate which of successive signals was regarded as distorted one. The audibility S, in %, was achieved from the ratio of the number of correct answers to the total number of signals offered for each frequency. The results, after ordering with respect to the number n of distorted periods, are shown in Fig. 3a.

Before the investigations the listeners underwent preliminary training in order to become generally accustomed to the kind of signals emitted.

It follows from Fig. 3a that the best audibility of distortions was obtained for low frequencies. For medium and, particularly, high frequencies high values of the audibility S occurred as the number of distorted periods increased. This results from the fact that the period of a signal decreases proportionally for higher frequencies, which signifies a decrease in the duration of distortions.

In order to verify in what way the audibility of distortions depends on their duration at different frequencies, the results in Fig. 3a were recalculated as a function of time and shown in Fig. 3b. These results show that the audibility of distortions involves different times necessary to recognize distortions of different frequency. This result differs from those of other psychoacoustic investigations, for example, in the case of perceiving echo, where the time needed for perceiving the phenomenon does not depend on frequency. It is interesting to note that recognition of distortions at a frequency of 2.5 kHz takes their duration of the order of 1-2 ms.

The method of subjective evaluation used in the present paper can provoke a number of objections, both to the principle of evaluation and the criteria of perceptibility used. An additional method which consisted in offering the lis-

tener pairs of signals was therefore used in the investigations. These pairs consisted either of a distorted signal and an undistorted one of different duration of distortions or of two undistorted signals, or of two signals distorted in the same way. The listeners' task was to evaluate which of the pairs of signals they regard as different.

The results obtained are shown in Fig. 3a, b in the form of ×, △ and ○. They show a character close to that of the results obtained using the previous method, which to a certain extent increases the reliability of evaluations made.

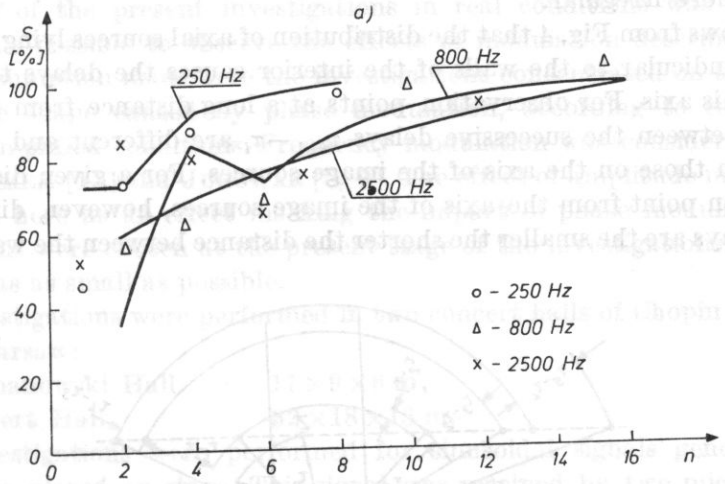

a) as a function of the number n of distorted periods

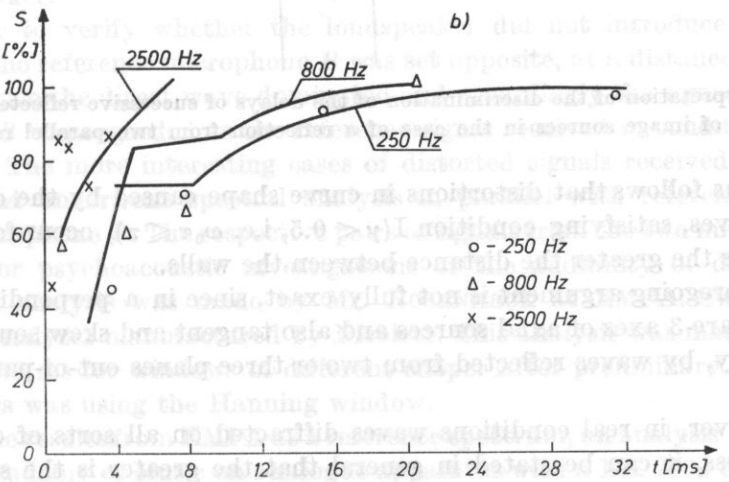

b) as a function of the duration of distortion

Fig. 3. The evaluation, in %, of the audibility S of distortions in a case of the simulated signal

4. Distortions in the shape of transient signals in real conditions

Condition (5) accepted in section 2 and regarding the same values of the delays τ of the signal and condition (4) assuming the equality of amplitudes are not satisfied in real conditions.

It is practically impossible to describe mathematically the distortions which occur then and it is only possible to make graphic analysis. It follows from this analysis that the effects of phase, frequency and amplitude modulation described for a simplified case also occur in real conditions although ther character is more irregular.

It follows from Fig. 4 that the distribution of axial sources lying on a straight line perpendicular to the walls of the interior causes the delays to be regular only on this axis. For observation points at a long distance from this axis differences between the successive delays $\tau_{i+1} - \tau_i$ are different and considerably lower than those on the axis of the image sources. For a given distance of the observation point from the axis of the image sources, however, differences between delays are the smaller the shorter the distance between the walls.

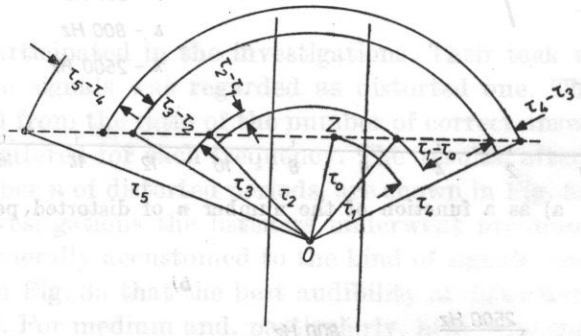

Fig. 4. Interpretation of the discrimination of the delays of successive reflected waves using the method of image sources in the case of a reflection from two parallel reflecting walls

It thus follows that distortions in curve shape caused by the delays of reflected waves, satisfying condition I($\gamma < 0.5$, i.e. $\omega_0 \tau \leqslant \pi$), occur for the lower frequencies the greater the distance between the walls.

The foregoing argument is not fully exact, since in a perpendicular-walled hall there are 3 axes of axial sources and also tangent and skew sources caused, respectively, by waves reflected from two or three planes out-of-parallel to one another.

Moreover, in real conditions waves diffracted on all sorts of edges occur. Nevertheless, it can be stated in general that the greater is the size of halls, the lower the frequency range in which the effect of distortions in the shape of the curve of the signal may occur when sound rises in the interior.

It follows from the analysis of the distribution of image sources that the

mean delay between successive signals can increase as the number of real sources increases or when soud-diffusing elements are introduced, which should cause an increase in the frequency at which distortions in the shape of the curve of the signal appear in a given hall. The above problem is the object of further investigations.

5. Experimental results

The aim of the present investigations in real conditions was to verify whether it was possible to observe the effects of modulation described above. Under the assumption made here the investigations concentrated on the distortion in curve shape caused by phase modulation, according to case I considered for simplified conditions. Frequency modulation was considered in the papers of OZIMEK [14] and JUGOWAR [8, 9]. The effect of amplitude modulation was regarded here as an effect masking the impact of phase modulation and such conditions were chosen at the present stage of the investigations, in which this effect was as small as possible.

The investigations were performed in two concert halls of Chopin Academy of Music, Warsaw:

I. Szymanowski Hall $17 \times 9 \times 6$ m,
II. Concert Hall $32 \times 18 \times 13$ m.

The investigations were performed for sinusoidal signals generated by a loudspeaker placed on stage. This signal was received by two microphones. The measurement microphone A was placed in the hall at a distance of 10 m from the loudspeaker.

In order to verify whether the loudspeaker did not introduce transient distortions, the reference microphone B was set opposite, at a distance of 0.5 m. At this distance the direct wave dominated and accordingly the signal from the microphone B was regarded as the reference signal received in conditions close to anechoic. The more interesting cases of distorted signals received from the microphone A underwent spectral analysis in parallel with reference signals from the microphone B. The respective pairs of signals from the two microphones were used for psychoacoustic investigations of the audibility of distortions.

Spectral analysis was made by Mr. ROSENHECK at EMPA, Switzerland, on an FFT analyzer manufactured by Nicolett. This analysis was made at time intervals of 40 ms for windows of different shape. After preliminary investigations analysis was using the Hanning window.

Using the results from EMPA as a reference spectrum, an analysis was made at Chopin Academy of Music on analogue apparatus with a BK 7502 digital register and a BK 2109 frequency analyzer. The block diagram of the measurement system for the signal A received from a long distance from the loudspeaker and for the signal B regarded as the reference signal is shown in Fig. 5 [18].

The changes in the signals A and B as a function of time obtained in Szymanowski Hall at a frequency of 180 Hz are shown in Fig. 6 for a time range of 160 ms calculated from the time of the arrival of the direct wave at the observation point. It follows from these curves that the duration of the distorted signal is relatively large, i.e. about 80 ms.

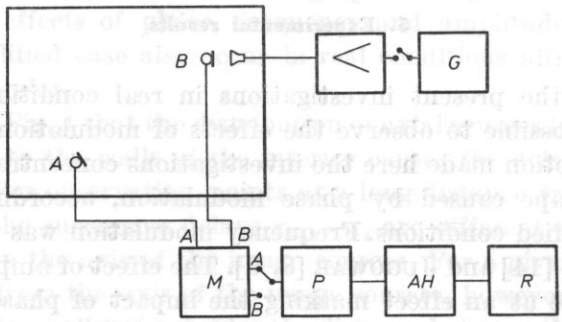

Fig. 5. A schematic diagram of the measurement system in the concert halls

A – the measuring microphone, B – the reference microphone, G – the generator of sinusoidal signals, M – a Nagra IV SJ tape recorder, P – digital memory, BK 7502, AH – heterodyne analyser, BK 2109, R – register, BK 2305

The results of the measurements of the frequency spectrum in the time ranges 0 - 40 ms, 40 - 80 ms and 80 - 120 ms for the signals A and B taken at EMPA are shown in Fig.7. The changes in the frequency spectrum of the same signals measured in the same ranges but obtained in the Academy of Music are shown in Fig. 8.

Comparison of changes in the frequency spectrum obtained using the two methods shows some differences which indicate the effect of measuring apparatus on the results. However, the general character of differences between the curves obtained from the measurement microphone A and the reference microphone B is similar. The differences between the spectra indicate a distinctly fuzzy frequency spectrum and the occurrence of an additional frequency in the time range 0-40 ms in the signal A, which are absent from the signal B. In the next time range 40-80 m the differences are smaller and disappear in the time range 80-120 ms.

This result indicates a distinct change in the frequency spectrum caused by quasi-nonlinear distortions in the first stage of the rise of the signal, which agrees with the behaviour of the signal observed in the time domain (Fig. 6).

Similar investigations were performed in the Concert Hall. In view of the larger size of the hall it was easier to obtain distortions in curve shape under consideration here for low frequencies of the order of 100-130 Hz. This frequency range has little practical significance, therefore the effect of distortion in curve shape was examined for slightly higher frequencies. In agreement with

predictions resulting from theoretical considerations, amplitude modulation dominated increasingly as the frequency of the signal increased. Nevertheless the effect of distortion in curve shape was very distinct for selected microphone positions in the frequency range up to 350 Hz.

Examples of signals obtained from the microphones A and B for a frequency of 340 Hz are shown in Fig. 9; their frequency spectra obtained in the Academy of Music, Warsaw, in Fig. 10.

As in the case of the measurements in Szymanowski Hall, the duration of the distorted signal was about 80 ms. The changes in the frequency spectrum measured in 40 ms time ranges show, as previously, greatest differences between the signals A and B in the first stage of sound rise in the interior.

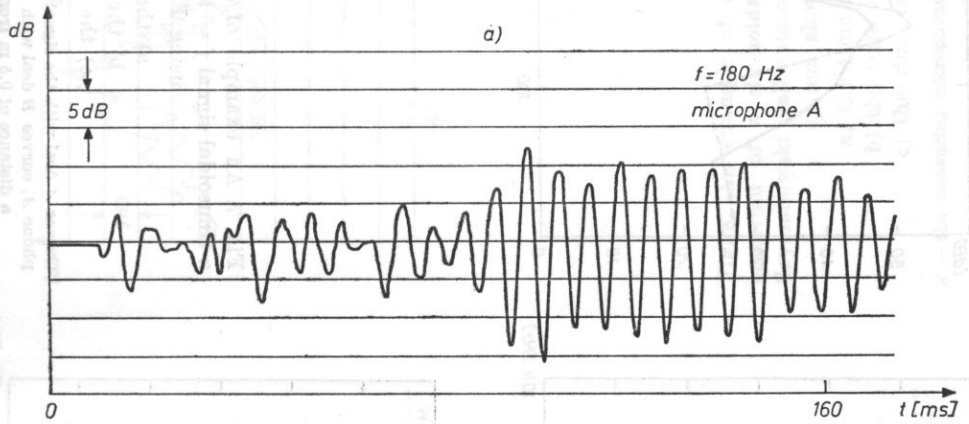

a) the measuring microphone A

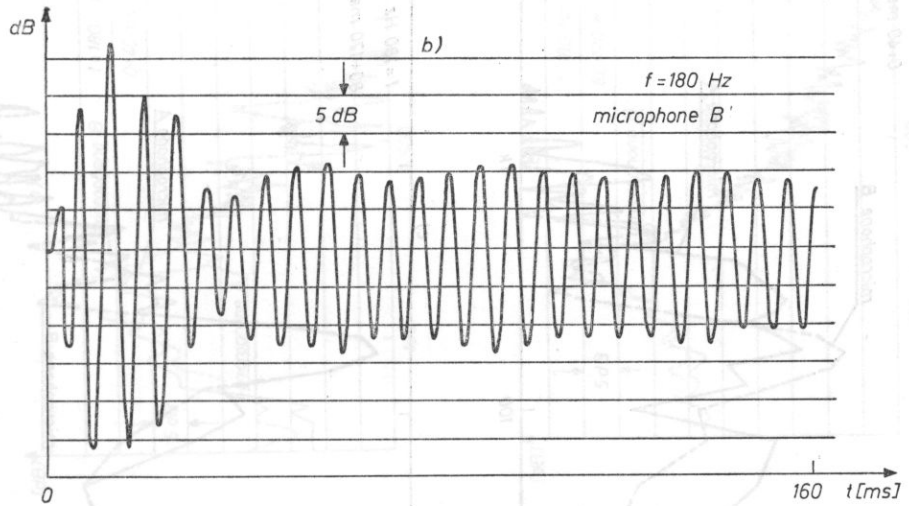

b) the reference microphone B

Fig. 6. An example of the rise of a sinusoidal signal of the frequency $f = 180$ Hz in Szymanowski Hall in Chopin Academy of Music, Warsaw

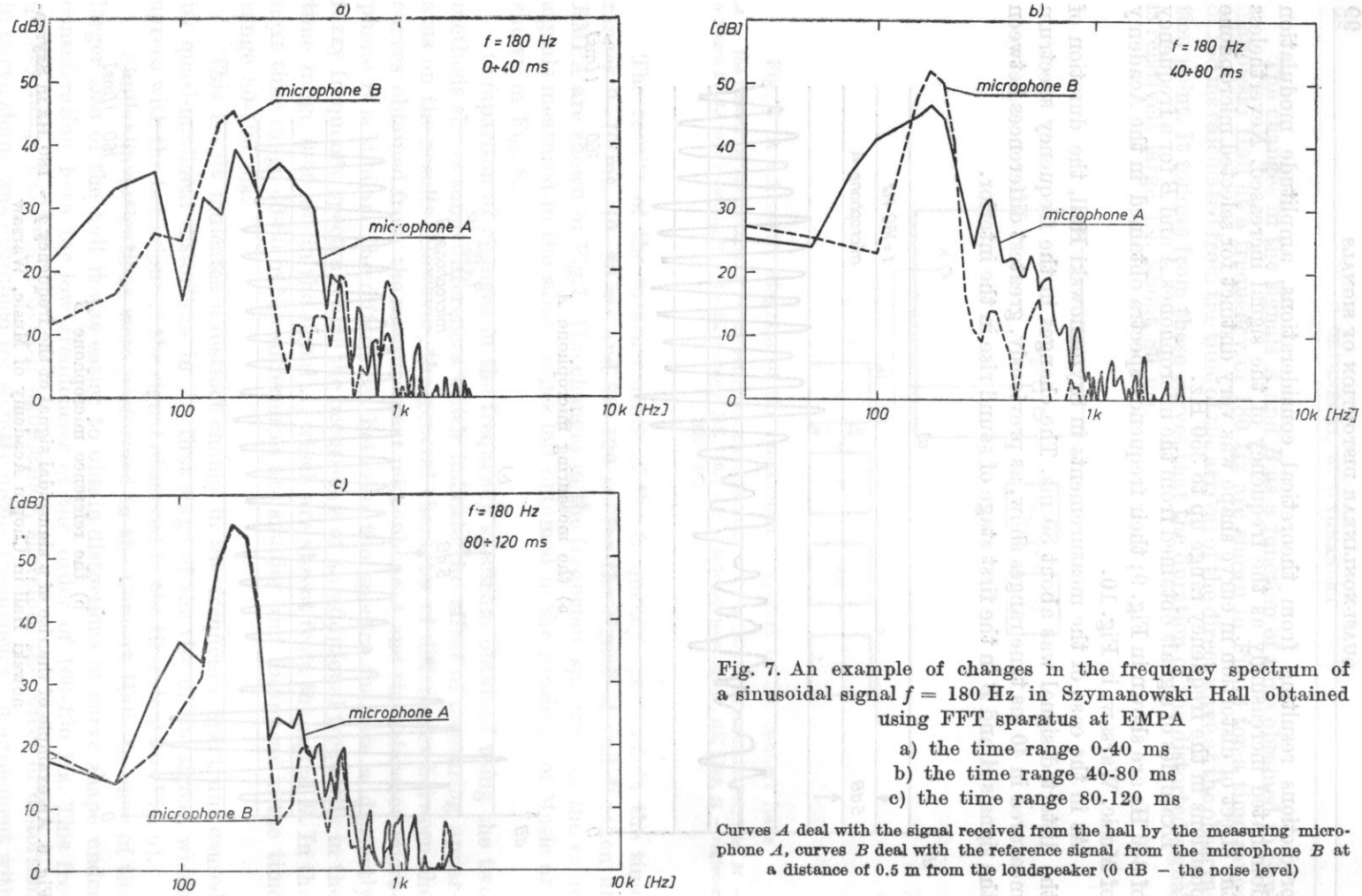

Fig. 7. An example of changes in the frequency spectrum of a sinusoidal signal $f = 180$ Hz in Szymanowski Hall obtained using FFT sparatus at EMPA

a) the time range 0-40 ms
b) the time range 40-80 ms
c) the time range 80-120 ms

Curves *A* deal with the signal received from the hall by the measuring microphone *A*, curves *B* deal with the reference signal from the microphone *B* at a distance of 0.5 m from the loudspeaker (0 dB – the noise level)

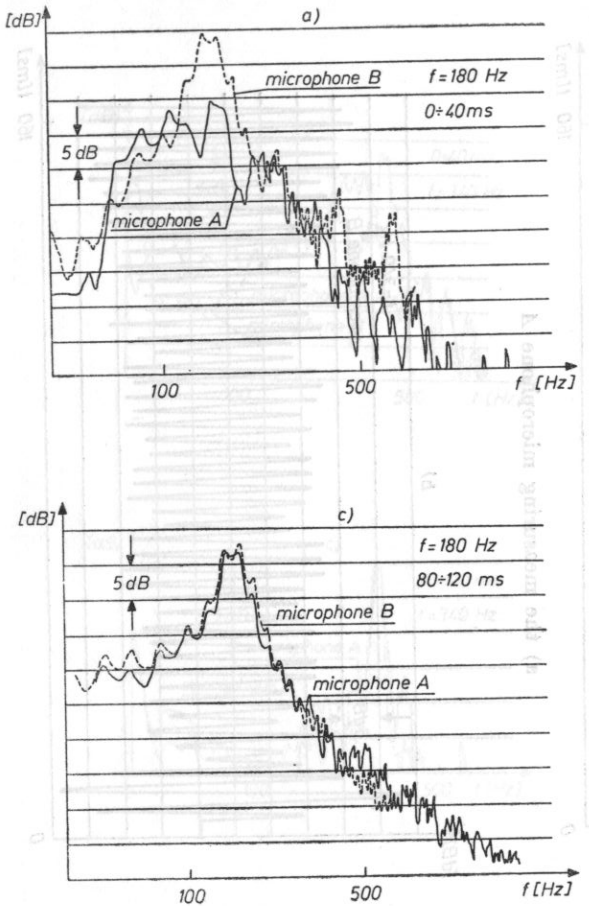

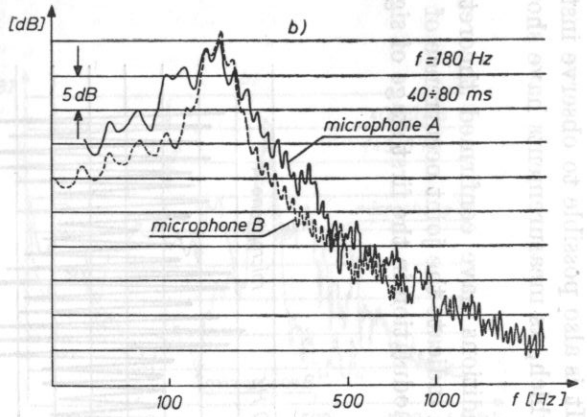

Fig. 8. An example of changes in the frequency spectrum of a sinusoidal signal $f = 180$ Hz in Szymanowski Hall obtained using the measurement system shown in Fig. 5

a) the time range 0-40 ms
b) the time range 40-80 ms
c) the time range 80-120 ms

A – the measuring microphone, B – the reference microphone

Observations of the signals A in the time domain (Figs. 7 and 9) have shown an irregularity in the time ranges of zero crossings of the signal, indicating instantaneous frequency changes, similar to frequency modulations, in the resultant signal in the first stage of its rise. It is also possible to observe instantaneous amplitude changes in the signal which, as measurements have shown, are much more distinct at high frequencies.

The measurements taken in real conditions have confirmed theoretical considerations for the simplified case which indicate the joint occurrence of the effects of phase, frequency and amplitude modulation in the first stage of signal rise in the interior.

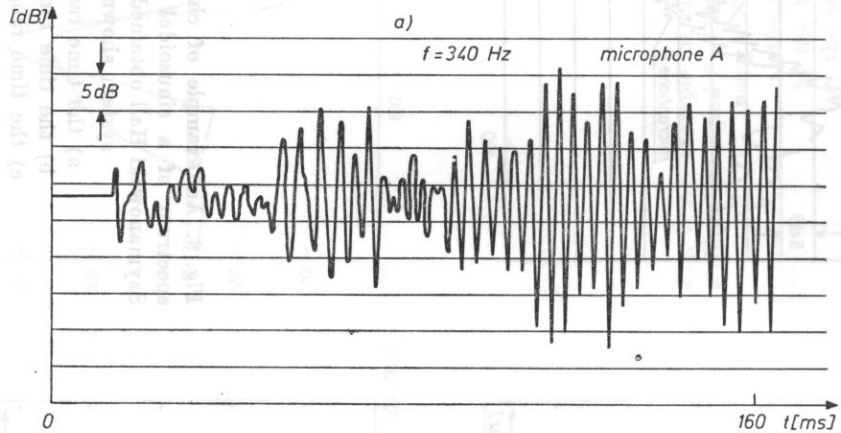

a) the measuring microphone A

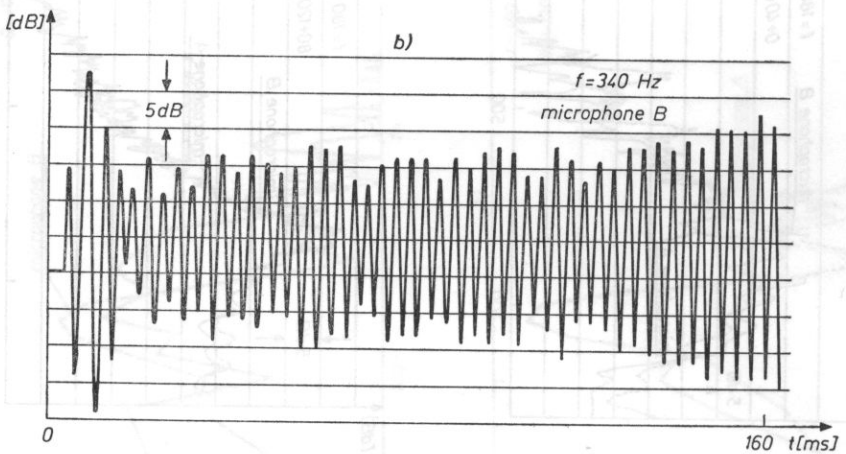

b) the reference microphone B

Fig. 9. An example of the rise of a sinusoidal signal at a frequency of 340 Mz in the Concert Hall of Chopin Academy of Music, Warsaw

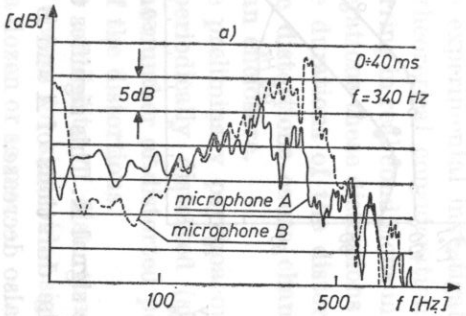

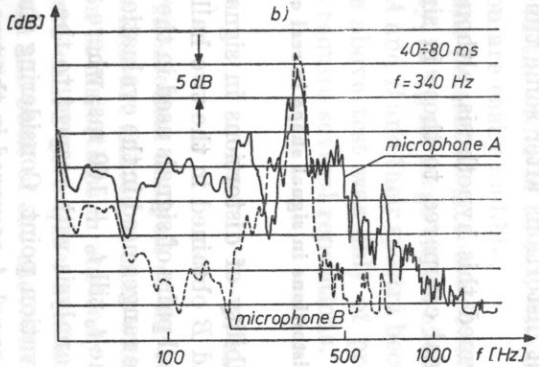

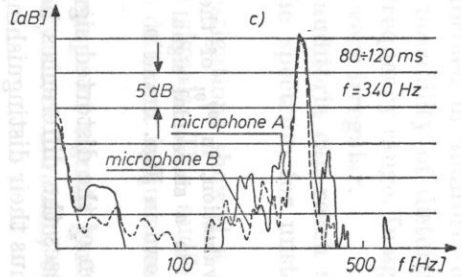

Fig. 10. An example of changes in the frequency spectrum of a sinusoidal signal at a frequency of 340 Hz in the Concert Hall obtained using the narrow-band analysis

a) the time range 0-40 ms
b) the time range 40-80 ms
c) the time range 80-120 ms

curves *A* deal with signals received by the measuring microphone, curves *B* with signals received by the reference microphone

The qualitative evaluation of the phenomena in real conditions performed in section 4 showed that the distortions are irregular and disappear after some time.

In practice, auditoria involve more complex signals, such as signals of speech and music. Naturally their character changes in time and accordingly one should not expect decay of the present distortions after some time in the process of sound rise in the interior.

The pilot results obtained have confirmed this hypothesis, although they have indicated smaller changes in the signal compared to those in sinusoidal signals.

6. Psychoacoustic evaluation of the audibility of distortions in signal shape in real conditions

Psychoacoustic evaluation of the audibility of distortions in signal shape was performed on pairs of the signals A and B obtained in the two halls which are shown in Figs. 6 and 9. The duration of all pairs of signals used in the evaluation was constant, i.e. 160 ms. Only the time ranges used in the evaluation of the pairs of signals were changed, from the time t_0 till $t_0 + 160$ ms, where t_0 is the delay of the onset of the signal chosen for analysis with respect to the time of the arrival of the direct wave at the observation point. Considering that most distinct distortions in the signal from the channel A occurred in the two halls in the time range of about 0-80 m, a change in the time t_0 involved a change

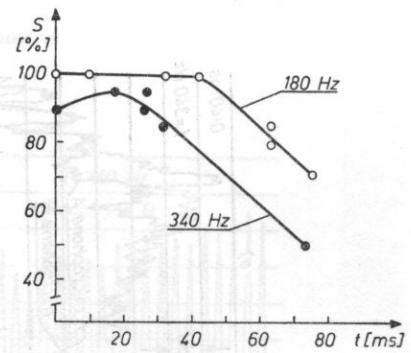

Fig. 11. The evaluation, in %, of the audibility S of distortions in a sinusoidal signal for signals shown in Figs. 6 and 9

in the duration of the distorted signal in the signal A. This signifies that as the time t_0 increases the differences between the durations of A and B should decrease; and thus their distinguishing should also decrease.

In the present psychoacoustic investigations the gaps between the signals within one pair compared were 1 s, while the pauses between pairs were about 5 s. The test consisted of 10 pairs for each hall and was estimated by 20 listeners, The order of selection of each pair was random.

The results of the evaluation are shown in Fig. 11. They indicate a very

high audibility close to 100 % of the differences between particular pairs of signals when the time $t_0 = 0$, i.e. in the time ranges chosen for evaluation the whole distorted fragments were within the signal A. As the time t_0 increased, i.e. as the distorted fragment became shorter, the distinguishing of signals fell but only after the time t_0 of the order of 40 ms, reaching a value of 70 % for the times t_0 of the order of 60 ms, which signifies that relatively short durations of distortion are easily audible.

At the present stage some doubt may arise from the excessive values of the audibility, in %, for large values of the time t_0 after which differences between the signals A and B and their spectra become much less distinct.

The above test was only of preliminary character and quantitative conclusions require several repetitions.

7. Conclusions

1. Theoretical analysis of the summing of sinusoidal signals with different phases which are shifted in time with respect to each other permits simple interpretation of distortions in unsteady state of sound in an enclosure. These distortions were called here quasi-nonlinear distortions.

2. On the basis of the theoretical considerations it is possible to determine in the simplified case which predetermines a constant value of the delay between successive signals the ranges in which distortions in signal shape caused by phase, frequency and amplitude modulations, respectively, dominate.

3. The experimental investigations performed in auditoria confirmed the results of theoretical considerations of the possibility of distortions in curve shape occurring in real conditions in the low frequency range. In agreement with the considerations these distortions are then very irregular.

4. The durations of the distortions in auditoria can reach several scores of ms. The distortions cause changes in the spectrum for unsteady state of signals in an enclosure.

5. The preliminary psychoacoustic investigations showed a distinct audibility of periodically distorted (simulated) signals. This audibility depends more on the number of distorted periods (at different frequencies) than on the duration of the distortions.

6. The audibility of distortion in the shape of signals generated in real conditions occurs for sinusoidal signals of very short duration, of the order of several to a dozen or so ms.

7. At the present stage it is difficult to evaluate the influence of distortions considered on the evaluation of the signals of speech and music quality in enclosures. Therefore the further investigations will follow in the three directions:

— analysis of factors increasing the effect of the distortions considered in this paper,

— investigation of the effect of the interior and its parameters on the distortions,

— psychoacoustic investigations of the effect of the distortions on the audibility of changes in the sound of speech and music signals.

References

[1] L.L. BERANEK, *Music, acoustics and architecture*, J. Wiley, New York 1962.

[2] S. CZARNECKI, *Analyse spectrale des ondes acoustiques en regime transitoire dans une chambre close*, Acustica, **8** (1958).

[3] S. CZARNECKI, M. VOGT, *Investigations of the effect of the interior on changes in transient acoustic behaviours* (in Polish), Archiwum Akustyki, **2**, 4, 313-322 (1967).

[4] S. CZARNECKI, B. OSIECKI, W. WYGNAŃSKI, *Quasi-nonlinear transient distortions in interiors and their preliminary subjective evaluation* (in Polish), Proc. XXVI Seminar on Acoustics, Wrocław – Oleśnica 1979.

[5] I.S. GRADSTEJN, I.M. RYZHIK, *Tablitsy integralov summ, riadov i proizvedenij*, Izd. Nauka, Moskwa 1971.

[6] H. HAAS, *Über den Einfluss eines Einfachechos auf die Hörsamkeit von Sprache*, Acustica, **1**, 49-58 (1951).

[7] V.L. JORDAN, *Acoustical design of concert halls and theatres*, Applied Science Publishers Ltd, London 1980.

[8] L. JUGOWAR, *Method of analysis of dynamic phase and frequency changes in transient sound* (in Polish), Proc. XXV Seminar on Acoustics, Poznań 1978.

[9] L. JUGOWAR, *Analysis of frequency changes in transient sound propagating in enclosure* (in Polish), doct. diss., Poznań 1980.

[10] A. KARCZEWSKA-NABELEK *Irregularities of sound decay for pure tones*, Proceedings of 4th Conference on Acoustics, Budapest 1967.

[11] E. MEYER, W. BURGTORF, *Über die Zeitabhängigkeit der Schallrichtungsverteilung in Räumen bei impulsartigen Anregung*, Acustica (A, B), 313 (1957).

[12] B.S. MISZCZAK, *Reflection distortions in enclosure* (in Polish), Zesz. Nauk. COBRIT, 1977.

[13] H. NIESE, *Vorschlag für die Definition und Messung der Deutlichkeit nach subiektiven Grundlagen*, Hochfrequenztechnik und Elektroakustik, **65**, 4 (1956).

[14] E. OZIMEK, *Deformation of the frequency spectra of sound propagating in enclosure*, The 13th Conference on Acoustics "Room and Building Acoustics", Tatranská Lomnica, 1975.

[15] W. STRASZEWICZ, *Geometrical analysis of the properties of the acoustic field in closed space* (in Polish), Prace Naukowe Politechniki Warszawskiej, Elektronika nr 11, Wyd. Polit. Warszawskiej 1974.

[16] R. THIELE, *Richtungsverteilung und Zeitfolge der Schallrückwurfe in Räumen*, Acustica (A, B), 291 (1953).

[17] W. WYGNAŃSKI, *Audibility of simulated transient non-linear distortion*, The 65th Convention AES, London, 25-28 February, 1980.

[18] W. WYGNAŃSKI, *Transient nonlinear distortion-duration and structure components*, The 66th Convention AES, Hamburg, 17-20 March, 1981.

[19] E. ZWICKER, *Subjektivc und objektive Dauer von Schallimpulsen und Schallpausen*, Acustica, **22**, 214 (1969/70).

Received on September 1, 1981; revised version on February 11, 1982

ARCHIVES OF ACOUSTICS
7, 2, 107-118 (1982)

PROPAGATION OF NOISE GENERATED BY SINGLE MOVING SOURCES IN OPEN AREA

J. JARZĘCKI, R. MAKAREWICZ

Institute of Acoustics, Mickiewicz University
(60-769 Poznań, ul. Matejki 48/49)

The sound level (L) of noise generated by a single moving source (e.g. vehicle) is a starting point for the determination of the resultant level of noise emitted by sets of moving sources (e.g. streams of vehicles). The aim of the investigations was to find the relations among L, the motion velocity and the distance of the observation point from the source for different weather conditions. The investigations were performed in a flat area covered with concrete and grass, taking into consideration two basic vehicle types: light and heavy. Logarithmic-and-linear relations between these quantities have been obtained.

1. Introduction

The major sources of urban noise are moving sources, i.e. means of transport, and, in particular, vehicles. Noise (assessed by means of so-called noise indexes) affects the quality of the environment of man from the acoustic viewpoint. The shaping of the environment so that the indexes of noise do not exceed some predetermined values is the object of environmental acoustics. This aim can be achieved when the acoustic field generated by single sources is known (since it is then possible to predict the values of the indexes of noise emitted by sets of these sources, i.e. streams of vehicles etc.).

The aim of the investigations was to find the dependence of the sound level L of noise on the distance and on the velocity of a single noise source. Two kinds of noise sources were considered: light vehicles (passenger cars) and heavy vehicles (lorries and buses). The measurements were made in a flat area covered with grass and concrete, typical for modern urban area. The present problem

This paper was written under the programme "Model investigations of acoustic parameters of urban systems" PR-5 coordinated by the Institute of Building Technology, Warsaw.

has been the object of investigations of many authors [1 - 4, 6 - 9]. The source of urban noise, traffic, is, however, different in each country. This fact was the reason why this problem was raised anew, the more so that the effect of weather conditions has not always been considered in other authors' papers.

This paper is a contribution to the development of methodology for predicting the acoustic climate in the vicinity of highways.

2. The dependence of the sound level on the distance

In a flat area of homogeneous cover and for the distance of the source from the observation point of the order of a dozen or so metres the pressure of noise generated by a single source is a monotonously decreasing function of the distance d (Figs. 1 and 2). In the literature the following two functions approximating this relation can be met most frequently,

$$p^2 = \frac{W \exp(-\alpha d)}{d^2}, \tag{1}$$

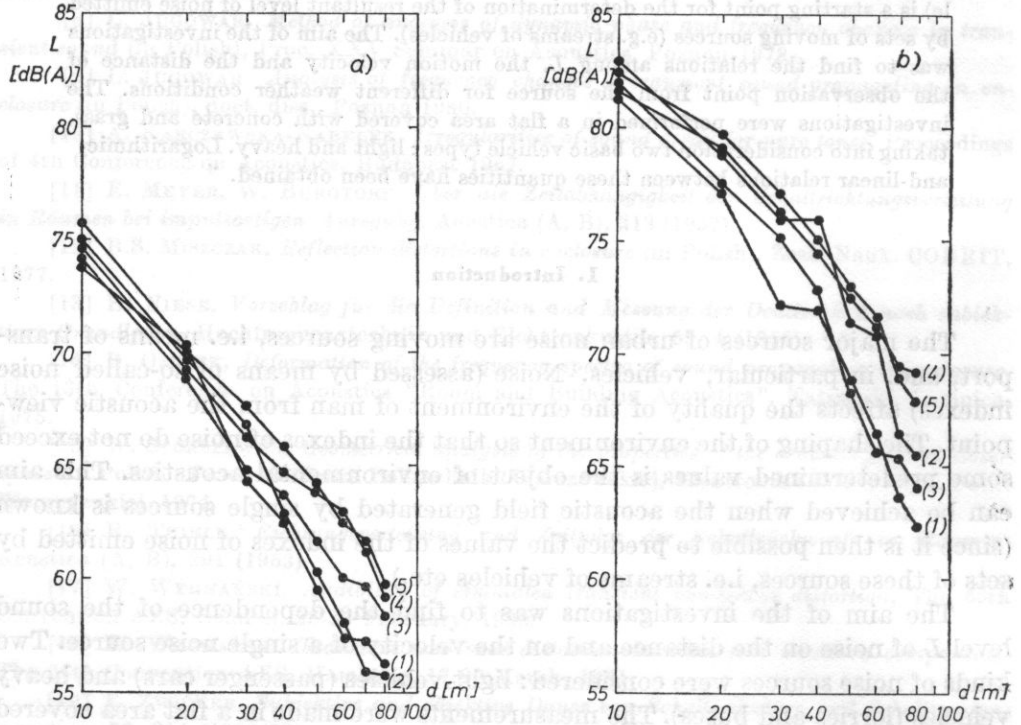

Fig. 1. The dependence of the sound level of noise generated by a single light (a) and heavy (b) vehicle on the distance d

the surface was covered with concrete, the number of measurement series corresponding to the weather conditions described in Fig. 5 is given in brackets

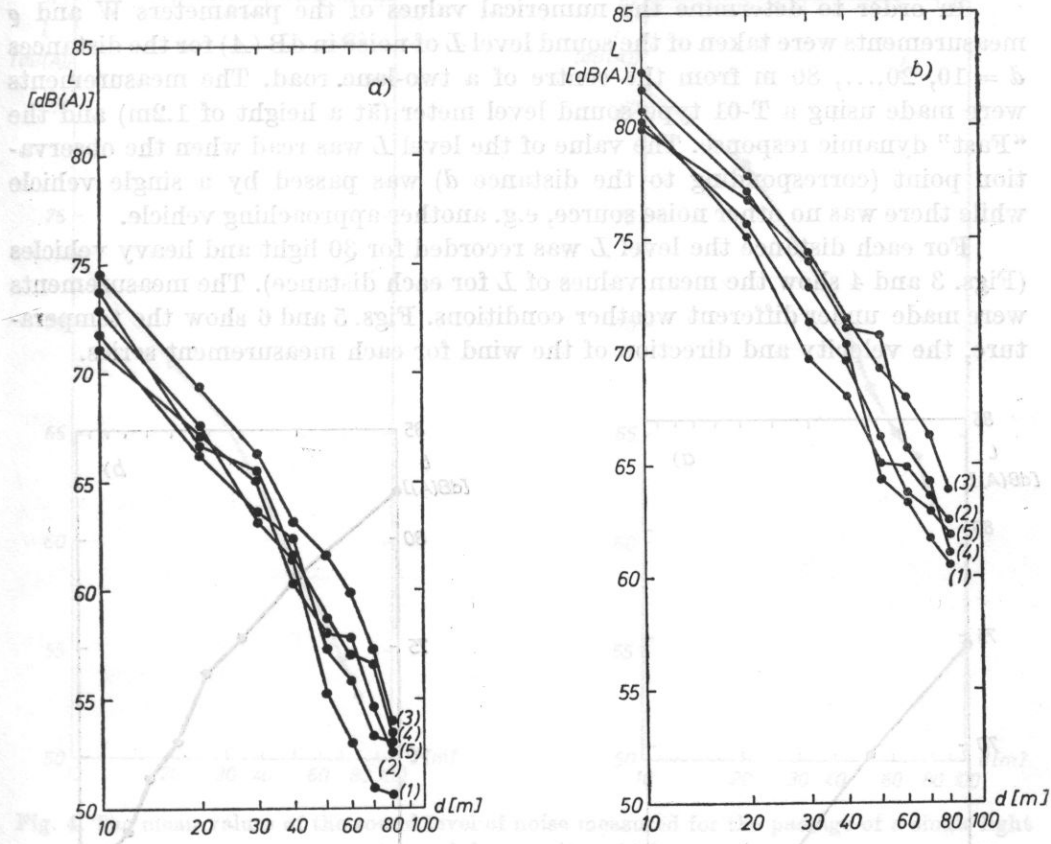

Fig. 2. The dependence of the sound level of noise generated by a single light (a) and heavy (b) vehicle on the distance d

the surface was covered with grass, the number of measurement series corresponding to the weather conditions described in Fig. 6 is given in brackets

where α is the coefficient of attenuation in air, and

$$p^2 = \frac{W}{d^\varrho}, \tag{2}$$

where W and ϱ are parameters describing the source and processes accompanying propagation. Function (1) involves the attenuation quantity expressed in dB per unit length, e.g. dB/m. According to relation (2), the attenuation is expressed as "level decrease per double distance". Paper [5] showed that if attenuation (for double distance) exceeds 8 dB, both functions approximate equally well the curves in Figs. 1 and 2. In the case of less attenuation (e.g. when noise propagates over a concrete-covered surface) much better approximation can be achieved using function (2). The further part of the present paper uses this relation.

In order to determine the numerical values of the parameters W and ϱ measurements were taken of the sound level L of noise in dB (A) for the distances $d = 10, 20, \ldots, 80$ m from the centre of a two-lane road. The measurements were made using a T-01 type sound level meter (at a height of 1.2m) and the "Fast" dynamic response. The value of the level L was read when the observation point (corresponding to the distance d) was passed by a single vehicle while there was no other noise source, e.g. another approaching vehicle.

For each distance the level L was recorded for 30 light and heavy vehicles (Figs. 3 and 4 show the mean values of L for each distance). The measurements were made under different weather conditions. Figs. 5 and 6 show the temperature, the velocity and direction of the wind for each measurement series.

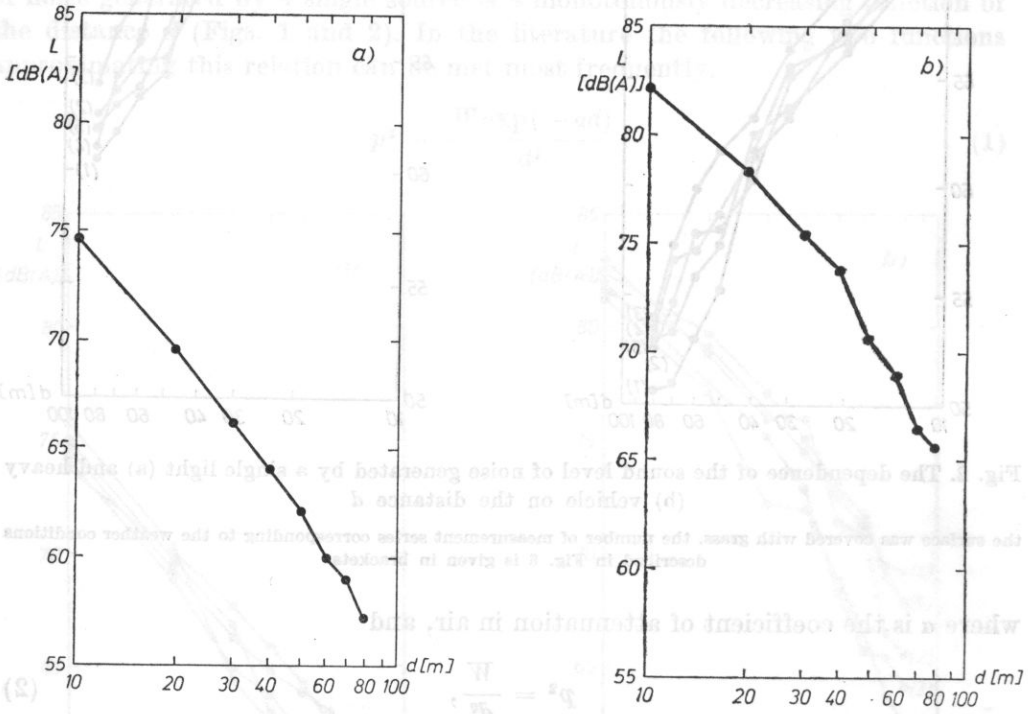

Fig. 3. The mean values of the sound level of noise measured for the passage of a single light (a) and heavy (b) vehicle
the surface was covered with concrete

It follows from the measurement results shown here that weather conditions do not clearly affect the values of the sound level. It is, for example, difficult to say whether a decrease on the sound level with increasing distance is slower or faster as the temperature decreases. This probably results from a too small number of measurements or from neglecting other parameters, essential in acoustic wave propagation, describing the weather conditions (e.g. the tempera-

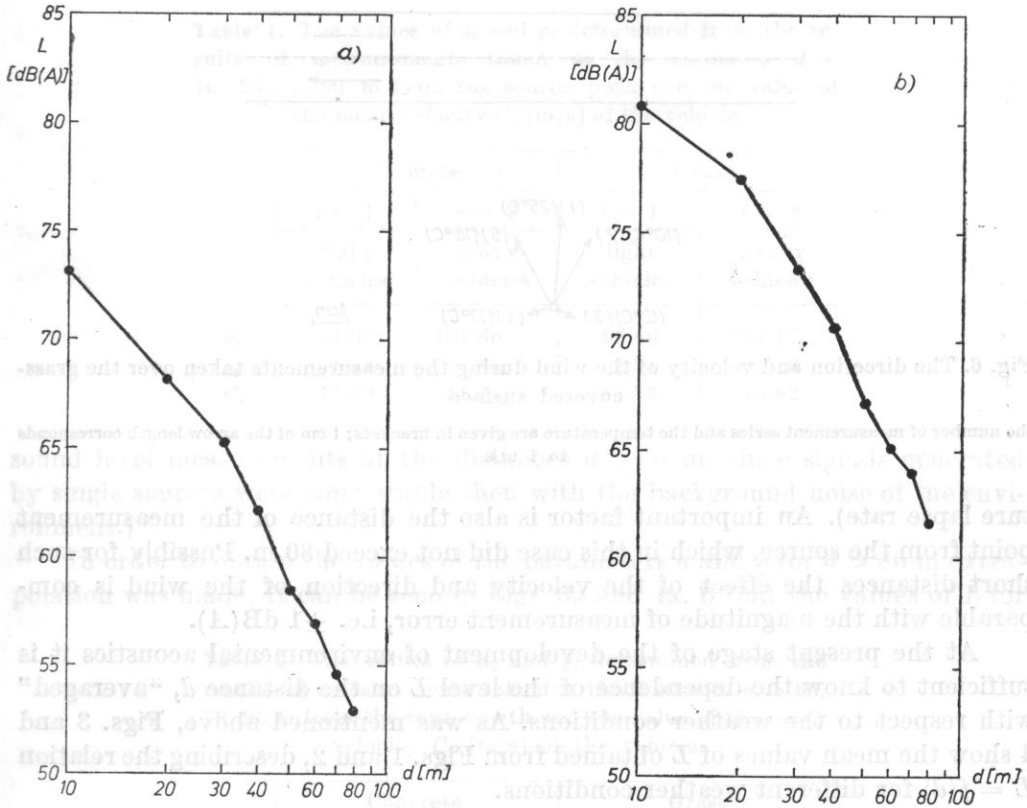

Fig. 4. The mean values of the sound level of noise measured for the passage of a single light (a) and heavy (b) vehicle

the surface was covered with grass

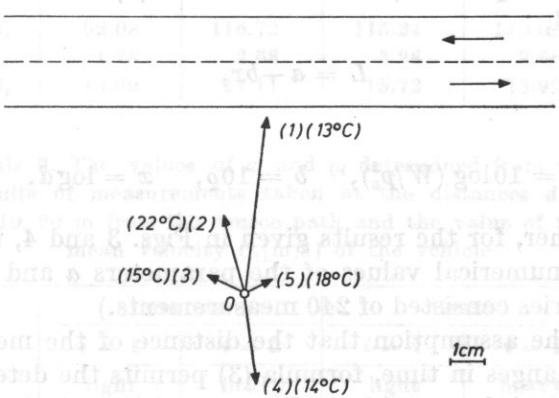

Fig. 5. The direction and velocity of the wind during the measurements taken over the concrete-covered surface

the number of measurement series and the temperature are given in brackets; 1 cm of the arrow length corresponds to 1 m/s

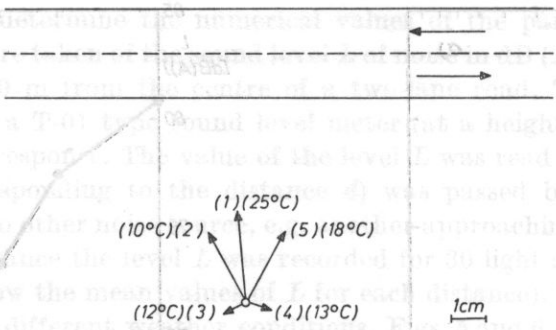

Fig. 6. The direction and velocity of the wind during the measurements taken over the grass-covered surface

the number of measurement series and the temperature are given in brackets; 1 cm of the arrow length corresponds to 1 m/s

ture lapse rate). An important factor is also the distance of the measurement point from the source, which in this case did not exceed 80 m. Possibly for such short distances the effect of the velocity and direction of the wind is comparable with the magnitude of measurement error, i.e. ± 1 dB(A).

At the present stage of the development of environmental acoustics it is sufficient to know the dependence of the level L on the distance d, "averaged" with respect to the weather conditions. As was mentioned above, Figs. 3 and 4 show the mean values of L obtained from Figs. 1 and 2, describing the relation $L = f(d)$ for different weather conditions.

From the definition of the level L

$$L = 10\log(p^2/p_0^2)$$

(p_0 being the reference pressure) and from formula (2) the following linear equation can be derived,

$$L = a - bx, \tag{3}$$

where

$$a = 10\log(W/p_0^2), \quad b = 10\varrho, \quad x = \log d. \tag{4}$$

Applying further, for the results given in Figs. 3 and 4, the linear regression analysis, the numerical values of the parameters a and ϱ were obtained (Table 1). (Each series consisted of 240 measurements.)

Thus, under the assumption that the distance of the measurement point from the source changes in time, formula (3) permits the determination of the instantaneous value of the sound level L generated by a single source, under the condition, however, that the source is at the distance $d < 80$ m from the observation point. Problems related to town planning require knowledge of L for longer distances. (It is necessary to explain that it was impossible to take

Table 1. The values of a_i and ϱ_i determined from the results of measurements taken at the distances $d = 10, 20, \ldots, 80$ m from the source path and the value of the mean velocity C_i [m/s] of the vehicle

	Concrete		Grass	
	$i = 1$	$i = 2$	$i = 1$	$i = 2$
	light vehicles	heavy vehicles	light vehicles	heavy vehicles
a_i	94.02	101.66	96.49	104.17
ϱ_i	1.89	1.83	2.24	2.18
C_i	13.69	11.11	15.72	13.92

sound level measurements at the distances $d > 80$ m, since signals generated by single sources were comparable then with the background noise of the environment.)

In order to obtain the values of the parameters a and ϱ for $d > 80$ m extrapolation was made. It can be seen in Figs. 3a and 4a, b that the values of L for

Table 2. The values of a_i and ϱ_i determined from the results of measurements taken at the distances $d = 60, 70, 80$ m from the source path and the value of the mean velocity C_i [m/s] of the vehicle

	Concrete		Grass	
	$i = 1$	$i = 2$	$i = 1$	$i = 2$
	light vehicles	heavy vehicles	light vehicles	heavy vehicles
a_i	92.08	116.72	115.24	110.60
ϱ_i	1.78	2.68	3.28	2.56
C_i	13.69	11.11	15.72	13.92

Table 3. The values of a_i and ϱ_i determined from the results of measurements taken at the distances $d = 10, 20$ m from the source path and the value of the mean velocity C_i[m/s] of the vehicle

	Concrete		Grass	
	$i = 1$	$i = 2$	$i = 1$	$i = 2$
	light vehicles	heavy vehicles	light vehicles	heavy vehicles
a_i	91.22	93.77	91.69	94.18
ϱ_i	1.64	1.17	1.86	1.32
C_i	13.69	11.11	15.72	13.92

$d = 60$, 70 and 80 m decrease faster than those for shorter distances. The results of other authors, e.g. COOK and VAN HAVERBECKE [1] show that this tendency should also sustain for $d > 80$ m. The linear regression analysis performed for the last three points leads to other values of a and ϱ (Table 2). Table 3 gives the parameters a and ϱ for the distances $d = 10$, 20 m. (These are useful, for example, in determining the level of noise near the edge of the road.)

In the course of measurements in an area covered with concrete (Fig. 3) and grass (Fig. 4) the mean velocities of light and heavy vehicles were, respectively, $C_1 = 13.69$ m/s, $C_2 = 11.11$ m/s and $C_1 = 15.72$ m/s, $C_2 = 13.92$ m/s.

3. The dependence of the sound level on the traffic velocity

Each highway is characterized among other things, by the traffic velocity V. In order to obtain quantitative information on the dependence of the sound level L dB (A) on the velocity of the source V, measurements were made at the distance $d_0 = 7.5$ m from the centre of the lane. As in the case of investigations aimed at determining L as a function of d (section 2), also in this case the sound level L was registered when a single source was "passing" the observation point. Each time its velocity V [m/s] was registered. The results are given in Figs. 7 and 8.

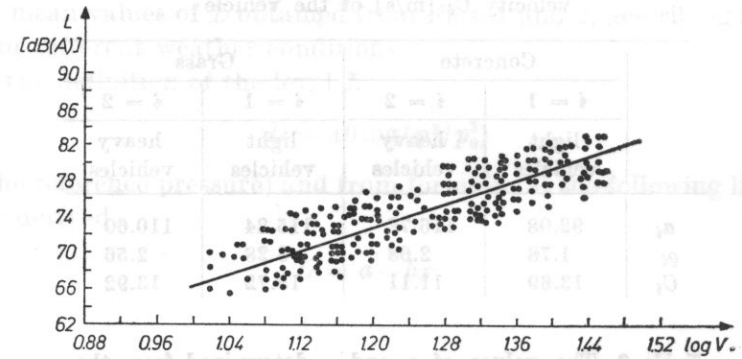

Fig. 7. The dependence of the sound level L, in dB (A), on the velocity V for light vehicles; $L = 34.0 \log V + 32.0$; $r = 0.93$ is the correlation coefficient

It was assumed for analytical description of the dependence of the level L on V that the parameter W (2) is the following function of the velocity

$$W = W_0 V^m. \tag{5}$$

Since the measurements were made at the distance $d_0 = 7.5$ m from the centre of the traffic lane, at the moment of "passing", the microphone was in the near field of the noise source (vehicle). In this case the simple dependence of the pressure on the distance, which is valid for the far field, $p^2 \sim d^{-\varrho}$ (formula

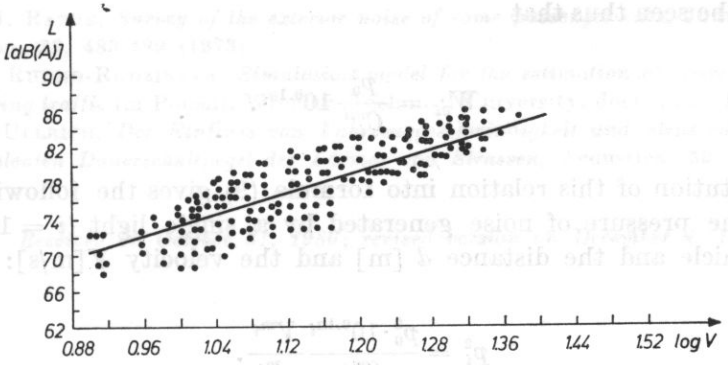

Fig. 8. The dependence of the sound level L, in dB (A), on the velocity V for heavy vehicles; $L = 29.0 \log V + 44.4$; $r = 0.84$ is the correlation coefficient

(2)) should be replaced with a more general one, $f(d)$. Finally, for $d = d_0$ this formula can be rewritten in the form

$$p^2 = W_0 V^m f(d_0). \tag{6}$$

(The explicit form of the function $f(d)$ is not important now.)

Using the definition of the level $L = 10 \log (p^2/p_0^2)$,

$$L = A + Bx', \tag{7}$$

where

$$A = 10 \log W_0 f(d_0)/p_0^2, \quad B = 10m, \quad x = \log V. \tag{8}$$

From the regression analysis for the results in Figs. 7 and 8, $m_1 = 3.4$ was obtained for light vehicles and $m_2 = 2.9$ for heavy ones. There is disagreement among the results obtained by other authors. This is caused by the differences in the set of vehicles (noise sources).

4. Conclusions

It follows from formulae (2) and (5) that if the observation point is at a distance of at least a dozen or so metres from the centre of the traffic lane,

$$p^2 = \frac{W_0 V^m}{d^\varrho}. \tag{9}$$

As was mentioned in section 2, the values of ϱ_i and $a_i = 10 \log (W_i/p_0^2)$ were obtained for the mean velocity C_i (Tables 1 and 2). It can be derived further from formula (5) that

$$a_i = 10 \log (W_{0i} C_i^m i/p_0^2).$$

It can be seen thus that

$$W_{0i} = \frac{p_0^2}{C_i^{mi}} 10^{0.1a_i}. \tag{10}$$

Substitution of this relation into formula (9) gives the following relation between the pressure of noise generated by a single light ($i = 1$) or heavy ($i = 2$) vehicle and the distance d [m] and the velocity V[m/s]:

$$p_i^2 = \frac{p_0^2 \cdot 10^{0.1a_i}}{C_i^{m_i}} \frac{V^{m_i}}{d^{\varrho_i}}. \tag{11}$$

The numerical values of the parameters a_i, ϱ_i, C_i are given in Tables 1-3, while $m_1 = 3.4$, $m_2 = 2.9$. From the definition $L = 10 \log(p^2/p_0^2)$,

$$L_i(t) = a_i - 10\varrho_i \log d(t) + 10\, m_i \log(V/C_i), \qquad i = 1, 2. \tag{12}$$

This formula makes it possible to determine the value of the sound level in dB (A) of noise generated by a single source (vehicle) moving at the velocity V constant in time, when its distance from the observation point is d at the time t. In view of the dependence of a_i and ϱ_i on wind velocity, its direction, air temperature, etc., equation (12) gives the relation $L_i(t) = f\{d(t), V\}$ for different weather conditions. The set of the values of a_i and ϱ_i given in this paper is at present complemented with the measurements of noise generated by single vehicles for the different weather conditions.

Acknowledgment. The authors wish to express their gratitude to J. TOMASZEWSKI, MSc., for taking part of the measurements and to Prof. Dr H. RYFFERT for assistance in preparation of this paper.

References

[1] D.I. COOK, D.F. VAN HAVERBECKE, *Trees and shrubs for noise abatement*, U.S. Department of Agriculture, Washington D.C., Research Bulletin, No 246 (1971).

[2] R.K. HILLQUIST, W.N. SCOTT, *Motor vehicle noise spectra*, JASA, **58**, 2-10 (1975).

[3] H.G. JONASSON, *The accuracy of traffic noise prediction*, Department of Build. Acoustics, Lund Institute of Technology, Lund, A41 (1975).

[4] P.T. LEWIS, *The noise generated by single vehicle in freely flowing traffic*, Journal of Sound and Vibration, **30**, 191-206 (1973).

[5] R. MAKAREWICZ, *The relationship between the noise emitted by a single source and the distance in open space*, Acoustics Letters, **3**, 112-114 (1979).

[6] N. OLSON, *Survey of motor vehicle noise*, JASA, **52**, 1291-1306 (1972).

[7] E.J. RATHE, *Survey of the exterior noise of some passenger cars*, Journal of Sound and Vibration, **29**, 483-499 (1973).

[8] B. RUDNO-RUDZIŃSKA, *Simulation model for the estimation of noise from vehicles in freely flowing traffic* (in Polish), Wrocław Technical University, doct. diss., 1981.

[9] S. ULLRICH, *Der Einfluss von Fahrzeuggeschwindigkeit und Strassenbelag auf den energieäquivalenten Dauerschallpegel des Lärmes von Strassen*, Acoustica, **30**, 90-99 (1974).

Received on October 31, 1980; revised version on December 4, 1981.

ARCHIVES OF ACOUSTICS
7, 2, 119-142 (1982)

INVESTIGATION OF THE WAVEGUIDE PROPERTIES OF A BOREHOLE AND THEIR USE FOR ACOUSTIC MEASUREMENTS IN SITU

ANNA JAROSZEWSKA

Institute of Fundamental Technological Research, Polish Academy of Sciences
(00-049 Warszawa, ul. Świętokrzyska 21)

A method of measurement of the velocity of a shear wave travelling in the vicinity of a borehole, using its waveguide properties, is both analyzed and verified. In particular, by this method, the shear wave velocity is determined from the velocity of the so-called tube wave which corresponds to the zero frequency limit of the lowest radial mode of propagation in the fluid filling the borehole. Investigations of the necessary conditions to obtain a tube wave and of its propagation were performed on a laboratory model of a borehole and in boreholes in situ. The results obtained show the possibility of a practical use of the method investigated for the determination of the mean velocities of shear waves in the rock mass surrounding the borehole.

1. Introduction

Geoacoustical investigations of boreholes in situ are performed in order to obtain the fullest possible information concerning the physical properties of the rock mass surrounding a borehole. One of the commonly used methods is sonic logging [17], which essentially provides data from the continuous measurement of the compressional wave propagation parameters along a borehole wall, i.e. as a function of depth (Fig. 1). Usually only one transmitter-receiver probe is used in sonic logging. The borehole is filled with a fluid, which couples acoustically the transducers of the logging tool with the formation. However, at present, the possible interpretation of the data obtained from sonic logging does not, in general, deliver all the information required about the formations. Analysis of the acoustical pulse travelling in the fluid-filled borehole and in its walls indicates that various elastic waves occur, depending on the geometry of the borehole and the physical properties of the two media involved. Detailed knowledge of the conditions necessary to excite the different specific

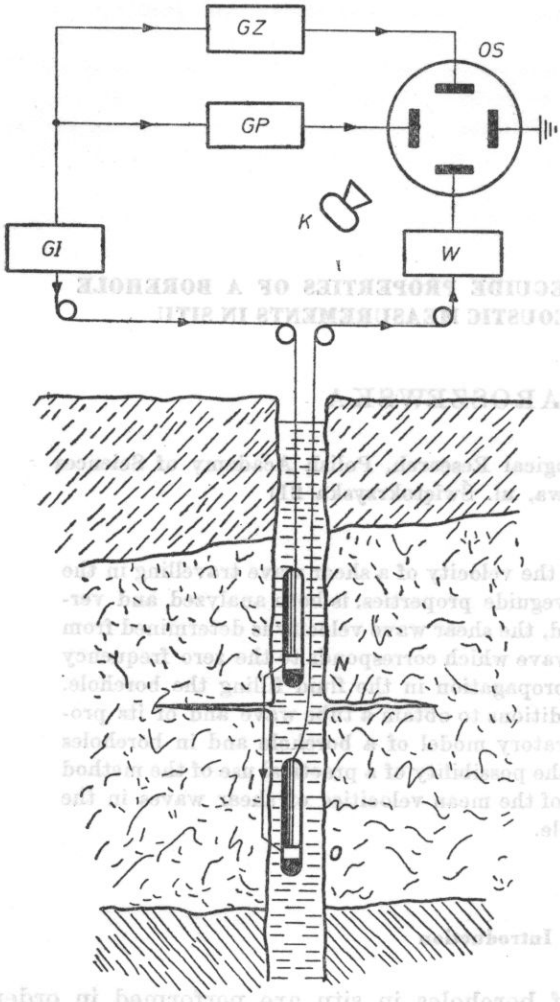

Fig. 1. The principle of geoacoustic measurement in the borehole

GI – pulse generator, *GZ* – time marker generator, *GP* – time base generator, *OS* – oscilloscope, *W* – amplifier, *K* – photographic camera, *N* – transmitter, *O* – receiver, *l* – the tested section of rock formation

waves and of the rules governing their propagation is potentially useful in the attempts to gain additional information on the properties of rock formation. This applies particularly to the shear waves propagating in the vicinity of a borehole. Shear wave velocities are used for the determination of the dynamic elastic constants of the rock formation. Propagation parameters of these waves are also particularly important as indicators of fracture and rock porosity. Read-out of the shear wave propagation data from the recorded response obtained from sonic logging is not accurate and may be ambiguous, as a result of the masking of their first times of arrival by refracted compressional waves and their multiple reflections. Direct measurement of the shear wave propagation data in the vicinity of a borehole, on the other hand, is very difficult, since access to a given location in a borehole is difficult.

In this paper, an analysis is presented of a method of determination of the velocities of shear wave travelling in the walls of a borehole, from the velocity of the so-called tube wave [10, 12, 14, 15, 20]. This wave corresponds to the zero-frequency limit of the lowest radial mode and travels in the borehole fluid. The tube wave velocity is a function of the elastic properties of this fluid and of the rock formation and in particular depends on the shear wave velocity in the formation surrounding the borehole. Investigations of the conditions of excitation and propagation of tube waves were carried out on a laboratory model of a borehole and in the field. The method for the determination of the tube wave velocities was developed from theoretical results describing elastic wave propagation in a fluid-filled cylindrical borehole in an infinite elastic solid. Such a model can be regarded as an approximation of a real borehole.

2. Propagation of acoustic waves in fluid-filled cylindrical boreholes surrounded by an infinite elastic solid

The propagation of acoustic waves in a fluid-filled cylindrical borehole surrounded by an infinite elastic solid was investigated both theoretically and experimentally and described in numerous papers (BIOT [1], GRATSINSKIJ [3 - 6], PETERSON [10], RIGGS [13], SOMERS [16], WHITE *et al.* [18, 20 - 22]). However, the formal representation of the propagation of acoustic waves excited in a borehole by an impulsive pressure point source was given by ROEVER *et al.* [14]. In this report, ordinary asymptotic results are also obtained on the basis of an expansion in terms of rays and on the basis of an analysis in terms of propagation modes. Solution of the wave equation in terms of the characteristic modes of propagation of the fluid-filled borehole is particularly representative for describing dispersive wavetrains at large axial distances from the source or long-time oscillations in the vicinity of the source. Ray theory, in contrast, has remarkable practical value in the analysis of the refracted compressional and shear waves, known also as head waves [7, 8, 14, 15], travelling in the solid medium surrounding a borehole.

The propagation of acoustic waves excited in a fluid-filled cylindrical borehole by an impulsive pressure point source was described by ROEVER *et al.* [14] for a homogeneous and isotropic solid medium, with idealized borehole geometry and neglecting the influence of the logging instrument on the configuration of the acoustic field.

2.1. *Results of mode theory.* According to mode theory, two types of modes of propagation can be excited in the borehole discussed, i.e. circumferential modes and radial modes differing with regard to the pressure distribution along the circumference and along the diameter of a borehole. Characteristic modes are labelled with the indexes l and n, where l refers to the number of nodal

planes through a borehole axis and n — to the number of pressure nodes along a borehole radius. Fig. 2 shows some of the first circumferential modes and the nodal diameters. For l even, the circumferential oscillations are symmetric with respect to the plane through the borehole axis, for l odd, the oscillations are antisymmetric with respect to this plane. The fundamental symmetric circumferential oscillations $l = 0$ propagate as a bulging and constriction of the borehole, whereas the fundamental antisymmetric $l = 1$ propagates as a bending of the borehole. Fig. 3 presents the first few radial modes in the borehole for $l = 0$. The concentric circles correspond to the pressure nodes in the borehole

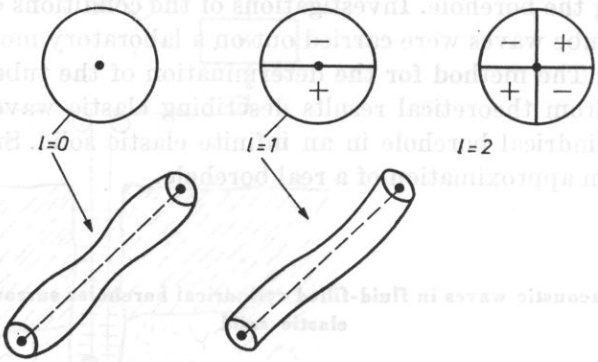

Fig. 2. Circumferential modes in the fluid filling a cylindrical borehole surrounded by an elastic solid

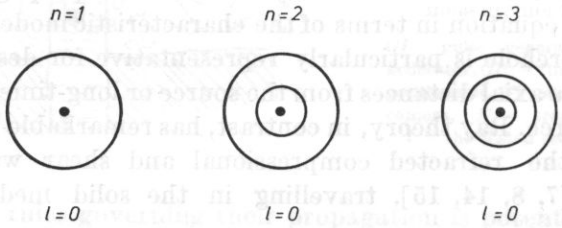

Fig. 3. Radial modes in the fluid filling a cylindrical borehole surrounded by an elastic solid

fluid. The lengths of successive radii of the nodal circles are proportional to the n zeros j_{ln} of the Bessel functions of the first kind, J_l. The fundamental radial mode $n = 0$ can exist for the two lowest circumferential modes, i.e. for $l = 0$ and $l = 1$. For $l > 0$, the pressure on the borehole axis is zero for all radial modes, i.e. for all values of n. For $l = 0$, in turn, the pressure is maximum on the borehole axis for all radial modes. i.e. all values of n. Hence, in the case of a source located on the borehole axis, only radial modes n associated with the fundamental symmetric circumferential mode $l = 0$ will be excited.

Propagation of sinusoidal, axially symmetric, radial waves in an infinitely

long fluid-filled borehole in an infinite homogeneous elastic medium has been described in detail by BIOT [1]. PETERSON [10] extended this theory for the case of a point source located on the borehole axis and also for the case of an impulsive source. These works [1, 10] present a detailed theory of dispersive wavetrains propagating in the borehole fluid, whereas the report by ROEVER [14] is devoted mainly to the description of refracted arrivals. Fig. 4 shows, after BIOT [1], the group velocity c_g dispersion curves for the radial modes, and

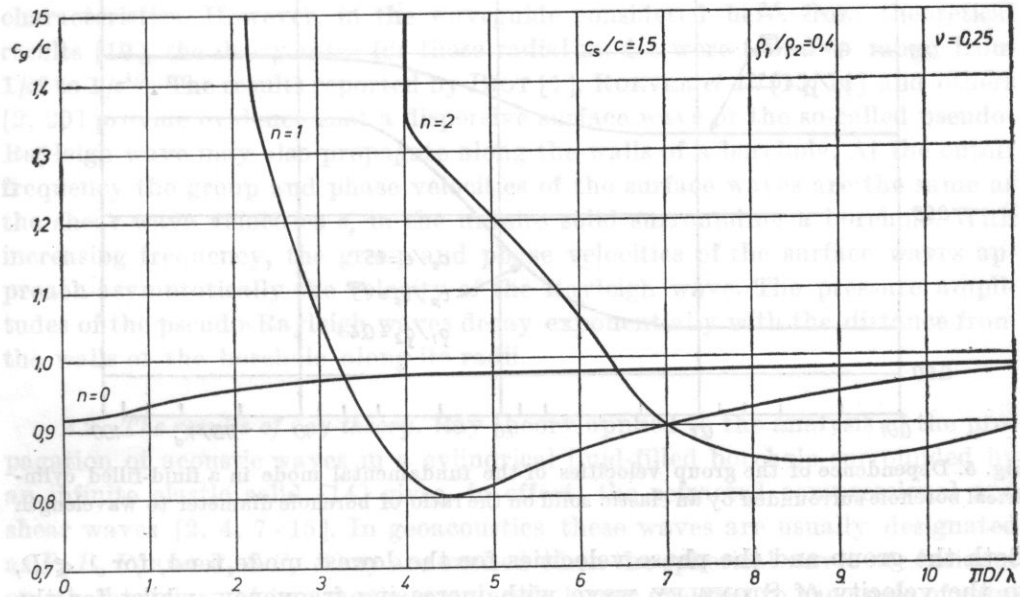

Fig. 4. Dependence of the group velocities of the first few radial modes in a fluid-filled cylindrical borehole surrounded by an elastic solid on the ratio of borehole diameter to wavelength

their dependence on the ratio of the borehole diameter D to the wavelength λ, for $c_p > c_s > c$, where c_p and c_s are the compressional and shear wave velocities, respectively, in the infinite solid surrounding the borehole, ν — Poisson's ratio for the solid medium, ϱ_1 — the density of the fluid in the borehole and ϱ_2 — the density of the solid. The group velocities are related here to the velocity of the dilatational wave c in the borehole fluid. It is easily seen from Fig. 4 that there is only one mode of the lowest order, i.e. for $l = 0$ and $n = 0$, which may propagate in the borehole over the whole range of frequencies, thus having no cutoff frequency. Both group and phase velocities of propagation for this mode are smaller than the dilatational wave velocity in the borehole fluid.

Group and phase velocities of the higher radial modes $n \geqslant 1$ reach, at the cutoff frequency, their maximum value which is equal to the shear wave velocity c_s in the solid surrounding the borehole. In the high frequency range, that is for $\lambda \ll D$, these velocities approach asymptotically the velocity c of dilata-

tional waves in the borehole fluid. For each of these modes a very pronounced minimum in the group velocity, or the so-called Airy phase, is observed.

Plots of the group velocity dispersion curves for the lowest mode $n = 0$, $l = 0$ as a function of the ratio of the borehole diameter to the dilatational wave wavelength λ_d in the fluid, for two solids characterized by different elastic constants, and for $c_p > c_s > c$ are presented after PETERSON [10] in Fig. 5.

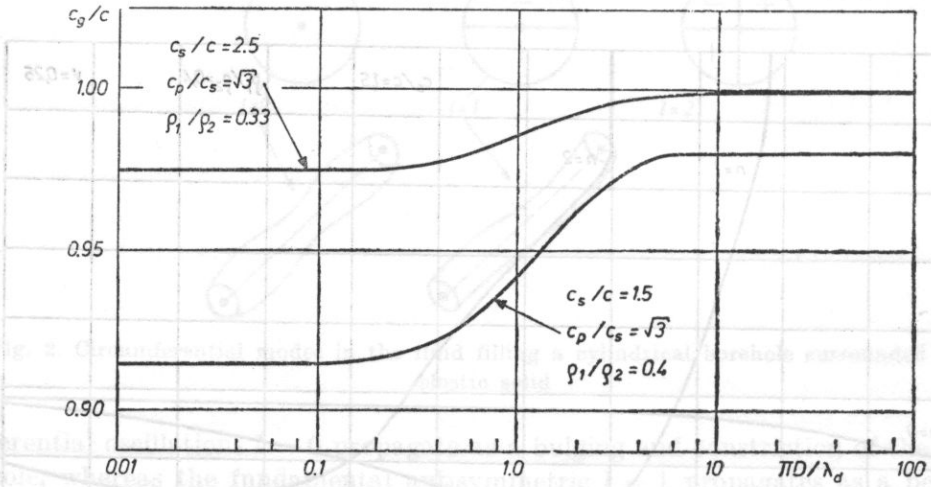

Fig. 5. Dependence of the group velocities of the fundamental mode in a fluid-filled cylindrical borehole surrounded by an elastic solid on the ratio of borehole diameter to wavelength

Both the group and the phase velocities for the lowest mode tend, for $\lambda \ll D$, to the velocity of STONELEY wave with increasing frequency, whilst for the sufficiently low frequencies ($\lambda \geqslant 5D$) they tend to the velocity of tube wave [10, 14, 15, 20], which coresponds to the so-called "waterhammer" phenomenon in a pipe. Minima of the group and phase velocity, in the case of fundamental radial mode, exist in the zero-frequency limit and thus correspond to the velocity of the tube wave c_T. The asymptotic value of this velocity is expressed by the following formula [1, 14, 20], which is valid for $\lambda \geqslant 5D$ and for $c_s > c$,

$$c_T = \frac{c}{\left[1 + \dfrac{\varrho_1 c^2}{\varrho_2 c_s^3}\right]^{1/2}}, \tag{1}$$

where c_T — the tube wave velocity, ϱ_1 and ϱ_2 — the densities of the fluid and solid, respectively, c — the dilatational wave velocity in the fluid, c_s — the shear waves velocity in the solid.

Equation (1) shows that the tube wave velocity depends only on the elastic properties of the borehole fluid (ϱ_i, c) and on the elastic properties of the surrounding solid; namely, on its shear modulus ($\varrho_2 c_s^2$).

According to PETERSON and ROEVER *et al.* [10, 14], the pressure ampli-

tudes for each of the radial modes, attenuation in both media being neglected, decay with the distance z from the impulsive point source, as $1/z^{1/2}$ along the borehole axis. The pressure amplitudes which correspond to the minima of the group velocities (the Airy phase) decay as $1/z^{1/3}$ [10, 14], whilst the tube wave propagates, according to PETERSON [10], without decaying along the borehole axis. It should be noted that in general the actual decay rates of the pressure amplitudes for all the normal radial modes depend on: the mode number, the frequency, the group velocity, the distance to the source and the source signal characteristics. However, in the waveguide considered here, from theoretical results [10], the decay rates for these radial modes were found to range from $1/z^0$ to $1/z^{1/2}$. The results reported by BIOT [1], ROEVER *et al.* [13, 14] and others [2, 20] provide evidence that a dispersive surface wave or the so-called pseudo-Rayleigh wave may also propagate along the walls of a borehole. At the cutoff frequency the group and phase velocities of the surface waves are the same as the shear wave velocities c_s in the infinite solid surrounding a borehole. With increasing frequency, the group and phase velocities of the surface waves approach asymptotically the velocity of the Rayleigh wave. The pressure amplitudes of the pseudo-Rayleigh waves decay exponentially with the distance from the walls of the borehole along its radii.

2.2. *The results of ray theory.* Ray theory applied to the analysis of the propagation of acoustic waves in a cylindrical fluid-filled borehole surrounded by an infinite elastic solid [14] gives, in effect, the refracted compressional and shear waves [2, 4, 7 - 15]. In geoacoustics these waves are usually designated as $P_1 P_2 P_1$ and $P_1 S P_1$. They are excited when the spherical waves are incident on the boundary of two media at an angle larger or equal to the angle of total internal reflection.

Refracted waves propagate along the paths characterized by the minimum travel time relative to the other waves, i.e. along the walls of a borehole. In the case of the propagation of acoustic pulses, the refracted waves thus arrive first at the points of observation in the borehole. The geometry of the borehole causes the rays of the acoustic waves propagating in it to be focused on the borehole axis, which leads to a caustic phenomenon and in effect they are totally reflected from the axis with a 90° phase shift. In the case of the propagation of acoustic pulses, the reflected pulse changes its shape according to a Hilbert transformation [14].

The results from the asymptotic ray theory reported by ROEVER [14] for a source on the borehole axis, and with attenuation in the medium being neglected, indicate that the amplitude of the first refracted compressional arrival decays with the distance z from the source as $1/z\log^2 z$ (i.e. approximately as $1/z$), whilst the amplitude of the first shear arrival decays as $1/z^2$. These results are also supported by empirical data [14] and by the analysis of the complex-valued sections of dispersion curves.

As shown by PETERSON [10], the decrease of the peak amplitude of the first refracted compressional arrival, with distance, z, from the source along the borehole axis, follows the formula $1/z^2 \log z$, which is not in agreement with the formula given by ROEVER [14]. On the other hand, TSANG [18], in his work pertaining to the propagation of compressional refracted waves in a borehole, obtained the same results as those of ROEVER [14], i.e. the decay rate of the amplitude for the first arrival is proportional to $1/z\log^2 z$. TSANG [18] has also shown that the expression for the decay rate of the first amplitude for these wave components along the borehole axis given by PETERSON [10] is erroneous. With reference to the decay rate of the amplitude for the first arrival of shear waves, however, the results obtained by these three authors are in complete agreement ($1/z^2$).

If the source is located in the borehole off its axis, the refracted waves travel in borehole walls along spiral pathways [2, 4, 5, 14]. The decay rate of the amplitude for the first arrival of these "spiral" refracted waves changes, according to ROEVER, with the distance between the source and the borehole walls as well as that between the receiver and the borehole walls and with their spacing along the borehole axis within the limits from $1/z$ to $1/z^2$, when attenuation is not taken into account.

The results by BULATOVA *et al.* [2] and by GRATSINSKIJ [6], obtained on the grounds of an approximate analysis using ray theory and empirical data, seem to indicate that the amplitudes of the first reflected arrivals of both compressional and shear waves travelling along the borehole walls fall off as $1/z^{3/2}$ for the case of a point source located on the axis. For a source off the axis they found that the first amplitudes of both compressional and shear arrivals fall off as $1/z^2$. These results were obtained for the conditions analogous to those assumed by ROEVER [14]. It seems, however, that in these two cases a significant difference should be pointed out, namely that ROEVER [14] measured the amplitude on the borehole axis and not close to its walls [2, 6]. If the attenuation in the surrounding rock-formation is taken into account, the total decrease of the amplitudes for an axial location of the source in the borehole follows the formula [2, 6]

$$A = \frac{A_0 \exp(-\alpha z)}{z^{3/2}}, \tag{2}$$

and for an off-axis location of the source

$$A = \frac{A_0 \exp(-\alpha z)}{z^2}, \tag{3}$$

where z – the cylindrical axial coordinate of the borehole, A_0 – the wave amplitude for $z = 0$, A – the wave amplitude at the distance z from the source, α – the attenuation coefficient in the rock formation.

In summary, the results presented in the reports cited indicate, in spite of differences, that the amplitudes of the refracted waves decrease more rapidly as a function of the distance from the source of acoustic waves in the borehole than the amplitudes of the dispersive wavetrains travelling in the borehole fluid. These conclusions hold, however, for the case where energy losses in both media are neglected.

2.3. *Acoustic response obtained from the borehole.* On the basis of the above description of acoustic wave propagation in a fluid-filled borehole surrounded by an elastic solid, the theoretical acoustic response from a borehole for the case of a short pulsed disturbance [9, 11] can be predicted. Fig. 6 illustrates schematically the acoustic waves propagating in a borehole from an impulsive source

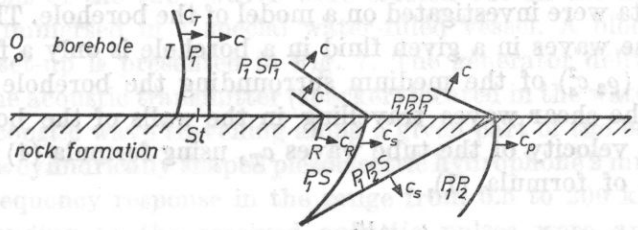

Fig. 6. Theoretical acoustic response in a borehole

$P_1P_2P_1$ – refracted compressional wave, $P_1\,S\,P_1$ – refracted shear wave, R – pseudo-Rayleigh wave, P_1 – direct wave, St – Stoneley wave, T – tube wave, c – velocity of dilatational waves in the fluid filling the borehole, c_p and c_s – velocity of compressional and shear waves in rock formation, c_T – tube wave velocity, O – acoustic source

o, situated in the figure on its left-hand side. For simplification, only one boundary of the borehole is shown. In the case of a pulse-like disturbance, at the point of observation located some distance from the source, refracted waves: compressional, $P_1\,P_2\,P_1$, and shear, $P_1\,S\,P_1$, arrive first, being characterized by minimum travel times, and propagating along the borehole walls with velocities c_p and c_s, respectively, and with velocity c in the borehole fluid. Next, with a short delay relative to the shear wave, a dispersive surface wave R and dispersive wavetrains in the borehole fluid arrive. Among the latter waves, the so-called direct wave P_1, characterized by high frequency components and travelling with velocity of a dilatational wave c in the fluid and the STONELEY wave can be distinguished. The tube wave T characterized by a relatively low frequency and travelling with velocity $c_T < c$ arrives last. In the tail of the pulse, oscillations, corresponding to the frequencies of the Airy phase of the first few modes, may also be observed.

It is obvious that the wider the spectrum of the pulse emitted in the borehole the more complex the received response will be, i.e. more of the various waves will be excited in the borehole. At large distances of the observation point from the source, relative to the wavelength, along the borehole axis, the waveform differs significantly from that for small distances, i.e. the vicinity of the source.

This results from the significantly different decay rates of the amplitude for various types of acoustic waves with the distance to the source discussed above, as well as their different attenuation in the medium. The present experimental data and the results of theoretical works thus indicate that, at sufficiently large distances from the transmitter, only dispersive wavetrains in which the amplitudes fall off relatively slowly with distance arrive at the point of observation. In particular, this pertains to the tube wave which is least attenuated, since its frequency is the lowest.

3. Propagation of acoustic waves investigated on the model of a borehole

3.1. *Technique.* The conditions necessary to excite a tube wave and its propagation data were investigated on a model of the borehole. The propagation velocity of these waves in a given fluid in a borehole is only a function of the shear modulus ($\varrho_2 c_s^2$) of the medium surrounding the borehole (1). Thus the velocity c_s of the shear waves travelling in the walls of the borehole can be found from the velocity of the tube waves c_T, using formula (4) obtained from transformation of formula (1),

$$c_s = \left(\frac{\varrho_1}{\varrho_2}\right)^{1/2} \frac{c}{\left[1-\left(\frac{c_T}{c}\right)^2\right]^{1/2}}. \tag{4}$$

The present idea of recording and measuring the velocity of the tube waves originated from the theoretical and experimental works discussed which indi-

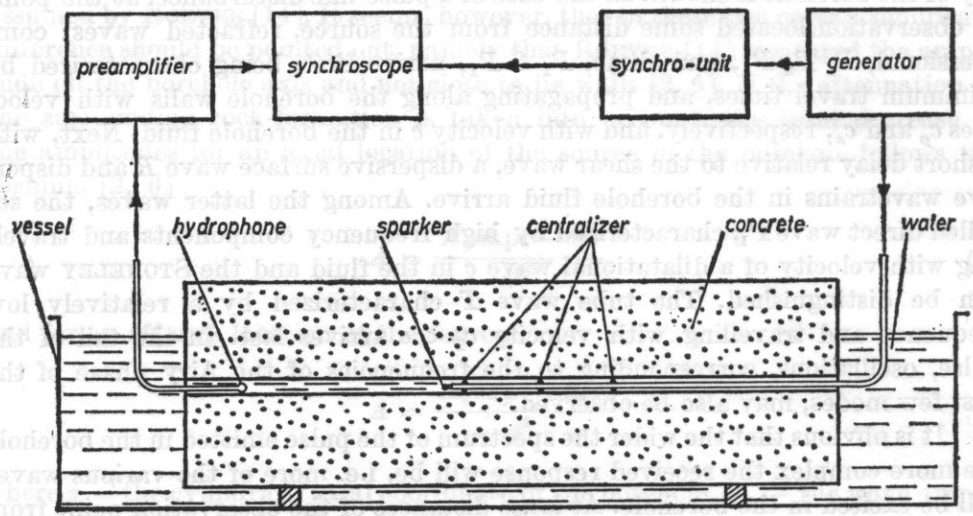

Fig. 7. Block diagram of the laboratory set-up for investigation of the propagation of acoustic waves in a model borehole

cate that the amplitudes of these waves fall off comparatively less relative to the amplitudes of the other waves as a function of distance from the source. To check the truth of this statement, the amplitudes of the first arrivals of the tube waves were measured on a laboratory model along the borehole axis as a function of distance from the source. To the present writer's knowledge such measurements have never previously been carried out.

A borehole model 12 mm in diameter was made along the axis of symmetry of a concrete block of 116 × 30 × 30 cm. The compressional and shear elastic wave velocities in the block determined using conventional techniques were $c_{p1} = 4562$ m/s and $c_{s1} = 2660$ m/s, respectively. The compressional wave velocity was measured using a transmission technique and the shear wave velocity using piezoelectric transducers with suitable electrical polarization.

Investigations of the tube waves were carried out on the model borehole with the block immersed in a special water-filled vessel. A block diagram of the laboratory set-up is presented in Fig. 7. The generator delivering electric pulses excited the acoustic transmitter (sparker) located in the water-filled model borehole. The acoustic wave travelling along a given part of the borehole length was received by a cylindrically shaped piezoelectric hydrophone 2 mm in diameter, having a flat frequency response in the range from 0.5 to 200 kHz. Electrical signals corresponding to the received acoustic pulses were amplified using a suitable preamplifier and fed to the synchroscope input. The generator delivering pulses to the transmitter and the synchroscope were triggered by a quartz-stabilized clock. To excite the wave in the model borehole, the sparker used emitted acoustic waves of a sufficiently low frequency spectrum, i.e. $\lambda \geqslant 5D$. The construction of the sparker used is presented in Fig. 8. It consists of a teflon-insulated copper wire 0.7 m min diameter and of a copper tube 1.5 mm in diameter pressed tight over the wire insulator. The inner wire is one, and the outer tube the other electrode of the sparker, which, due to its dimensions, was regarded as a point source. The frequency spectrum emitted by such a transmitter depends on its geometry and on the duration of the electric pulse leading to the spark discharge. In the present experiments, 4.5 kV rectangular *dc* pulses were used. Their duration was adjustable in the range from 5 to 100 μs and the repetition frequency in the range from 1 to 50 pulses per second.

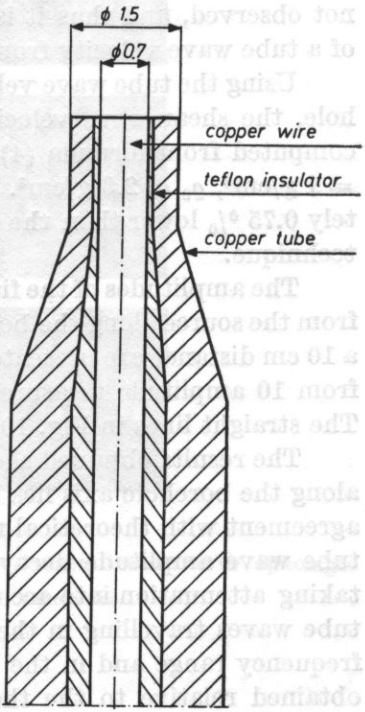

Fig. 8. Sparker cross-section

The wave forms were photographed from a synchroscope screen as a function of the transmitter-receiver distance along the borehole axis. This distance was changed from 10 to 90 cm in 10 cm steps. Both transducers used in the measurement of the tube wave amplitudes were constrained to be on the borehole model axis by mechanical centralizers.

3.2. *Results of the laboratory measurements.* Fig. 9 shows the oscillograms of the acoustic signals obtained on the borehole model at constant amplification and sweep frequency for various transmitter-receiver spacings. As can be easily observed from these oscillograms, the most pronounced frequency component in the received pulses amounts to about 25 kHz.

At front of the received pulses, a very weak wave component is observed. The travel-times of this wave indicate that it is a refracted shear arrival. The subsequent segment of the received pulses contains a large amplitude wave of approximately the same frequency (25 kHz) travelling at a velocity of about 1390 m/s, i.e. lower than the velocity of dilatational waves in water. This indicates the dispersive character of this wave. For this wave and the borehole diameter $D = 12$ mm, the relation $\lambda \geqslant 5D$ is valid. In the range of wavelengths thus determined, only the fundamental radial mode, at the tube wave velocity may propagate according to the mode theory. As can be readily seen from Fig. 9, a very substantial part of the pulse energy travels at the tube wave velocity. With large transmitter-receiver spacings other waves than tube waves are not observed, and thus it is possible to achieve a very accurate determination of a tube wave velocity from its travel time.

Using the tube wave velocity $c_T = 1390$ m/s as measured on the model borehole, the shear wave velocity $c_{s2} = 2640$ m/s in the concrete block itself was computed from formula (4) for the following parameters: $c = 1482$ m/s, $\varrho_1 = 1$ g/cm^3, $\varrho_2 = 2.3$ g/cm^3. The obtained velocity $c_{s2} = 2640$ m/s is approximately 0.75 % lower than the velocity $c_{s1} = 2660$ m/s obtained using the classical technique.

The amplitudes of the first arrivals of the tube wave as a function of distance from the source along the borehole axis normalized relative to the amplitude at a 10 cm distance are presented in Fig. 10. The data points in the graph are means from 10 amplitude measurements. Standard deviation never exceeded 0.3 dB. The straight lines in Fig. 10 have slopes of $1/z^{1/2}$, $1/z^{2/3}$ and $1/z$.

The results obtained show that the decay rate for the tube wave amplitude along the borehole axis lies between $1/z^{2/3}$ and $1/z$. These results are not in full agreement with theoretical results which determine the maximum slopes of the tube wave amplitude decay rate, due to the geometrical factors and without taking attenuation into account, as not exceeding $1/z^{1/2}$. The attenuation of the tube waves travelling in the water medium in the borehole is negligible in the frequency range and in the borehole segments examined [8]. The discrepancy obtained relative to the theoretical works may thus have resulted from the

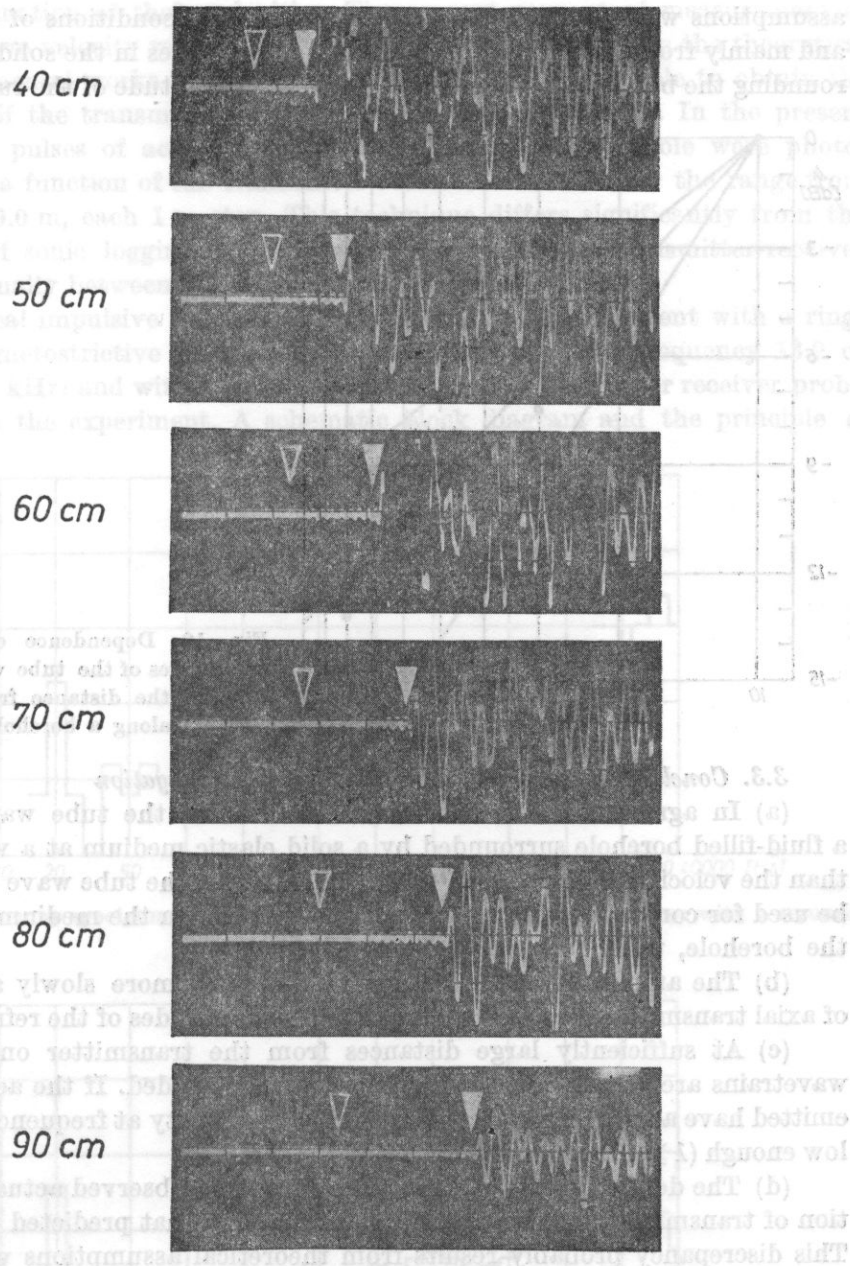

Fig. 9. Oscillograms of acoustic model responses for various transmitter-receiver spacings
time base – 100 μs/cm; ▽ – shear wave, ▼ – tube wave

assumptions which simplify and idealize the actual conditions of measurement and mainly from the assumption that the energy losses in the solid medium surrounding the borehole have no influence on the amplitude of the tube wave.

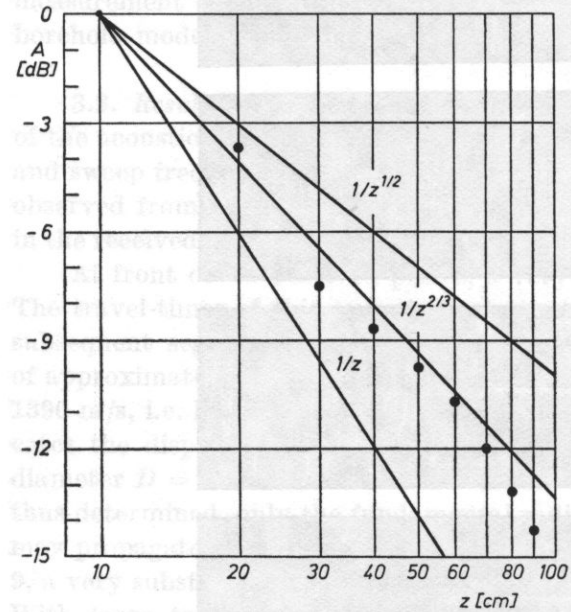

Fig. 10. Dependence of the relative amplitudes of the tube wave frist arrivals on the distance from transmitter along a borehole axis

3.3. Concluding remarks on the laboratory investigation

(a) In agreement with the theoretical results, the tube wave travels in a fluid-filled borehole surrounded by a solid elastic medium at a velocity lower than the velocity of dilatational waves in the fluid. The tube wave velocity may be used for computation of the shear wave velocity in the medium surrounding the borehole, using formula (4).

(b) The amplitude of the tube wave decreases more slowly as a function of axial transmitter-receiver spacing than the amplitudes of the refracted waves.

(c) At sufficiently large distances from the transmitter only dispersive wavetrains are observed in the model response recorded. If the acoustic pulses emitted have a frequency spectrum of sufficient density at frequencies which are low enough ($\lambda \geqslant 5D$), then the tube wave is observed.

(d) The decay rate of the tube wave amplitude observed actually as a function of transmitter-receiver spacing is larger than that predicted theoretically. This discrepancy probably results from theoretical assumptions which idealize and simplify the actual conditions of the measurement.

4. Field measurements

4.1. *Method.* Investigations in boreholes in situ pertaining to the conditions of excitation and propagation data of tube waves were aimed chiefly at

the determination of their velocities. The present concept of measurement of the tube wave velocity results, as it was already discussed, from the theoretical and experimental works which point out that it is only possible to obtain the tube wave if the transmitter-receiver spacing is large enough. In the present project the pulses of acoustic waves travelling in the borehole were photographed as a function of the transmitter-receiver distance over the range from 0.5 m to 10.0 m, each 1 m step. This technique differs significantly from the technique of sonic logging in which, as a rule, a constant transmitter-receiver spacing (usually between 0.5 m and 1.8 m) is used.

A typical impulsive geoacoustic Petroscope PT-13 equipment with a ring-shaped magnetostrictive transmitter probe (radial resonant frequency 13.9 or 25.4 or 31.5 kHz) and with a piezoelectric ring-shaped transducer receiver probe was used in the experiment. A schematic block diagram and the principle of

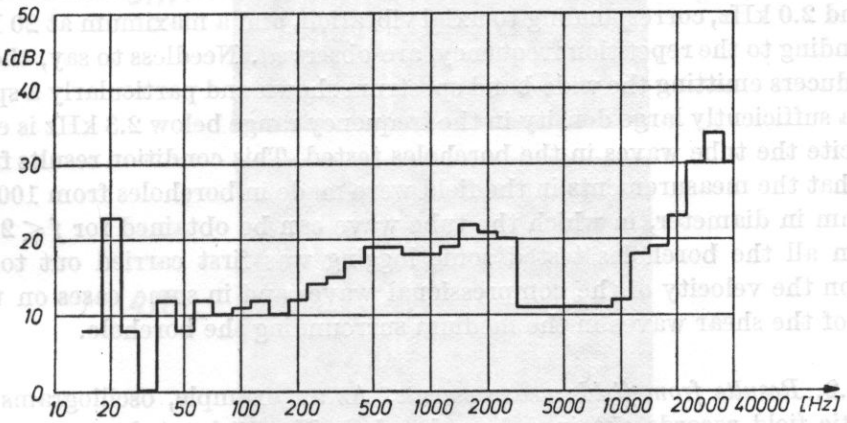

Fig. 11. Frequency spectrum of the ring-shaped magnetostrictive transducer with a resonant frequency of 13.9 kHz

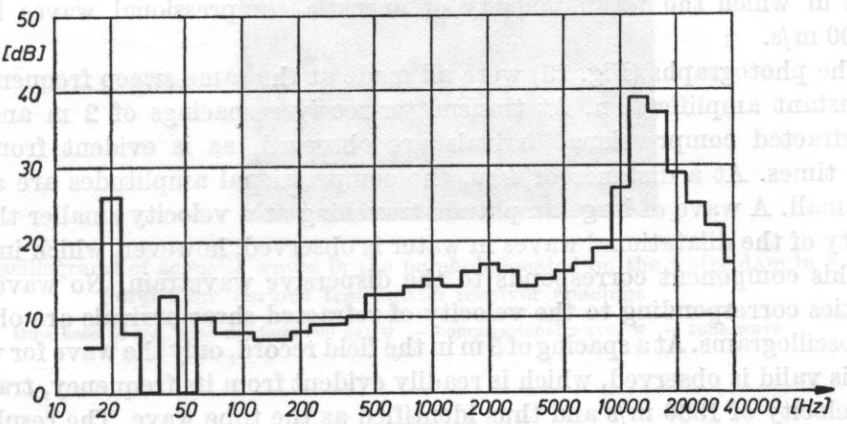

Fig. 12. Frequency spectrum of the ring-shaped magnetostrictive transducer with a resonant frequency of 31.5 kHz

operation of the equipment are given in Fig. 1. Transmitting transducers were set into vibration using *dc* pulses at a repetition frequency of 20 Hz.

The frequency spectrum of the transmitter transducers used was measured using a sphere-shaped piezoelectric hydrophone 10 mm in diameter and with a frequency response flat over the range from 2 Hz to 40 kHz. Acoustic waves were also received using the probe of a typical Petroscope PT-13 equipment. The frequency spectra of magnetostrictive transducers operating at resonant frequencies of 13.9 and 31.5 kHz, obtained from a 1/3 octave spectral analyzer (corrected for the frequency response of the PT-13 receiver channel) as being most representative are presented in Figs. 11 and 12. The measurements of these frequency spectra were carried out in a large water basin (lake) and with a transmitter-receiver spacing of 1 m. The spectra obtained provide evidence that the transducers used emitted wide-band signals. Except for the maximum at 13.9 or 31.5 kHz, which corresponds to the radial resonance, a maximum between 1.5 and 2.0 kHz, corresponding to axial vibration, and a maximum at 20 Hz, corresponding to the repetition frequency, are observed. Needless to say, the use of transducers emitting the wide-band spectrum shown and particularly a spectrum with a sufficiently large density in the frequency range below 2.3 kHz is essential to excite the tube waves in the boreholes tested. This condition results from the fact that the measurements in the field were made in boreholes from 100 mm to 130 mm in diameter, in which the tube wave can be obtained for $f \leqslant 2.3$ kHz.

In all the boreholes tested sonic logging was first carried out to obtain data on the velocity of the compressional waves and in some cases on the velocity of the shear waves in the medium surrounding the borehole.

4.2. *Results from field measurements.* As an example, oscillograms of the acoustic field records obtained from borehole No. 15 located on a water dam in Swinna Poręba for various transmitter-receiver spacings are presented in Fig. 13. The formations surrounding the borehole are chalk shale-layered sandstones in which the mean velocity of acoustic compressional waves is $c_p = 3700$ m/s.

The photographs (Fig. 13) were all made at the same sweep frequency and at constant amplification. At transmitter-receiver spacings of 2 m and 3 m, the refracted compressional arrivals are observed, as is evident from their travel times. At a distance of 4 m, the compressional amplitudes are already very small. A wave of large amplitude travelling at a velocity smaller than the velocity of the dilatational waves in water is observed, however, which indicates that this component corresponds to the dispersive wavetrain. No waves with velocities corresponding to the velocity of refracted shear arrivals are observed in the oscillograms. At a spacing of 5 m in the field record, only the wave for which $\lambda \geqslant 5D$ is valid is observed, which is readily evident from its frequency, travelling at a velocity of 1380 m/s and thus identified as the tube wave. The results presented of acoustic signals travelling in the borehole illustrate the character of

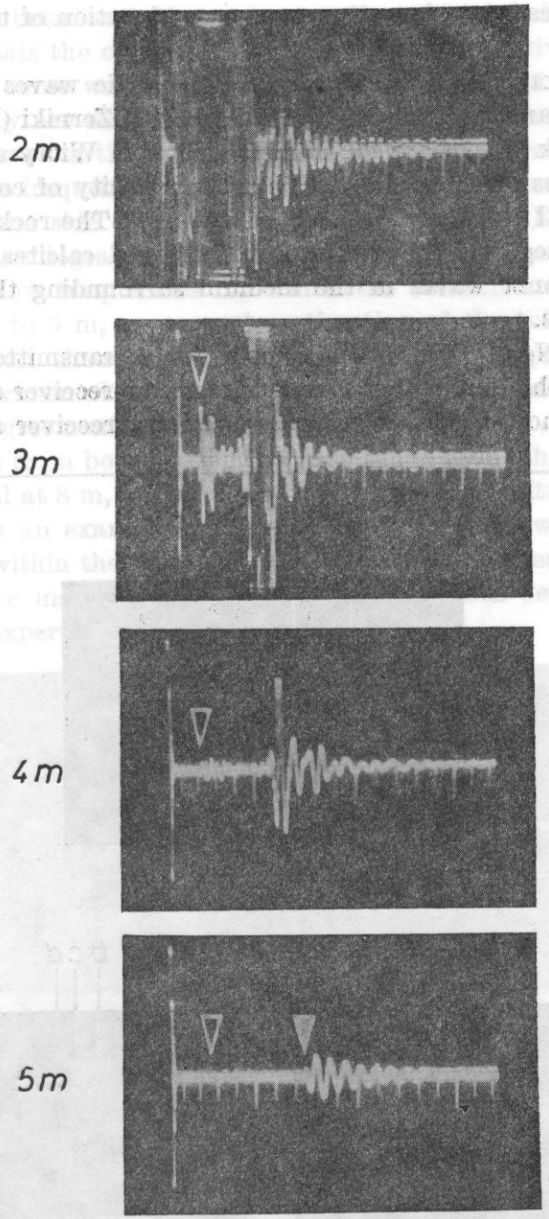

Fig. 13. Oscillograms of acoustic waves in the borehole located on the water dam in Swinna Poręba for various transmitter-receiver spacings

time base 10 ms, time markers 500 μs; ▽ – compressional wave, ▼ – tube wave

the amplitude decay rate for some waves as a function of transmitter-receiver distance.

The other examples of oscillograms of acoustic waves in boreholes were taken on water dams in Wióry (No. 1) and Brzegi-Żerniki (Nos. 2 and 3). The characteristic rock formations on the water dam in Wióry are chiefly medium grained sandstones of lower Trias. The mean velocity of compressional waves in these geological formations was $c_p = 2700$ m/s. The rock formations at the water dam in Brzegi-Zerniki are Jurassic fractured calcites. The mean velocity of compressional waves in the medium surrounding the borehole tested was $c_p = 3150$ m/s.

Photograph No. 1 (Fig. 14) was made for a transmitter-receiver spacing of 4 m, photographs Nos. 2 and 3 for a transmitter-receiver spacing of 5 m but with various borehole depths. For these transmitter-receiver spacings it is poss-

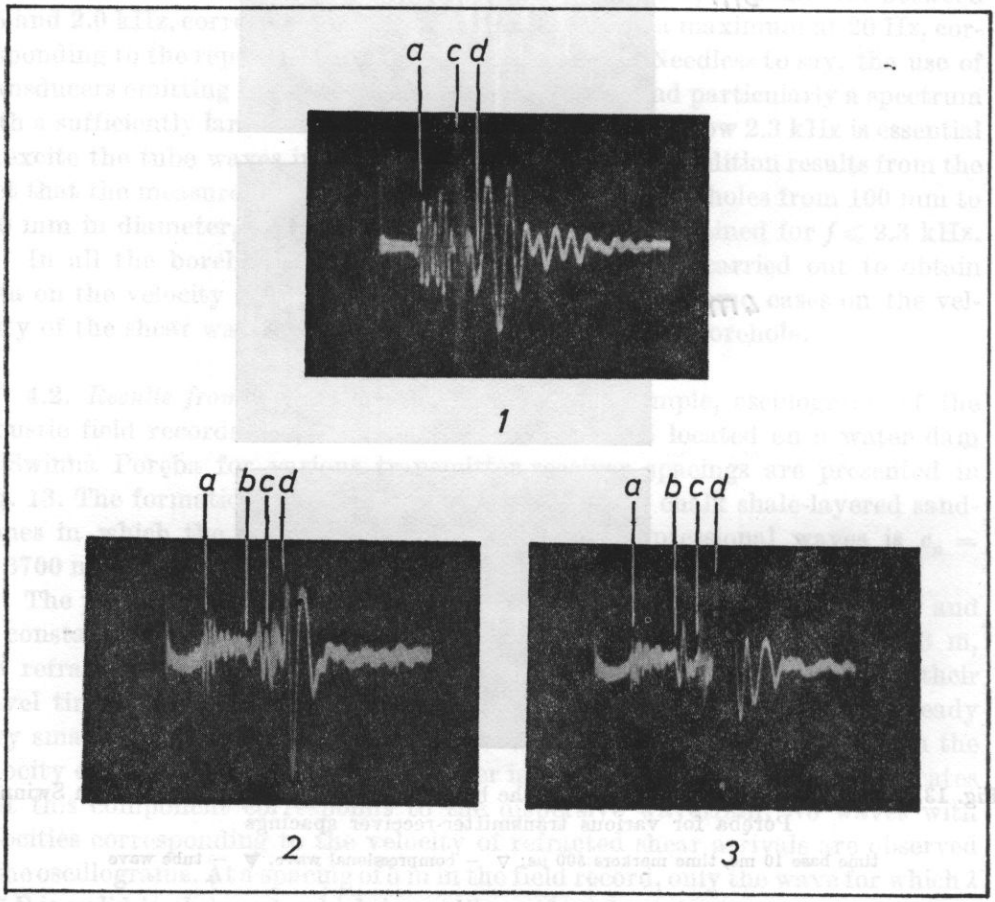

Fig. 14. Oscillograms of acoustic waves in the borehole located on the water dam in Brzegi-Żerniki and Wióry

time base 10 ms, time markers 500 μs; *a* – compressional wave, *b* – shear wave, *c* – direct wave, *d* – tube wave

ible to distinguish between various waves on the basis of their travel time. At the fronts of the signals the compressional waves of comparatively high frequency are observed; in some waveforms, i.e. photographs Nos. 2 and 3 shear waves of lower frequency are also present. Direct waves travelling at the velocity of the dilatational wave in the water filling the borehole, characterized by the components of highest frequencies contained in the spectrum emitted, in agreement with the right-hand side of the group velocity curves in Fig. 4, can be easily found in all the oscillograms. Pulse tails correspond to tube waves having large amplitudes and low frequencies for which the condition $\lambda \geqslant 5D$ is valid. At distances from 4 to 5 m, an accurate estimation of the tube wave velocity is, in the oscillograms shown, rather difficult, due to the presence of the other waves. The experimental results for acoustic waves travelling in boreholes in situ are in good agreement with theoretical predictions.

Oscillograms from boreholes in the rock foundation (shale) of a water dam in Młoty obtained at 8 m, i.e. for a relatively large transmitter-receiver spacing, are presented by an example in Fig. 15. Only the tube waves for which the wavelengths lie within the limit $\lambda \geqslant 5D$ are observed in these oscillograms. The photographs were made in borehole No. 82 at various depths but otherwise under the same experimental conditions throughout.

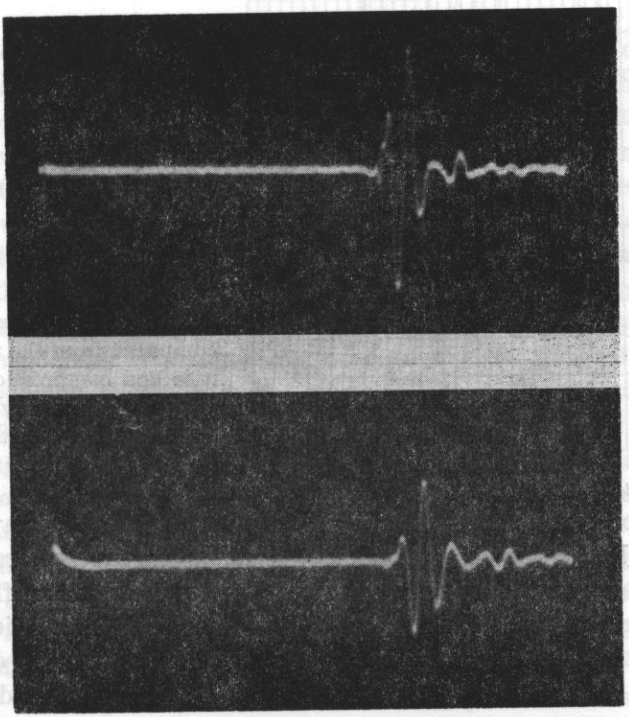

Fig. 15. Oscillograms of acoustic waves from various depths of the borehole located on the water basin in Młoty for 8 m distance to the transmitter. Time base 10 ms, time markers 500 μs

The mean values of the compressional wave velocity in the rock formation surrounding borehole No. 82 in Młoty, computed from the tube wave velocity using relation (4), as a function of depth, are presented in Fig. 16 together with the compressional wave velocities for comparison.

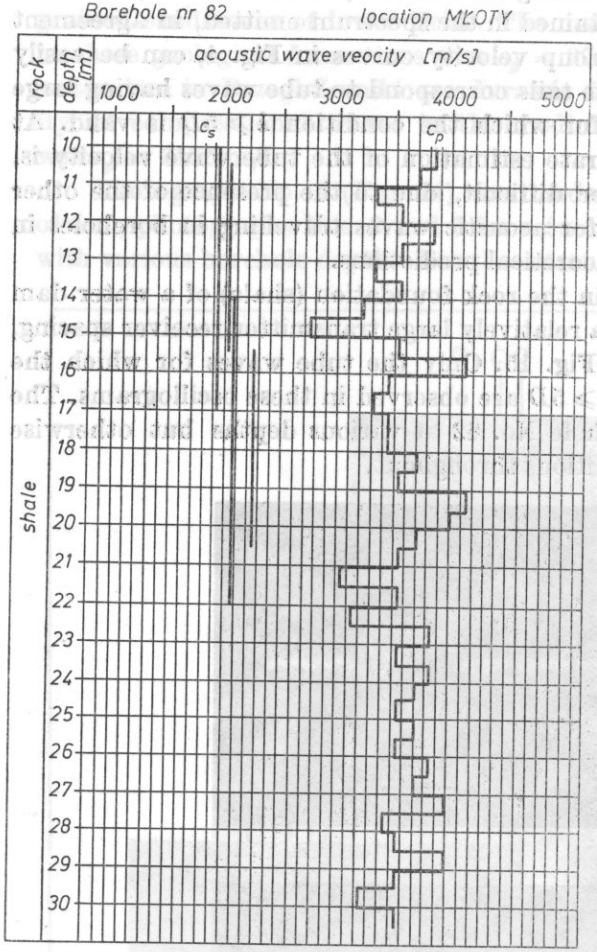

Fig. 16. Mean shear wave velocities computed from the tube wave velocities and compressional wave velocities in the vicinity of the borehole at Młoty as a function of its depth

4.3. Concluding remarks on field measurements

1. The records presented here illustrate the multitude of wave types which are excited in boreholes using ring-shaped magnetostrictive transducers, and also the decay rates of their amplitudes along the borehole axis in field conditions. In complete agreement with the recent data from both theoretical and experimental works, the present data also provide evidence that the decay rates for refracted waves travelling in the borehole walls as a function of distance are the largest.

2. For large transmitter-receiver spacing only dispersive wavetrains propagating in the borehole fluid were observed in the field records.

3. Using the tube wave velocity, the mean shear wave velocity in the rock mass surrounding the borehole can be computed using relation (4). The use of equation (4) for computation of the shear wave velocity, c_s, from the measured tube wave velocity, c_T, introduces an additional error σ_W determined by the general formula [19]

$$\sigma_W = \sigma_{\bar{x}} \frac{\partial W}{\partial x}, \tag{5}$$

where $\sigma_{\bar{x}}$ — the standard deviation of the mean of the measured quantity $\bar{x}$, W — a function of the measured quantity, x — the measured quantity.

Using function (4), the following dependence is obtained

$$\frac{\partial W}{\partial x} = \frac{\partial c_s}{\partial c_T} = \left(\frac{\varrho_1}{\varrho_2}\right)^{1/2} \frac{1}{\left[1-\left(\frac{c_T}{c}\right)^2\right]^{3/2}}, \tag{6}$$

and hence

$$\sigma_W = \sigma_{c_s} = \sigma_{\bar{c}_T} \left(\frac{\varrho_1}{\varrho_2}\right)^{1/2} \frac{1}{\left[1-\left(\frac{c_T}{c}\right)^2\right]^{3/2}}. \tag{7}$$

As can be seen from (7), the error $\sigma_{\bar{c}_s}$ resulting from the use of function (4), for the computation of the shear wave velocity, becomes much larger as the tube wave velocity approaches the velocity of the dilatational wave in the borehole fluid. These values are, in practice, of the same order and thus the error, σ_{c_s}, in determining the velocity of the shear wave may be significantly larger than the standard deviation ,$\sigma_{\bar{c}_T}$, of the mean value of the measured tube wave velocity c_T. The greatly increased transfer of tube wave velocity measurement errors to the errors of their function (4) indicates some deficiency of the method investigated. This deficiency can be well illustrated by the following examples. The tube wave velocities determined for borehole No. 82 located on the hydro-electric power station Młoty were the means of 10 measurements with a standard deviation not exceeding ± 0.1 dB. The error σ_{c_s} of the shear wave determination according to formula (7) for the tube wave velocity $c_T = 1333$ m/s was in this case $\sigma_{c_s} = 7.4\ \sigma_{\bar{c}_T}$, i.e. ± 0.74 dB, for $c_T = 1351$ m/s, correspondingly, $\sigma_{c_s} = 9.0\ \sigma_{\bar{c}_T}$, i.e. ± 0.9 dB.

4. The shear wave velocity computed from the mean tube velocity for sections of the borehole some meters long can be used for the determination of the mean dynamic elastic constants of the rock mass. These constants are particularly useful and significant for engineering geology.

5. The use of two receivers that are relatively close to each other with a spacing of 0.5 m for example, at some meters' distance from the transmitter should improve, as far as can be predicted, the resolution of the method discussed.

6. Identification of the tube wave and the very accurate determination of its propagation velocity using the described method is not possible in all specific borehole conditions and is particularly difficult if the attenuation in the rock formation is small.

7. Further research in the field using the described method in lithologically different geological formation seems promising.

Acknowledgements The author wishes to express thanks to W. MIKIEL for his efficient technical assistance in the measurements of frequency spectra emitted by the ring-shaped magnetostrictive transducers used in the field measurements.

References

[1] M.A. BIOT, *Propagation of elastic waves motion in a cylindrical hole containing a fluid*, J. Appl. Phys., **23**, 9, 997-1005 (1952).

[2] Z.M. BULATOVA, E.A. VOLKOWA, E.F. DUBROV, *Akusticheskij karotazh*, Izd. "Nedra" Leningrad 1970, pp. 31-45.

[3] W.G. GRATSINSKIJ, *Kinematicheskiye osobiennosti volnovey kartiny pri ultrazvukovom karotazhe skvazhin*, Izv. Ak. Nauk SSSR, ser. geofiz., **7**, 1021-1039 (1963).

[4] W.G. GRATSINSKIJ, *Kinematika volnovykh frontov pri karotazhe skvazhin a raspredelonnymi preobrazovatelami*, Izv. Ak. Nauk SSSR, ser. geofiz., **8**, 1178-1197 (1963).

[5] W.G. GRATSINSKIJ, *Issledovanie uprugich voln v modeli skvazhiny*, Izv. Ak. Nauk SSSR, ser, geofiz., **3**, 322-338 (1964).

[6] W.G. GRATSINSKIJ, *Amplitudy skolzyashchikh voln na poverkhnosti skvazhiny*, Izv. Ak. Nauk SSSR. ser. geofiz., **6**, 819-838 (1964).

[7] A. JAROSZEWSKA, *Investigation of the conditions for excitation and propagation of refracted acoustic waves in rock samples* (in Polish), Archiwum Akustyki, **15**, 4. 385-398 (1980).

[8] I. MALECKI, *Physical foundations of technical acoustics*, Pergamon Press, PWN, 1969, pp. 134, 267.

[9] R.L. MORRIS, D.R. GRINE, T.E. ARKFELD, *Using compressional and shear acoustic amplitudes for the location of fractures*, Jour. Pet. Techn., **16**, 6, 623-632 (1964).

[10] E.W. PETERSON, *Acoustic wave propagation along a fluid-filled cylinder*, J. Appl. Phys., **45**, 8, 3340-3350 (1974).

[11] G.R. PICKETT, *Acoustic character logs and their applications in formation evaluation*, Jour. Pet. Techn., **15**, 6, 659-667 (1963).

[12] S. PLEWA, *Prospecting geophysics* (in Polish), Śląsk, Katowice 1972.

[13] E.D. RIGGS, *Seismic wave types in a borehole*, Geophysics, **20**, 1, 53-67 (1955).

[14] W.L. ROEVER, J.H. ROSENBAUM, T.F. VINING, *Acoustic waves from an impulsive sources in a fluid-filled borehole*, JASA, **55**, 6, 1144-1157 (1974).

[15] W.L. ROEVER, T.F. VINING, E. STRICK, *Propagation of elastic wave motion from an impulsive source along a fluid-solid interface, I. Experimental pressure response, II. Theoretical pressure response*, Phil. Trans. R. Soc., **A 251**, 455-488 (1959).

[16] E.V. SOMERS, *Propagation of acoustic waves in a liquid-filled cylindrical hole surrounded by an elastic solid*, J. Appl. Phys., **24**, 5, 515-521 (1953).

[17] G.C. SUMMERS, R.A. BRODING, *Continuous velocity logging*, Geophysics, **18**, 3, 598 (1952).

[18] L. TSANG, J.A. KONG, *Asymptotic methods for the first compressional head wave arrival in a fluid-filled borehole*, JASA, **65**, 3, 647-654 (1979).

[19] J. WEHR, *Measurements of velocities and attenuation of ultrasonic waves* (in Polish), PWN, Warszawa 1972, p. 78.

[20] J.E. WHITE, *Seismic waves radiation, transmission, and attenuation*, McGraw-Hill, New York 1965, p. 142-211.

[21] J.E. WHITE, H.H. FROST, *Unexpected waves observed in fluid-filled boreholes*, JASA, 28, 5, 924-927 (1956).

[22] J.E. WHITE, R.E. ZECHMAN, *Computed response of an acoustic logging tool*, Geophysics, 33, 2, 302-310 (1968).

Received on September 30, 1980; revised version on June 10, 1981.

ARCHIVES OF ACOUSTICS
7, 2, 143-154 (1982)

ON THE DIFFRACTION OF SOUND WAVE BY A WEDGE

ROMAN WYRZYKOWSKI, JAN K. SNAKOWSKI

Institute of Physics, WSP Rzeszów (35-311 Rzeszów, ul. Rejtana 16a)

This paper presents calculations for plane wave diffraction by a right-angled wedge. Using the UFIMTSEV and OBERHETTINGER'S theoretical approach, formulae are obtained for the diffracted field potential on the shaded wall of the wedge in the form of a series of cylindrical functions and a real integral. Some results of numerical calculations are also presented.

1. Introduction

More and more attention has been paid recently to the problems in the field of the applications of the theory of acoustic wave diffraction in the protection of the environment and of working posts. This field includes research related to all kinds of acoustic protecting devices, investigation of intensity decrease in rooms etc.

The present paper aims to discuss the following problem: to what extent one wall of a wedge (e.g. the corner of a building) is affected by a sound wave which propagates along the other wall (Fig. 1). The evident theoretical basis is here the theory of wave diffraction by a wedge of which the present problem is a special case.

Since it is impossible to find a compact solution of the problem of diffraction by a wedge, three theoretical approaches have been formulated to date:

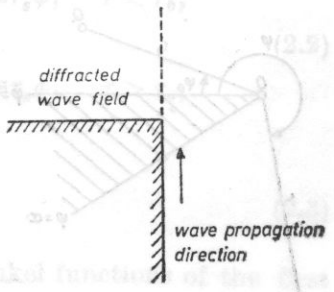

Fig. 1. A schematic diagram of the right-angled wedge

1) of SOMMERFELD [8, 9] which can be briefly summarized by saying that it uses the image source method and such a conformal transformation that straightens the wedge to a plane. This leads to an integral in a complex plane, which can be subsequently expanded into a series or calculated directly in a numerical way;

2) of OBERHETTINGER [4] which consists in relevant integral transformations of the function representing the incident wave and the diffracted wave, and subsequently in summing up of the two waves so that the boundary conditions on the wedge are satisfied. In turn, there follows an expansion into a series whose coefficients are found from these boundary conditions. An advantage of the OBERHETTINGER method is the interesting proposal of this author that an imaginary frequency should be formally introduced, thus simplifying the necessary mathematical operations and permitting a transition to pulses;

3) of UFIMTSEV [1] which proceeds in a direction different from those of the other two in that it assumes the acoustic potential in the form of a series and shows subsequently that it can be summed into a SOMMERFELD integral.

The initial part of the present paper is based on the UFIMTSEV theory, or rather part of it, which is adapted here to the present purposes and the mathematical part of which is developed later on.

2. Formulation of the problem and its analytical solution

The starting point are general formulae for the acoustic field of a wave diffracted by a wedge. The geometry of the wedge is shown in Fig. 2. It is possible to take a system of the cylindrical coordinates (r, φ, z) in which the axis z is perpendicular to the plane of the figure, the pole is placed at a point which is the trace of the point of the wedge on the plane of the figure and the angle φ is measured in a positive direction from the "upper" edge of the wedge. The source of the wave is a "thread" that is a straight line with densely set points radiating a cylindrical wave. Fig. 1 shows the trace of this straight line in the form of the point Q with the coordinates r_0 and φ_0. The desired field is sought at the point P with the coordinates r and φ. It is possible to begin with a formulation

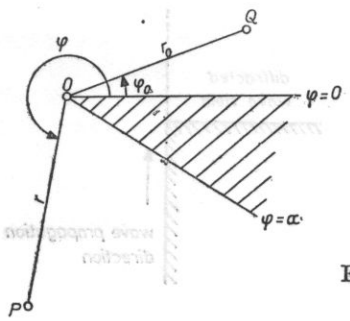

Fig. 2. Geometry of the problem of diffraction by a wedge in general case

of the general formulae and proceed subsequently to the limit $r_0 \to \infty$. This transition does not have to give, as UFIMTSEV proposed in [1], an exact value of the acoustic field potential for a plane wave, which can be certain only when diffraction by an object of finite dimensions is considered. In the case of an infinite edge it is possible to obtain a solution which can be used at relatively long distances from the edge of the wedge. It is interesting to add here that other works of the present authors in progress show that the point source field in space gives, in the case of the wedge, different expressions for the transition $r_0 \to \infty$ but both expressions agree for $r \to 0$.

Bearing in mind the fact that a cylindrical model of plane wave is used here, it is possible to proceed in the later part to the value $\alpha = \varphi = 3/2$. It is also possible to assume simultaneously the harmonic time dependence in the form $\exp(-\omega t)$. In the present case the boundary condition is the assumption that the walls of the wedge are perfectly rigid and therefore the acoustic pontential must satisfy the boundary conditions

$$\frac{\partial \Phi}{\partial \varphi} = 0 \quad \text{for } \varphi = 0 \text{ and } \varphi = \alpha. \tag{2.1}$$

It is known [2, 5, 6] that a solution of the Helmholtz equation for the acoustic potential in a cylindrical system of coordinates can have the form of a sum of terms, i.e. of the product of cylindrical and trigonometric functions, where the order of the cylindrical function must be equal to the coeficient for the angle φ in the argument of the trigonometric function. The basic solution of the Helmholtz equation should be the sum of components containing Hankel functions of the first kind (which is related to the assumption of the dependence $\exp(-i\omega t)$) and cosines. For $r = 0$, however, the Hankel function has a discontinuity of the type of $-\infty$ and therefore only the real part, i.e. the Bessel function, can be assumed. It is convenient to break the solution into two intervals: the Bessel function must occur for $r < r_0$ and the Hankel function for $r > r_0$. In order to make the solution continuous for $r = r_0$, the first solution must be multiplied by the Hankel function of r_0 and the other, by the Bessel function of r_0. This gives the solution in the form of the following series

$$\Phi(r, \varphi) = \begin{cases} \sum_{s=0}^{\infty} c_s J_{r_s}(kr) H_{r_s}^{(1)}(k r_0) \cos r_s \varphi_0 \cos r_s \varphi, & r < r_0, \\ \sum_{s=0}^{\infty} c_s J_{r_s}(kr_0) H_{r_s}^{(1)}(k r) \cos r_s \varphi_0 \cos r_s \varphi, & r > r_0, \end{cases} \tag{2.2}$$

where

$$r_s = s \frac{\pi}{\alpha}, \tag{2.3}$$

and J_{r_s} and $H_{r_s}^{(1)}$ denote, respectively, Bessel and Hankel functions of the first kind, of the order r_s. The choice of $H_{r_s}^{(1)}$ is, as was mentioned above, related to

the choice of the time factor in the form $\exp(-i\omega t)$ [2, 6]. It can be seen from (2.2) and (2.3) that for $\varphi = 0$ and $\varphi = \alpha$ all the terms of the derivative $\partial\Phi/\partial\varphi$ become zero, thus satisfying the boundary condition (2.1).

The coefficients c_s can now be calculated. This can be done applying the identity

$$\iint_s \frac{\partial \Phi}{\partial \overline{n}}\, ds = \iiint_V \Delta\Phi dV \tag{2.4}$$

to a solid with its base limited by the contour L (Fig. 3) and the thickness dz. For $\Phi = \Phi(r, \varphi)$

$$\oint_L \frac{\partial \Phi}{\partial \overline{n}}\, dl = \int_s \Delta\Phi d\sigma. \tag{2.5}$$

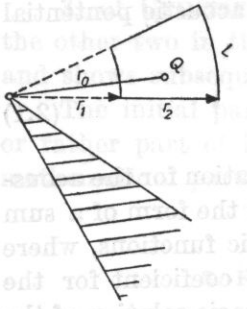

Fig. 3. Integration contour in formula (2.5)

Transition to the limit $r_1 \to r_0$ and $r_2 \to r_0$ gives

$$\int \left(\left.\frac{\partial \Phi}{\partial r}\right|_{r_0+0} - \left.\frac{\partial \Phi}{\partial r}\right|_{r_0-0} \right) r_0 d\varphi = \int_{s\to 0} \Delta\Phi d\sigma. \tag{2.6}$$

In the case of a linear source in space, and in the present case, of the point source Q, the acoustic potential must satisfy the inhomogeneous Helmholtz equation in the form [1, 5]

$$\Delta\Phi + k^2\Phi = A\,\frac{\delta(r-r_0, \varphi-\varphi_0)}{r}, \tag{2.7}$$

where A is a constant which can be normalized subsequently to the effectiveness of the source; $\delta(\ )$ is a Dirac distribution which when multiplied by r provides the integration properties of this distribution in a cylindrical coordinate system. In calculating $\Delta\Phi$ from equation (2.7), in order to substitute it on the right side of (2.6), it should be borne in mind that for $s \to 0$ integration of the term containing Φ gives a result tending to zero and that an integral containing the Dirac distribution δ only remains. Thus, from equation (2.6)

$$\int \left(\left.\frac{\partial \Phi}{\partial r}\right|_{r_0+0} - \left.\frac{\partial \Phi}{\partial r}\right|_{r_0-0} \right) r_0 d\varphi = A \lim_{r\to 0} \int_{s\to 0} \frac{\delta(r-r_0)\,\delta(\varphi-\varphi_0)}{r}\, r dr d\varphi. \tag{2.8}$$

Integration with respect to the variable r gives

$$\int \left(\left.\frac{\partial \Phi}{\partial r}\right|_{r_0+0} - \left.\frac{\partial \Phi}{\partial r}\right|_{r_0-0} \right) r_0 d\varphi = \frac{A}{r_0} \int \delta(\varphi - \varphi_0) r_0 d\varphi . \tag{2.9}$$

Since the size of the contour L is fully arbitrary, the identity of the integrals in formula (2.9) involves the equality of the integrands and thus

$$\left.\frac{\partial \Phi}{\partial r}\right|_{r_0+0} - \left.\frac{\partial \Phi}{\partial r}\right|_{r_0-0} = \frac{A}{r_0} \delta(\varphi - \varphi_0) . \tag{2.10}$$

It is possible to substitute on the left side of formula (2.10) the corresponding formula for Φ with $r < r_0$ and $r > r_0$, i.e. the first and second formulae of (2.2). Because of their complex form it is best to consider a single component of the sum first. Marking with a dash the integration with respect to the whole parameter under a cylindrical function, this gives

$$kc_s J_{r_s}(kr_0) H^{(1)\prime}_{r_s}(kr_0) - kc_s J'_{r_s}(k r_0) H^{(1)}_{r_s}(kr_0) = \\ = kc_s W\left[J_{r_s}(kr_0), H^{(1)}_{r_s}(kr_0) = kc_s \frac{2i}{\pi k r_0} \right], \tag{2.11}$$

where W is a wronskian which for the functions $J_{r_s}(kr_0)$ and $H^{(1)}_{r_s}(kr_0)$ has the form of (2.11) (cf. [7], p. 68). Formula (2.10) takes now the form

$$\frac{2i}{\pi r_0} \sum_{s=0}^{\infty} c_s \cos(r_s \varphi_0) \cos(r_s \varphi) = \frac{A}{r_0} \delta(\varphi - \varphi_0) . \tag{2.12}$$

Both sides of (2.12) can be divided by $r_0 \cos(r_s \varphi)$ and integrated with respect to φ in the interval from 0 to α. Since this interval must contain the value φ_0, the right side becomes $A r_0^{-1} \cos(r_t \varphi_0)$. On the left side, however, because of the orthogonality of the system of the function $\cos(r_s \varphi)$, integration of the particular terms leads to their value of zero, except the term containing $s = t \neq 0$. Thus

$$\frac{2i}{\pi} c_t \cos(r \varphi_0) \int_0^{\alpha} \cos^2(r_t \varphi) d\varphi = A \cos(r_t \varphi_0), \tag{2.13}$$

i.e.

$$c_t = \frac{A\pi}{i\alpha} . \tag{2.14}$$

It can be seen that the coefficient c_s is constant for all $s \neq 0$. For $s = 0$, however, $\cos(r_s \varphi) = 1$, i.e. it can be noted easily that integration of the left side of (2.13) gives a result greater by a factor of two than before. It can thus be written jointly,

$$c_s = \varepsilon_s \frac{A\pi}{i\alpha} , \tag{2.15}$$

where the symbol ε_s takes the values

$$\varepsilon_s = \begin{cases} \frac{1}{2}, & s = 0, \\ 1, & s \neq 0. \end{cases} \tag{2.16}$$

The formula for the potential becomes

$$\Phi(r, \varphi) = \begin{cases} \frac{A\pi}{ia} \sum_{s=0}^{\infty} \varepsilon_s J_{r_s}(kr) H_{r_s}^{(1)}(kr_0) \cos(r_s\varphi_0) \cos(r_s\varphi), & r < r_0, \\ \frac{A\pi}{ia} \sum_{s=0}^{\infty} \varepsilon_s J_{r_s}(kr_0) H_{r_s}^{(1)}(kr) \cos(r_s\varphi_0) \cos(r_s\varphi), & r > r_0. \end{cases} \tag{2.17}$$

Proceeding to the problem of a plane wave propagating along one of the walls of the wedge (with the qualification given above), the transition $r_0 \to \infty$ must first be considered. The following asymptotic formula can then be used for $H_{r_s}^{(1)}(kr_0)$ [2, 7],

$$H_{r_s}^{(1)}(kr_0) = \sqrt{\frac{2}{\pi k r_0}} \exp\left[i\left(kr_0 - \frac{\pi}{4} - \frac{\pi}{2} r_s\right)\right] = H_0^{(1)}(kr_0) \exp\left(-i\frac{\pi}{2} r_s\right). \tag{2.18}$$

What remains is only the acoustic field for $r < r_0$ and thus

$$\Phi(r, \varphi) = \frac{A\pi}{2ia} H_0^{(1)}(kr_0) \sum_{s=0}^{\infty} \varepsilon_s \exp\left(-i\frac{\pi}{2} r_s\right) J_{r_s}(kr) [\cos r_s(\varphi - \varphi_0) + \cos r_s(\varphi + \varphi_0)]. \tag{2.19}$$

In the case of a cylindrical wave source in a free space, the potential at a given point must be proportional to the function $H_0^{(1)}(kr_0)$ where r_0 is the distance of this point from the source. In the case when $kr_0 \gg l$ and $kr_0 \gg kr$ it can be assumed that for an arbitrary value of r the distance PQ (Fig. 2), which in reality is

$$PQ = (r^2 + r^2 - 2r\, r_0 \cos(\varphi - \varphi_0))^{1/2} \tag{2.20}$$

can be taken for r_0. It can certainly be so assumed for a plane wave which corresponds to an infinitely great value of r_0. In general, the acoustic potential can be given by

$$\Phi(r, \varphi) = F[u(r, \varphi - \varphi_0) + u(r, \varphi + \varphi_0)], \tag{2.21}$$

where F is the amplitude of the free wave and the function u represents the diffraction phenomena.

Approximately, for large values of $kr_0 \gg kr$, for a cylindrical wave

$$F = \frac{A}{i} H_0^{(1)}(k\, r_0), \tag{2.22}$$

while for a plane wave from the direction of φ_0

$$\Phi_0 = A_0 \exp[-ikr\cos(\varphi-\varphi_0)] \tag{2.23}$$

and the acoustic potential of a diffracted wave can be represented in the form of the product of the amplitude A_0 and the function u, as in (2.21). In turn, the function defining the diffraction phenomena is equal to (when ψ denotes the value $\varphi-\varphi_0$ or $\varphi+\varphi_0$)

$$u(r, \psi) = \frac{\pi}{2a} \sum_{s=0}^{\infty} \varepsilon_s \exp\left(-i\frac{\pi}{2} r_s\right) J_{r_s}(k\,r)\cos(r_s\psi). \tag{2.24}$$

It should be stressed that for $r\to 0$ $J_{r_s}(k\,r) = 0$, except for $s = 0$, since $J_0(0) = 1$. Therefore in the limits (for an arbitrary value of φ)

$$u(0, \psi) = \frac{\pi}{4a}. \tag{2.25}$$

Formula (2.23) permits, if necessary, the constant A_0 to be normalized to the output of the source for a plane wave. This problem is not considered here in view of the aim of the present paper, i.e. a calculation of a decrease in the amplitude along the wall of the wedge. It is interesting to note, however, that it is useless to check here whether the solution assumed satisfies the so-called edge condition since UFIMTSEV himself reduces the results of his theory to a SOMMERFELD integral [8, 9] whose properties have been investigated in this respect.

3. The case of a plane wave propagating along the wall of the edge — the potential in the form of a series

Returning to the case of interest shown in Fig. 2 when the plane wave propagates along one of the walls of the wedge, and the interest here is in the acoustic field on the other wall, the following values occur in the formulae in section 2

$$\varphi_0 = 0, \qquad \varphi = a = \frac{3\pi}{2}. \tag{3.1}$$

The index of the Bessel function under the sign of sum is now

$$r_s = s\frac{\pi}{a} = \frac{2}{3}s. \tag{3.2}$$

Since for the values of the angles assumed

$$\varphi-\varphi_0 = \varphi+\varphi_0, \tag{3.3}$$

the difference $\varphi - \varphi_0$ or the sum $\varphi + \varphi_0$, symbolically represented by ψ, can in the present case be reduced to one value

$$\psi = \varphi = \alpha = \frac{3\pi}{2}, \tag{3.4}$$

i.e. the factor 2 occurs in the formula for Φ. Thus

$$\Phi(r) = \frac{2A_0}{3} \sum_{s=0}^{\infty} (-1)^s \varepsilon_s \exp\left(-i\frac{\pi}{3}s\right) J_{2s/3}(kr). \tag{3.5}$$

This gives $\Phi(r)$ in the form of a rapidly convergent series of Bessel functions.

Before making numerical calculations and drawing conclusions from the theory given here, it is useful to present a completely different approach to the same problem, which leads to an integral form of the expression for the potential Φ.

4. Integral expression for the potential

In order to reduce equation (2.24) to an integral form, it is possible to use the purely formal transition to an imaginary wave number, proposed by OBERHETTINGER [4], in the form

$$k = i\gamma, \tag{4.1}$$

and thus passing to the so-called modified Bessel functions. On the basis of the known relation for these functions ([3], 6.406),

$$I_\nu(z) = \exp\left(-\nu\frac{\pi}{2}i\right) J_\nu\left(z\exp\left(\frac{\pi}{2}i\right)\right), \tag{4.2}$$

it is possible to rewrite formula (2.24) in the form

$$u(r, \varphi) = \frac{\pi}{2a} \sum_{s=0}^{\infty} \varepsilon_s I_{r_s}(\gamma r)\cos(r_s \psi). \tag{4.3}$$

In accordance with the aim of the present paper, it is possible to assume the boundary case $kr_0 \to \infty$, i.e. formula (2.22) and that $\varphi_0 = 0$, and retaining still the arbitrary value of the angle, it is possible to write

$$\Phi(r, \varphi) = \frac{\pi}{a} \sum_{s=0}^{\infty} \varepsilon_s I_{s\pi/a}(\gamma r)\cos\left(\frac{s\pi}{a}\varphi\right). \tag{4.4}$$

An integral representation of the modified Bessel function $I_p(z)$ ([3], 6.443)

can now be used,

$$I_p(z) = \frac{1}{\pi}\int_0^{\pi} \exp(z\cos x)\cos(px)\,dx - \frac{\sin(p\pi)}{\pi}\int_0^{\infty} \exp(-z\,ch\,x)\exp(-px)dx. \quad (4.5)$$

Inserting expression (4.5) into (4.4), two modifications of this formula can be performed simultaneously: the order of summation and integration can be changed and summation can be performed up to an arbitrary finite N and then from N to infinity. This gives

$$a\Phi(r,\varphi) = \lim_{N\leftarrow\infty}\int_0^{\pi} \exp(\gamma r\cos x)\left\{\sum_{s=0}^{N}\varepsilon_s\cos\left(\frac{s\pi}{a}x\right)\cos\left(\frac{s\pi}{a}\varphi\right)\right\}dx +$$

$$-\int_0^{\infty}\exp(-\gamma r\,ch\,x)\left\{\sum_{s=0}^{\infty}\varepsilon_s\cos\left(\frac{s\pi}{a}\varphi\right)\sin\left(\frac{s\pi^2}{a}\right)\exp\left(-\frac{s\pi}{a}x\right)\right\}dx =$$

$$\stackrel{\mathrm{df}}{=} \lim\int_0^{\infty}\exp(\gamma r\cos x)s_1(x,\varphi)\,dx - \int_0^{\infty}\exp(-\gamma r ch x)s_2(x,\varphi)\,dx. \quad (4.6)$$

The sums s_1 and s_2 in formula (4.6) can now be calculated. The first calculation, using elementary trigonometric formulae, gives the sum s_1 in the form

$$s_1 = \sum_{s=0}^{N}\varepsilon_s\left[\cos\frac{s\pi(x+\varphi)}{a} + \cos\frac{s\pi(x-\varphi)}{a}\right]. \quad (4.7)$$

The two sums on the right side of formula (4.7) can be gathered by means of a known formula ([3], 1.341.2), giving

$$s_1 = \frac{1}{2}\left\{\frac{\sin\left(\frac{\pi}{2a}(2N+1)(x+\varphi)\right)}{\sin\left(\frac{a}{2\pi}(x+\varphi)\right)} + \frac{\sin\left(\frac{\pi}{2a}(2N+1)(x-\varphi)\right)}{\sin\left(\frac{\pi}{2a}(x-\varphi)\right)}\right\}. \quad (4.8)$$

The components of the first expression tend in the limits for $N\to\infty$ to the Dirac distribution δ if the argument $x+\varphi$ and $x-\varphi$ [5]. It can be noted that when $\varphi > \pi$, the first of the integrals in (4.6) disappears, since the two values fall outside the integration interval.

In turn, the second sum in (4.6) can be transformed into the form

$$s_2 = \sum_{s=0}^{\infty}\varepsilon_s\exp\left(-s\frac{\pi}{a}x\right)\left[\sin\frac{s\pi(\pi+\varphi)}{a} + \sin\frac{s\pi(\pi-\varphi)}{a}\right] =$$

$$= \sum_{s=0}^{\infty}\exp\left(-s\frac{\pi}{a}x\right)\sin\frac{s\pi(\pi+\varphi)}{a} + \sum_{s=1}^{\infty}\exp\left(-s\frac{\pi}{a}x\right)\sin\frac{s\pi(\pi-\varphi)}{a}. \quad (4.9)$$

Using a relevant formula ([3], 1.461), it is possible to write that

$$s_2 = \frac{1}{2}\left(\frac{\sin\left(\frac{\pi}{\alpha}(\pi+\varphi)\right)}{ch\frac{\pi}{\alpha}x - \cos\left(\frac{\pi}{\alpha}(\pi+\varphi)\right)} + \frac{\sin\left(\frac{\pi}{\alpha}(\pi-\varphi)\right)}{ch\frac{\pi}{\alpha}x - \cos\left(\frac{\pi}{\alpha}(\pi-\varphi)\right)} \right). \tag{4.10}$$

The form of the sum can now be determined for the case of interest when $\varphi = \alpha = \frac{3}{2}\pi$. Substitution and calculation of the values of the relevant trigonometric functions give

$$s_2 = -\frac{\sqrt{3}}{2}\frac{1}{ch\frac{2}{3}x - \frac{1}{2}}. \tag{4.11}$$

Substitution of this result into (4.6) and consideration that the first integral disappears lead to

$$\Phi\left(r, \frac{3}{2}\pi\right) = \frac{1}{\sqrt{3}\pi}\int_0^\infty \frac{\exp(-\gamma r ch x)}{ch\frac{2}{3}x - \frac{1}{2}}dx. \tag{4.12}$$

It is necessary to return now to the real value of the wave number k, assuming in formula (4.12) that $\gamma = -ik$ (cf. (4.1)). This gives the final formula which expresses in integral form the acoustic potential along the wall of the edge

$$\Phi\left(r, \frac{3}{2}\pi\right) = \frac{1}{\sqrt{3}\pi}\int_0^\infty \frac{\exp(ikr\,ch\,x)}{ch\frac{2}{3}x - \frac{1}{2}}dx. \tag{4.13}$$

The integral obtained on the real semi-axis is a rapidly converging one and, in addition to (3.5), can be used to calculate the diffracted field of a plane wave on the wall of the wedge.

5. Conclusions

On the basis of the final formula (4.13), which gives in integral form the expression for the acoustic potential of a plane wave diffracted by a right-angled wedge, numerical calculations were made of the squared value of the modulus of the sound pressure on the wall of the wedge. The following formula which is valid in the case of a harmonic time dependence was used

$$|p| = \varrho\omega|\Phi|. \tag{5.1}$$

The results of the numerical calculations are given in Figs. 4 and 5. Fig. 4 shows, in dB, a decrease in the sound pressure on the wedge as a function of the relative distance $kr = 2\pi r/\lambda$ (lower curve) and, for comparison, for a spherical wave (dashed curve). Since the source of a spherical wave, placed on the edge of the wedge, would have to show there an infinite value of the sound pressure, therefore in this case its value at a point where $kr = l$ was assumed

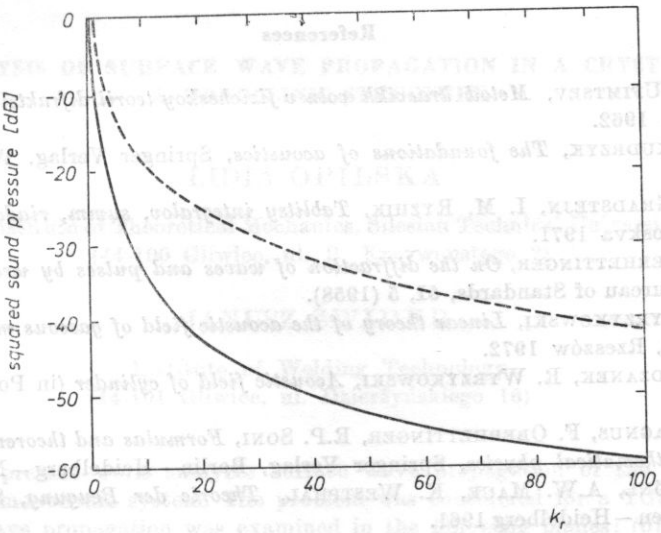

Fig. 4. Drop of the level of the squared modulus of sound pressure along the shaded wall of the right-angled wedge as a function of the normalized distance from the edge (solid line), compared with the curve characteristic of a spherical wave (dashed line)

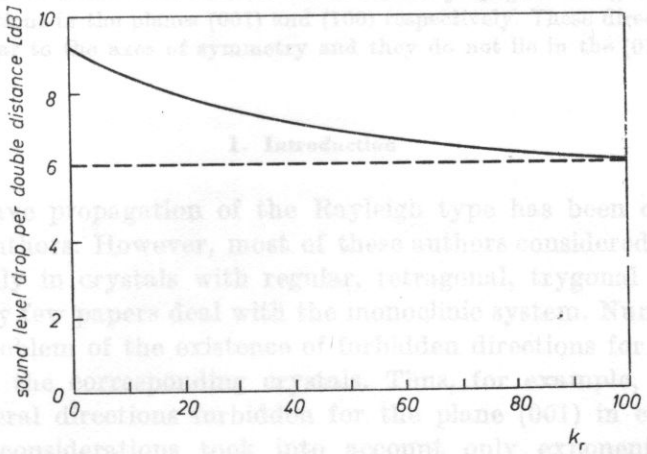

Fig. 5. Drop in the level of the squared modulus of sound pressure along the shaded wall of the right-angled wedge per double distance (solid line), compared with the value characteristic of a spherical wave (dashed line)

as the reference point. Fig. 5 shows a drop in the sound pressure per double distance as a function of a double distance.

It can be seen in the two diagrams that the sound pressure on the wedge decreases initially at a much faster rate than that for a spherical wave and subsequently stabilizes on the level characteristic for a spherical wave.

References

[1] P.Y. UFIMTSEV, *Metod kraevikh voln v fizicheskoy teorii difraktsii*, Izd. Sovetskoe Radio, Moskva 1962.

[2] E. SKUDRZYK, *The foundations of acoustics*, Springer Verlag, Wien – New York 1971.

[3] I.S. GRADSTEJN, I. M. RYZHIK, *Tablitsy integralov, summ, riadov i proizvedenij*, Izd. Nauka, Moskva 1971.

[4] F. OBERHETTINGER, *On the diffraction of waves and pulses by wedges and corners*, J. Res. Natl. Bureau of Standards, **61**, 5 (1958).

[5] R. WYRZYKOWSKI, *Linear theory of the acoustic field of gaseous media* (in Polish), RTPN – WSP, Rzeszów 1972.

[6] W. RDZANEK, R. WYRZYKOWSKI, *Acoustic field of cylinder* (in Polish), WSP Rzeszów 1972.

[7] W. MAGNUS, F. OBERHETTINGER, R.P. SONI, *Formulas and theorems for the special functions of mathematical physics*, Springer Verlag, Berlin – Heidelberg – New York 1966

[8] H. HÖNL, A.W. MAUE, K. WESTPHAL, *Theorie der Beugung*, Springer Verlag Berlin – Gottingen – Heidelberg 1961.

[9] A. SOMMERFELD, *Optik*, Akademische Verlagsgesellschaft, Leipzig 1964.

Received on June 25, 1980; revised version on September 28, 1981.

ARCHIVES OF ACOUSTICS
7, 2, 155-162 (1982)

THE ANALYSIS OF SURFACE WAVE PROPAGATION IN A CRYSTAL WITH A MONOCLINIC STRUCTURE

LIDIA OPILSKA

Institute of Theoretical Mechanics, Silesian Technical University
(44-100 Gliwice, ul. B. Krzywoustego 2)

JANUSZ ŚWIDER

Institute of Welding Technology
(44-101 Gliwice, ul. Dzierżyńskiego 16)

The present work analyzes surface wave propagation of the Rayleigh type in a monoclinic system. The problem was considered for a TGS crystal. Surface wave propagation was examined in the following planes: (010) in the ⟨100⟩, ⟨001⟩ directions and in some chosen directions forming angles 20°, 40°, 60°, 130°, 150°, 170°, 180° corresponding to the ⟨100⟩ direction, (100) in ⟨010⟩, ⟨001⟩ directions, and (001) in ⟨100⟩ and ⟨010⟩ directions. The above analysis was made using an electronic computation technique. As a result of our calculations we have found that surface waves cannot propagate along ⟨100⟩ and ⟨001⟩ directions in the planes (001) and (100) respectively. These directions are perpendicular to the axes of symmetry and they do not lie in the (010) plane.

1. Introduction

Surface wave propagation of the Rayleigh type has been considered by a number of authors. However, most of these authors considered surface wave propagation only in crystals with regular, tetragonal, trygonal or hexagonal symmetry. Very few papers deal with the monoclinic system. Numerous papers consider the problem of the existence of forbidden directions for surface wave propagation in the corresponding crystals. Thus, for example, STONLEY [1] discovered several directions forbidden for the plane (001) in cubic crystals. However, his considerations took into account only exponential terms of damping. GAZIS [2] calculated the velocities of surface wave propagation for a free surface in the (001) plane of many cubic crystals. Moreover, he proved that for aluminium and copper, surface waves do not exist in the range of ⟨110⟩ direc-

tions. BUCHWALD and DAVIS [3] show that surface waves in anisotropic media are possible only if the free plane is a symmetry plane of the crystal. In a medium with cubic symmetry surface wave propagation is possible only in the planes (001) and (100). Their calculations show the ranges of a forbidden direction: ⟨100⟩ in the (001) plane of aluminium, iron and lead. In their paper [4] other authors prove that in all cubic crystals surface waves cannot propagate in the (001) plane. The criterion given (necessary but not sufficient) for surface wave propagation has the following form: $c_{11}(c_{11}-c_{44}) > (c_{12}+c_{44})^2$.

Computations of a similar nature for LiF and Cu have been published by TURSONOV [5], who showed that the direction ⟨110⟩ in the (001) plane is forbidden for surface wave propagation. The author presents the results of numerical computations for LiF, for a propagation direction forming an angle of 15° with the axis, x_1, of the coordinate system.

The problem of the existence of the forbidden directions for regular systems has mainly been considered. Our aim was to investigate this problem in a crystal with a monoclinic structure. It was performed for a TGS crystal.

2. Calculation procedure

The general surface wave problem is formulated by assuming that the equation of motion is given by

$$\varrho \frac{\partial^2 u_i}{\partial t_2} = c_{ijkl} \frac{\partial^2 u_k}{\partial x_i \partial x_l}, \tag{1}$$

where ϱ is the density of the material, u_i are the particle displacements and c_{ijkl} is the the elastic stiffness tensor.

For example the solution of equation (1) for the (010) plane is as follows

$$u_i = \sum_{n/1}^{3} C_n a_i^{(n)} \exp\left[ik(l_1 x_1 + l_2 x_2 + l_3^{(n)} x_3 - vt)\right], \tag{2}$$

where a_i is the amplitude of the wave, depending on polarization, $\exp(ikl_3^{(n)} x_3)$ is the factor assuring the properties of a surface wave, l_3 is the parameter which characterizes the wave decaying into the depth of the solid, and $\exp[ik(l_1 x_1 + l_2 x_2 - vt)]$ is the change of amplitude in time and space, as it is in case of bulk wave.

Substituting equation (2) into (1) the relation between a and k is obtained. Using the stress-free boundary conditions on $x_3 = 0$,

$$\sigma_{3j} = c_{3jkl} \frac{\partial u_k}{\partial x_l} = 0 \quad (j, k, l = 1, 2, 3), \tag{3}$$

the parameters a_1, a_2, a_3, the velocity of surface wave, and also the vector components of the particle displacements were obtained.

In this work an analysis of surface wave propagation for the TGS crystal in the three following planes has been made: (010), (100) and (001). In the plane (010), the propagation of the surface wave was analyzed along the ⟨100⟩ and ⟨001⟩ directions and in the directions which form angles of 20°, 40°, 60°, 120°, 150°, 170°, 180° with the ⟨100⟩ direction. In both remaining cases our calculations were made in the (001) plane in the ⟨100⟩, ⟨001⟩ directions and in the (100) plane along the ⟨010⟩, ⟨001⟩ directions.

The coordinate system assumed for surface waves is presented in Fig. 1, where a, b, c are the crystallographic axes of the TGS monocrystal, x_1, x_2, x_3 are the axes of an orthogonal system with respect to which surface wave propagation has been considered. The above calculations were made by applying an electronic computation technique using an ODRA 1305 computer. The values of the velocity as a parameter were changed with a step of ± 0.4 m/s.

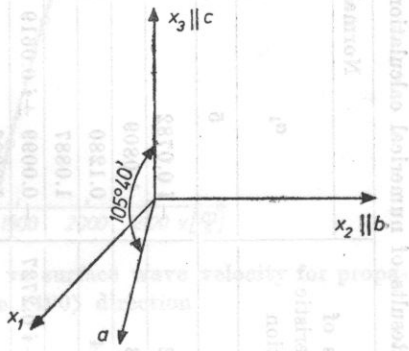

Fig. 1. Coordinate system for surface wave propagation in TGS crystal

3. Calculation results

Table 1 presents the values obtained for the surface wave propagation velocity, the roots of the characteristic equation, the normalized values of the eigenvector, and the values of the boundary condition determinant for the surface wave propagation directions considered in the present work. Fig. 2 presents, as example, the magnitude of the boundary condition determinant of surface propagation velocity in the (010) plane along the ⟨100⟩ direction. Fig. 3 shows the dependence of the surface wave propagation velocity on the direction in the (010) plane.

Moreover, the components of the particle displacement along the directions determined by the axes of the coordinate system have been calculated. These components in the (010) plane in the ⟨100⟩ direction are as follows:

$$u_1 = C_1[0.0782 \exp(0.127\, kx_2) - 0.429 \exp(1.0035\, kx_2) - \\ - 0.0166 \exp(0.0308\, kx_2)] \sin k(x_1 - vt), \qquad (4a)$$

Table 1. Results of numerical calculations

Plane	Direction of surface wave propagation	$V\left[\frac{m}{s}\right]$	D_{min}	Roots of characteristic equation	Normalized values of eigenvectors		
					a_1	a_2	a_3
1	2	3		4	5	6	7
(010) (001) (100)	⟨100⟩	1875.2	0.04	$-i$ 0.12762	$-i$ 0.0782	−1.0035	$-i$ 0.0308
				$-i$ 1.90833	− 1.0809	i 0.4145	0.0588
				− i 0.71644	0.1280	− i 0.1032	0.9974
	20°	1868.0	0.11	− i 1.7437	1.0887	− i 0.4315	0.0316
				± 0.1243 − i 0.2727	−0.0099 ± i 0.0619	±0.8898 − i 0.2719	0.6515 ± i 0.3724
	40°	1704.0	0.02	$-i$ 1.4812	1.0906	$-i$ 0.4383	0.0531
				± 0.3839 − i 0.1430	−0.1777 ∓ i 0.0587	∓ 0.6304 − i 0.0089	0.7583 ∓ i 0.0212
	60°	1664.0	0.12	$-i$ 1.1505	−1.0506	±0.3238	0.0323
				± 0.5795 − i 0.1811	−0.1132 ∓ i 0.0688	∓ 0.6965 − i 0.0340	0.7140 ∓ i 0.0441
	⟨001⟩	1726.0	0.21	$-i$ 1.04933	− 1.0053	$-i$ 0.2122	0.1853
				± 0.6595 − i0.2026	0.3423 ± i 0.0308	∓ 0.6929 − i 0.04423	0.6402 ∓ i 0.0644
	130°	1926.0	0.45	$-i$ 1.6245	−1.05982	$-i$ 0.4660	0.3065
				± 0.3179 − i 0.1567	0.4620 ∓ i 0.0510	± 0.5704 ∓ i 0.0079	0.6816 + i 0.0280
	150°	1999.2	0.46	$-i$0.2156	$-i$ 0.0343	− 1.0582	$-i$ 0.3443
				$-i$ 1.8323	−1.06635	$-i$ 0.4371	0.2323
				$-i$ 0.4772	0.3993	$-i$ 0.6879	1.1462
	170°	1903.2	0.30	$-i$ 0.1277	i0.0705	− 1.0027	$-i$ 0.0234
				$-i$ 1.9258	−1.0765	$-i$ 0.4152	0.1158
				$-i$ 0.7460	0.2013	$-i$ 0.0466	0.9806
	⟨010⟩	1810.0	0.10	$-i$ 0.2506	−1.0000	i 0.0065	0.0019
				± 0.7638 − i 0.2999	0.3009 ± i0.0187	±0.5878 + i 0.0907	0.7592 ± i 0.0628
	⟨010⟩	1868.0		$-i$ 0.1147	1.0031	i 0.1027	0.0655
				$-i$ 1.5071	i 0.3699	− 1.0682	i 0.0661
				$-i$ 0.5760	0.0738	i 0.0264	0.9976

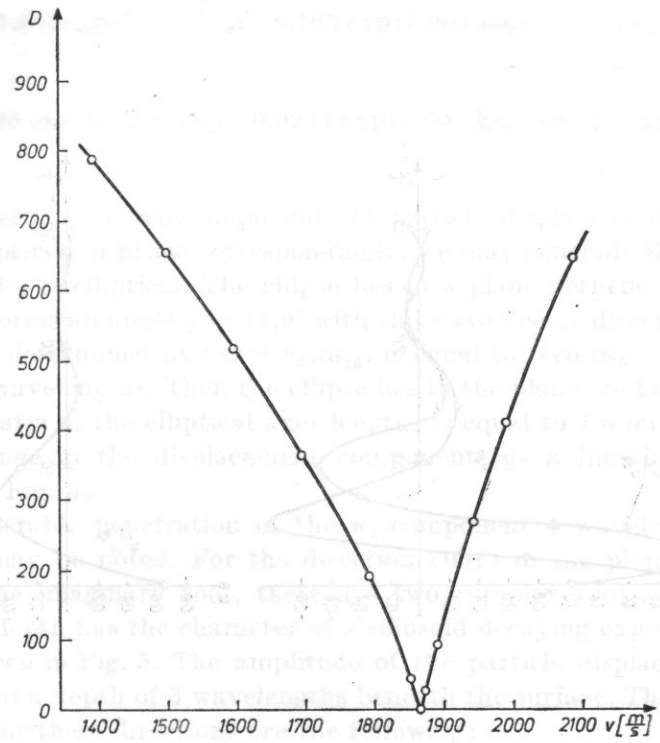

Fig. 2. Magnitude of boundary - condition determinant vs surface wave velocity for propagation in the (010) plane along the ⟨100⟩ direction

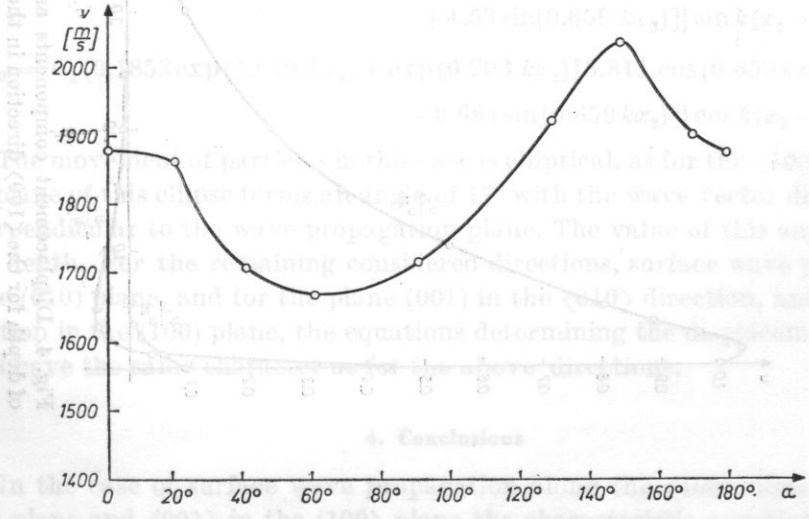

Fig. 3. Dependence surface wave velocity on the direction for the (010) plane

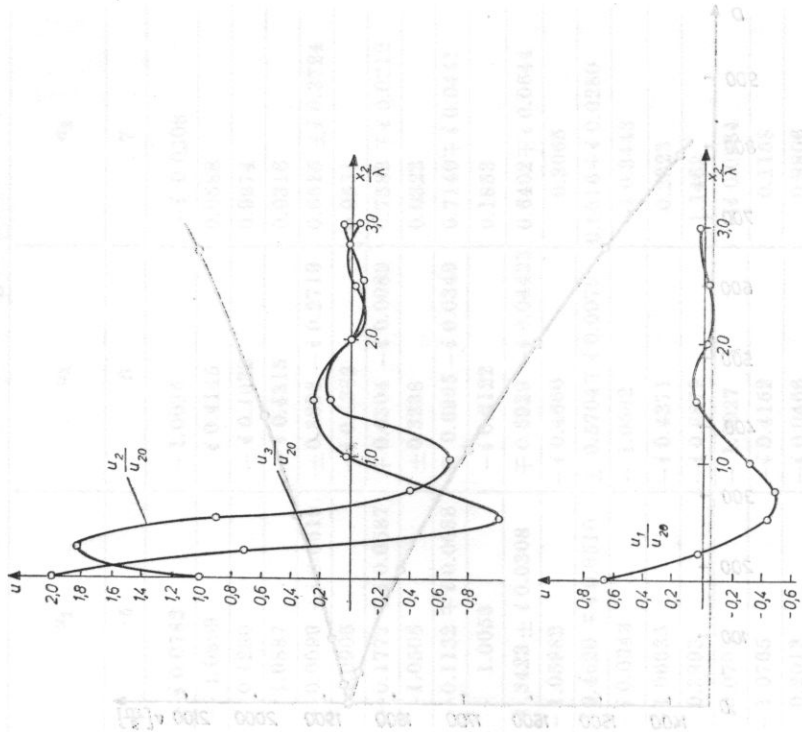

Fig. 5. Displacement components as a function of depth for the ⟨001⟩ direction in the (010) plane

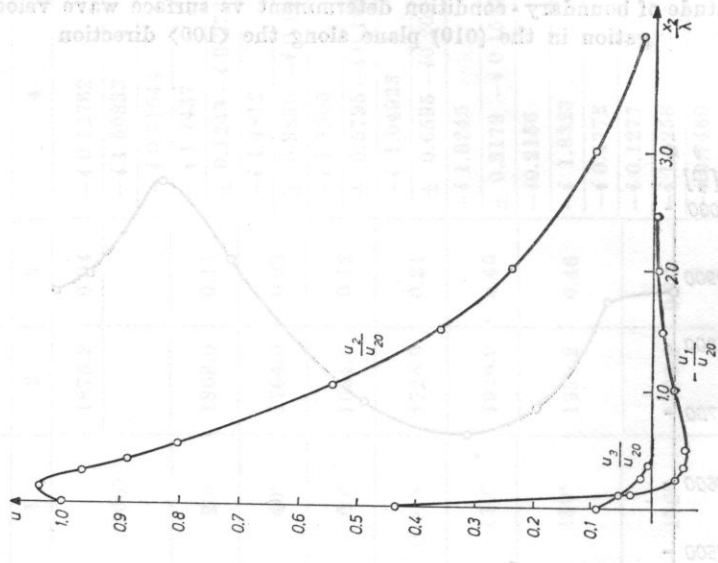

Fig. 4. Displacement components as a function of depth for the ⟨100⟩ direction in the (010) plane

$$u_2 = C_1[1.003\exp(0.127\ kx_2) - 0.165\exp(1.003\ kx_2) - 0.13\exp(0.0308\ kx_2)] \times \times \cos k(x_1 - vt), \quad (4b)$$

$$u_3 = C_1[0.0308\exp(0.1276\ kx_2) + 0.0234\exp(1.003\ kx_2) - 0.123\exp(0.031\ kx_2)] \times \times \sin k(x_1 - vt). \quad (4c)$$

Since there are three components of particle displacement not equal to zero, and displaced in phase correspondingly, we may conclude that the motion of the particles is elliptical. The ellipse lies in a plane perpendicular to a free surface and forms an angle $\varphi = 11.9°$ with the wave vector direction. The value of this angle, determined by $\tan^{-1} u_{30}/u_{10}$, is equal to zero ($u_3 = 0$), at a depth equal to 0.5 wavelengths. Then the ellipse lies in the plane containing the wave vector. The ratio of the elliptical axes lengths is equal to 1.6 on a free surface.

The change in the displacement components as a function of depth is presented in Fig. 4.

A considerable penetration of the u_2 component 4 wavelengths beneath the surface may be noted. For the direction ⟨001⟩ in the plane (010) where, except for one imaginary root, there are two complex roots, the amplitude change with depth has the character of a sinusoid decaying exponentially. This change is shown in Fig. 5. The amplitude of the particle displacement components decays at a depth of 3 wavelengths beneath the surface. The displacement components for these directions are the following:

$$u_1 = C_1\{-1.005\exp(1.049\ kx_2) + \exp(0.203\ kx_2)[2.27\cos(0.659\ kx_2) - -1.024\sin(0.659\ kx_2)]\}\cos k(x_3 - vt), \quad (5a)$$

$$u_2 = C_1\{-0.212\exp(1.049\ kx_2) + \exp(0.203\ kx_2)[2.187\cos(0.659\ kx_2) + +4.53\sin(0.659\ kx_2)]\}\sin k(x_3 - vt), \quad (5b)$$

$$u_3 = C_1\{0.1853\exp(1.049\ kx_2) + \exp(0.203\ kx_2)[3.811\cos(0.659 kx_2) - -2.684\sin(0.659 kx_2)]\}\cos k(x_3 - vt). \quad (5c)$$

The movement of particles in this case is elliptical, as for the ⟨100⟩ direction. The plane of this ellipse forms an angle of 17° with the wave vector direction and is perpendicular to the wave propagation plane. The value of this angle changes with depth. For the remaining considered directions, surface wave propagation in the (010) plane, and for the plane (001) in the ⟨010⟩ direction, and the ⟨010⟩ direction in the (100) plane, the equations determining the displacement components have the same character as for the above directions.

4. Conclusions

In the case of surface wave propagation along the ⟨100⟩ direction in the (001) plane and ⟨001⟩ in the (100) plane the characteristic equation is divided into two equations of the second order and of the fourth order. Analyzing the

second order equation and assuming stress-free surface boundary conditions, it has been proved that only a transverse bulk wave can propagate in the ⟨100⟩ direction in the (001) plane. This wave propagates at an angle of $\tan^{-1} l_3^1 = 1.6°$ to the free surface. The velocity which corresponds to the wave is equal to $V = 1919.9$ m/s. The calculated displacement components of the particles in this wave are as follows

$$u_1 = u_3 = 0, \quad u_2 = C\exp[ik(0.027\, x_3 + x_1 - vt)]. \tag{6}$$

While solving the equation of fourth order roots with the imaginary part not equal to zero have not been found. It is known that only these roots correspond to a surface wave which would simultaneously satisfy the boundary conditions. The boundary conditions were satisfied only in the range of real roots. Therefore, it may be assumed that only transverse bulk waves can propagate in the direction considered. This wave propagates at an angle equal to 10.6° to the free surface with a velocity $V = 2038$ m/s.

Similar results for the ⟨001⟩ direction in the (100) plane have also been obtained. Thus, in the case of the TGS crystal considered the ⟨100⟩ direction in the (001) plane, and ⟨001⟩ in the plane (100) are forbidden for surface wave propagation.

References

[1] R. Stonley, *The propagation of surface elastic waves in a cubic crystal*, Proc. Roy. Soc., **A 232**, 44 (1955).

[2] A.C. Gazis, R. Herman, R. Vallis, *Surface elastic waves in cubic crystals*, Phys. Rev., **119**, 533 (1960).

[3] T.C. Lim, G.W. Farnell, *Search for forbidden directions of elastic surface-wave propagation in anisotropic crystals*, Journal of Applied Physics, **39**, 9, 4319 (1968).

[4] L.F. Protopopova, A.M. Fiedorchenko, *Volny Rayleigha v poluprovodnikach i yannych kristalach z kubicheskoy symetrej*, Nauch. trudy vysshich ucheb. zaved. Litevskoy CCR, Ultrazvuk, **3**, 61 (1971).

[5] A.D. Tursonov, *Obobshchennye poverchnostnye volny v kubicheskich kristalach*, Acust. Journal, **13**, 100 (1967).

Received on December 16, 1980; revised version on November 3, 1981.

ARCHIVES OF ACOUSTICS
7, 2, 163-170 (1982)

ACOUSTICAL RELAXATION IN HETEROCYCLIC LIQUIDS

BOGUMIŁ LINDE

Department of Physics, University of Gdańsk
(80-952 Gdańsk, ul. W. Stwosza 57)

Measurements of ultrasonic velocity and ultrasonic absorption coefficient have been carried out for several organic liquids in the frequency range from 10 to 1300 MHz at 293 K temperature.

The ultrasonic measurements and the infrared spectra of the liquids have been used for determination of vibrational degrees of freedom which take part in acoustical relaxation process.

1. Introduction

Based on the Kneser acoustical relaxation times measured by the authors [1] and using published data of optical frequencies, the active vibrational degrees of freedom were determined for thiazole [2] and pirimidine [3]. The lack of complete IR spectra for α-picoline, tetrahydrofuran and piperidine [11, 12] prevented a similar analysis for these substances.

Comparing these in complete IR data and the measured acoustical results, it has been possible to show that not all the degrees of freedom are active within the acoustical relaxation processes observed.

2. Experiment

The ultrasonic absorption spectra $\alpha/f^2(f)$ were measured by the ultrasonic pulse method from 10 to 1300 MHz [4, 5] and ultrasonic velocities were obtained using an ultrasound pulse-phase interferometer [4]. The temperature was stabilized with an accuracy of 0.01 K.

The measuring errors ranged from 7 to 4 per cent for attenuation in the frequency range 10-60 MHz, and from 3.5 to 5.5 per cent in the frequency range 400-1300 MHz.

The liquids used (made by Fluka AG, Bucks IG) were of analytical purity and were used after distillation.

3. Theory

In the case of acoustical relaxation the $\alpha/f^2(f)$ and $\mu(f)$ absorption curves can be described as follows

$$\frac{\alpha}{f^2} = \frac{A}{1+(\omega\tau)^2} + B, \tag{1}$$

$$\mu = \alpha\lambda = \left(\frac{A}{1+(\omega\tau)^2} + B\right) fc, \tag{2}$$

when the process is characterized by a single relaxation time. (Where A is the relaxational absorption, B the residual absorption after the process has relaxed, and $\tau = 1/2\pi fc$.)

The determination of the internal vibrational degrees of freedom involved in the acoustical relaxation process is possible using the Herzfeld formula [6]

$$\tau_i = \frac{C_p - C_i}{C_p}\tau_{\text{opt}}, \quad \tau_{\text{opt}} = \frac{Ac}{2\pi^2}\frac{C_p C_v}{(C_p - C_v)C_i}, \tag{3}$$

(where c is the velocity of ultrasound, C_i is the vibrational specific heat, C_p and C_v are the specific heats at constant pressure and volume); and the Planck-Einstein formula

$$C_i = R\sum \frac{\left(\frac{h\nu_i}{kT}\right)^2}{\exp\left(\frac{h\nu_i}{kT}\right)\left[1-\exp\left(\frac{h\nu_i}{kT}\right)\right]^2}, \tag{4}$$

using the frequencies of fundamental vibrations ν_i measured from the infrared spectra.

Comparing τ_{ac} and τ_{opt} one can determine the degrees of freedom active in the process [7].

4. Results and discussion

Pirimidine

The variations of sound absorption $\alpha/f^2(f)$ and $\mu(f)$ for pirimidine are shown in Figs. 1 and 2 and can be described by equations (1) and (2). In these figures the solid lines represent curves of a single relaxation.

The relaxation time τ_{ac} determined from the acoustical measurements is $1.2\cdot10^{-10}$s whereas the value of τ_{opt} calculated according to formula (3) is smaller and is equal to $0.3\cdot10^{-10}$s. Hence it is possible to conclude that in the given range of frequencies of ultrasound and hypersound waves not all of the internal degrees of freedom take part in the energy transfer between vibrational and

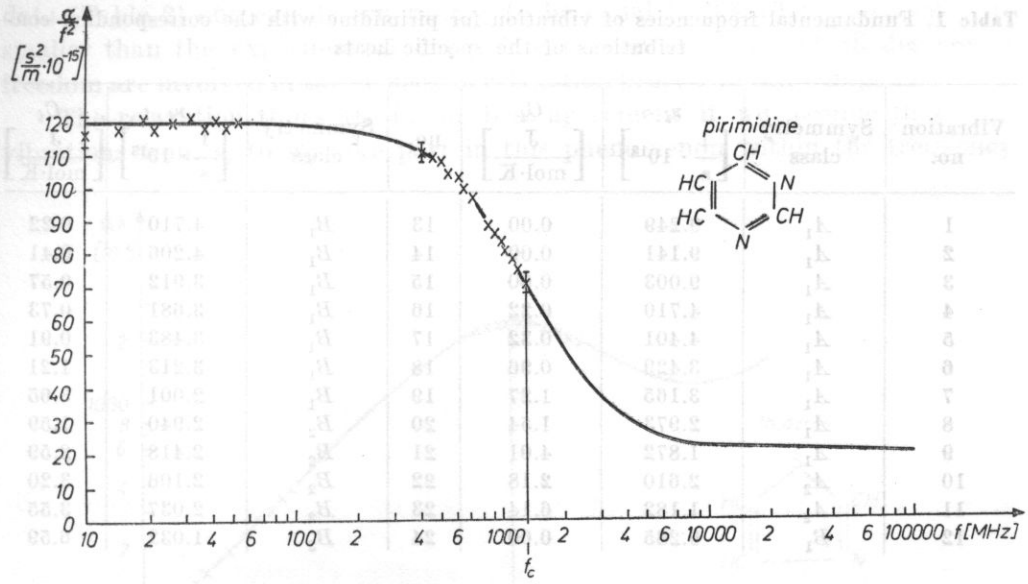

Fig. 1. Frequency dependence of the ultrasound absorption α/f^2 in pirimidine at 293 K temperature

in Figs. 1-5: — calculated, × — measured

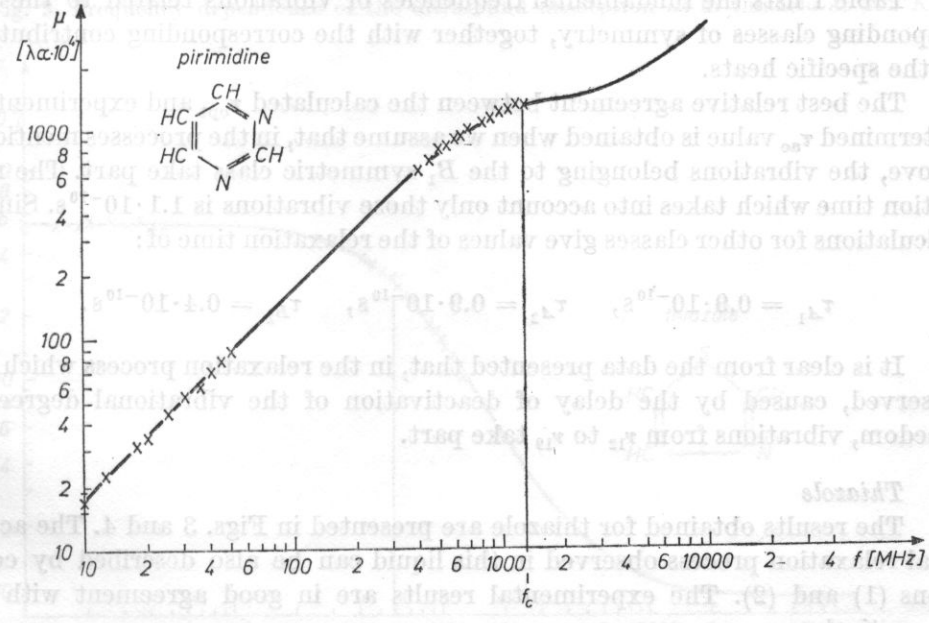

Fig. 2. Absorption μ measurements as a function of frequency in pirimidine

Table 1. Fundamental frequencies of vibration for pirimidine with the corresponding contributions of the specific heats

Vibration no.	Symmetry class	ν_i $\left[\frac{1}{s} \cdot 10^{13}\right]$	C_i $\left[\frac{J}{mol \cdot K}\right]$	no.	Symmetry class	ν_i $\left[\frac{1}{s} \cdot 10^{13}\right]$	C_i $\left[\frac{J}{mol \cdot K}\right]$
1	A_1	9.249	0.00	13	B_1	4.710	0.22
2	A_1	9.141	0.00	14	B_1	4.206	0.41
3	A_1	9.003	0.00	15	B_1	3.912	0.57
4	A_1	4.710	0.22	16	B_1	3.681	0.73
5	A_1	4.401	0.32	17	B_1	3.483	0.91
6	A_1	3.429	0.96	18	B_1	3.213	1.21
7	A_1	3.165	1.27	19	B_1	2.001	3.65
8	A_1	2.973	1.54	20	B_2	2.940	1.59
9	A_1	1.872	4.01	21	B_2	2.418	2.59
10	A_2	2.610	2.18	22	B_2	2.106	3.20
11	A_2	1.182	6.14	23	B_2	2.037	3.55
12	B_1	9.285	0.00	24	B_2	1.032	6.59

translational degrees of freedom, or in other words, the relaxation times of different degrees of freedom are different.

The complete spectroscopic data of IR for pirimidine listed in Table 1 [3] gives the possibility of determining, with a high probability, which of the vibrational degrees of freedom take part in the observed acoustical relaxation process.

Table 1 lists the fundamental frequencies of vibrations related to the corresponding classes of symmetry, together with the corresponding contributions of the specific heats.

The best relative agreement between the calculated τ_{opt} and experimentally determined τ_{ac} value is obtained when we assume that, in the processes mentioned above, the vibrations belonging to the B_1 symmetric class take part. The relaxation time which takes into account only those vibrations is $1.1 \cdot 10^{-10}$ s. Similar calculations for other classes give values of the relaxation time of:

$$\tau_{A_1} = 0.9 \cdot 10^{-10}\,\mathrm{s}, \quad \tau_{A_2} = 0.9 \cdot 10^{-10}\,\mathrm{s}, \quad \tau_{B_2} = 0.4 \cdot 10^{-10}\,\mathrm{s}.$$

It is clear from the data presented that, in the relaxation process which was observed, caused by the delay of deactivation of the vibrational degrees of freedom, vibrations from ν_{12} to ν_{19} take part.

Thiazole

The results obtained for thiazole are presented in Figs. 3 and 4. The acoustical relaxation process observed in this liquid can be also described by equations (1) and (2). The experimental results are in good agreement with the theoretical ones.

The relaxation time τ_{ac} estimated on the basis of the experimental results is equal to $2.7 \cdot 10^{-10}$ s. Using the fundamental vibrational degrees of freedom

data (Table 2) one can determine τ_{opt} to be equal to $2.3 \cdot 10^{-10}$s, so that it is smaller than the experimental one. We can conclude that not all degrees of freedom are involved in the acoustical relaxation process in this compound.

The relaxation times are in the best agreement if we assume that only vibrations from ν_2 to ν_{18} take part in this phenomenon within the frequency

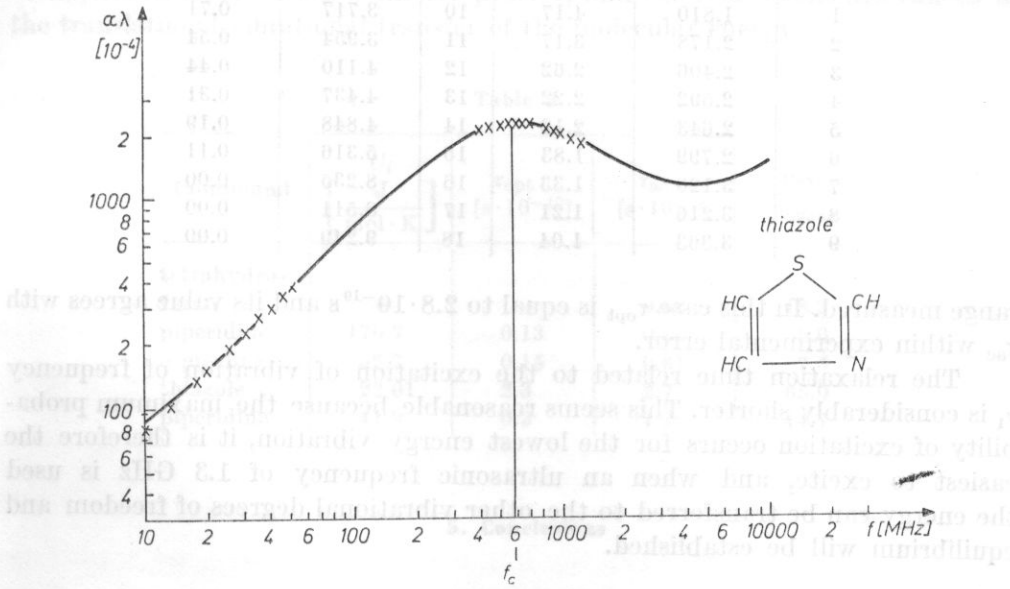

Fig. 3. Frequency dependence of the ultrasound absorption $\alpha\lambda$ in thiazole at 293 K

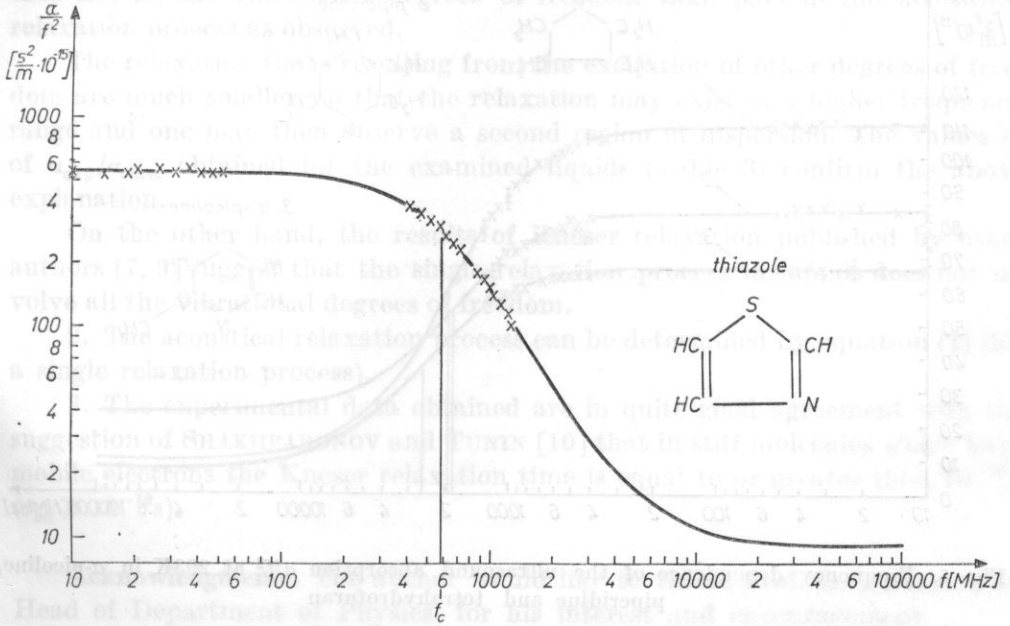

Fig. 4. Absorption α/f^2 measurements as a function of frequency in thiazole

Table 2. Fundamental frequencies of vibration for thiazole with the corresponding contributions of the specific heats

Vibration no.	ν_i $\left[\frac{1}{s}\cdot 10^{13}\right]$	C_i $\left[\frac{J}{mol\cdot K}\right]$	no.	ν_i $\left[\frac{1}{s}\cdot 10^{13}\right]$	C_i $\left[\frac{J}{mol\cdot K}\right]$
1	1.810	4.17	10	3.717	0.71
2	2.178	3.17	11	3.954	0.54
3	2.406	2.62	12	4.110	0.44
4	2.592	2.22	13	4.437	0.31
5	2.643	2.12	14	4.848	0.19
6	2.799	1.83	15	5.316	0.11
7	3.120	1.33	16	8.235	0.00
8	3.216	1.21	17	8.511	0.00
9	3.363	1.04	18	9.249	0.00

range measured. In this case τ_{opt} is equal to $2.8\cdot 10^{-10}$s and its value agrees with τ_{ac} within experimental error.

The relaxation time related to the excitation of vibration of frequency ν_1 is considerably shorter. This seems reasonable because the maximum probability of excitation occurs for the lowest energy vibration, it is therefore the easiest to excite, and when an ultrasonic frequency of 1.3 GHz is used the energy can be transferred to the other vibrational degrees of freedom and equilibrium will be established.

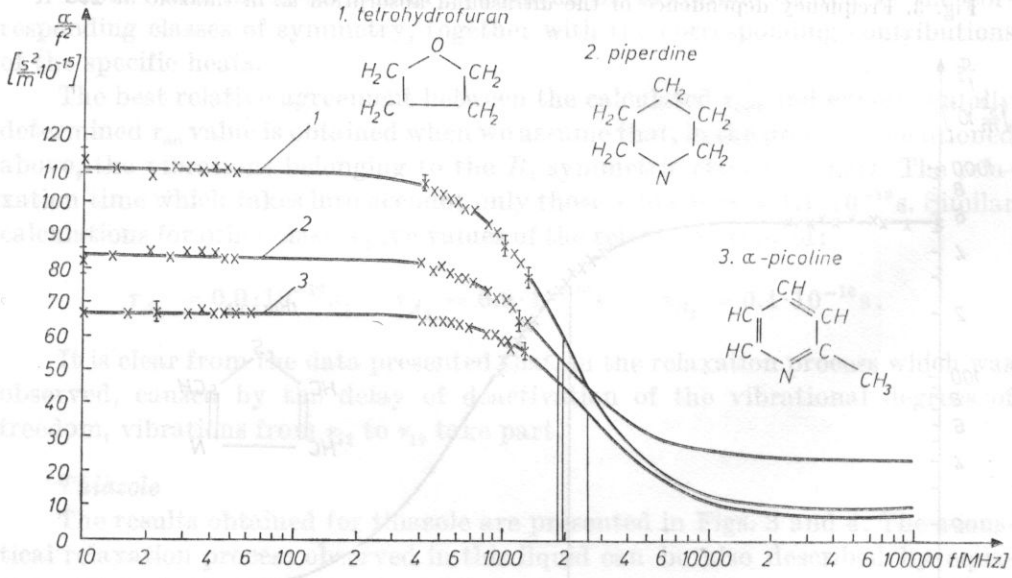

Fig. 5. Frequency dependence of the ultrasound absorption α/f^2 at 293K in α-picoline, piperidine and tetrahydrofuran

In these liquids the inflection points of the curves $\alpha/f^2(f)$ occur outside the measurement frequency range experimentally available, but they can be calculated from equation (1) [8].

It seems from the comparison of the values of τ_{ac} obtained from the acoustical measurements with the calculated τ_{opt} (Table 3) that the observed region of dispersion results from a Kneser process, and the relaxations are caused by the translational-vibrational transfer of the molecular energy.

Table 3

Compound	C_i $\left[\frac{\text{J}}{\text{mol}\cdot\text{K}}\right]$	τ_{opt} $[\text{s}\cdot 10^{-10}]$	τ_{ac} $[\text{s}\cdot 10^{-10}$	$\frac{\alpha_{exp}}{\alpha_{class}}$
tetrahydro-furan	—	—	0.82	18.3
piperidine	170.7	0.13	0.86	5.0
α-picoline	52.7	0.15	0.61	7.5
thiazole	22.01	2.3	2.7	65.0
piperidine	41.9	0.3	1.2	14.7

5. Conclusions

1. From the above considerations it appears that in the compounds examined not all the vibrational degrees of freedom take part in the acoustical relaxation process as observed.

The relaxation times resulting from the excitation of other degrees of freedom are much smaller, so that the relaxation may exist in a higher frequency range and one may then observe a second region of dispersion. The values of of $\alpha_{exp}/\alpha_{class}$ obtained for the examined liquids (Table 3) confirm the above explanation.

On the other hand, the results of Kneser relaxation published by other authors [7, 9] suggest that the single relaxation process in liquids does not involve all the vibrational degrees of freedom.

2. The acoustical relaxation process can be determined by equation (1) (for a single relaxation process).

3. The experimental data obtained are in quite good agreement with the suggestion of SHAKHPARONOV and TUNIN [10] that in stiff molecules which have mobile electrons the Kneser relaxation time is equal to or greater than 10^{-10} s ($\tau_{ac} \geqslant 10^{-10}$s).

Acknowledgments. The author would like to thank Prof. dr A. ŚLIWIŃSKI, Head of Department of Physics, for his interest and encouragement.

References

[1] B. LINDE, A. ŚLIWIŃSKI, *Ultrasound attenuation of benzene-similar and heterocyclic liquids within the frequency range 10 - 1300 MHz*, Acoustics Letters, **2**, 65-68 (1978).

[2] G. DAVIDOVICS, Ch. GARRIGOU-LAGRANGE, J. CHOUTEAU, J. METZGER, *Contribution á l'ètude des spectres de vibration du thiazole*, Spectrochimica Acta, **23A**, 1477-1487 (1967).

[3] L.M. SVERDLOV, M.A. KOVNER, E.A. KARAINOV, *Kolebatelnyie spektry mnogoatomnykh molekul*, Nauka, Moskva 1979.

[4] J. WEHR, *Measurements of velocity and damping of ultrasound* (in Polish), PWN, Warsaw 1972.

[5] L.A. DAVIDOVICH, S. MAKHMAKOV, L. PULATOVA, P. K. KHABIBULAIEV, M. G. KHALIULIN, *Isledovanie akusticheskikh svoistv nekotorykh organicheskikh zhidkostei na chastotakh 0.3-3 GHz*, Akust. Zh., **XVIII**, W 2, 318-320 (1972).

[6] K.F HERZFELD, T.A. LITOWITZ, *Absorption and dispersion of ultrasonic waves*, Academic Press, New York and London, 1959.

[7] A.S. LAGUNOV, B.A. BELINSKII, *Isledovanie akusticheskikh svoistv zhidkikh: benzola, piridina, pirola i phurana v diapazonie chastot 6-900 MHz*, Uchonyie Zapiski, Primenenie ultraakustyki k isledovaniu veshchestva, **XXII**, 85-96 (1967).

[8] W. BOCH, *Investigations of zinc chloride solutions in methyl alcohol by methods of molecular acoustics* (in Polish), Poznań 1975.

[9] Z. KLESZCZEWSKI, *Thermal relaxation processes in some organic liquids* (in Polish), Archiwum Akustyki, **11**, 1, 59-66 (1976).

[10] M.I. SHAKHPARONOV, M.S. TUNIN, *Giperakusticheskiie svoistva zhidkosti i struktura molekul*, Primenenie ultraakustiki k isledovaniu veshchestva, **XV**, 19-29 (1961).

[11] *Arbeitsatlas der Infrarotspektroskopie*, Butterworth-Verlag Chemie, London – Weinheim 1972.

[12] J.H.S. GREEN, W. KYNASTON, H.M. PAISLEY, *Vibrational spectra of monosubstituted pyridines*, Spectrochimica Acta, **19**, 549 (1963).

Received on January 6, 1981; revised version on October 26, 1981.